ERRATA

Page

Abstract line 10: having its V-O axis inclined at an angle of

Abstract second line from bottom: of the reduced vanadyl signal

13 line 1: vanadyl ion surrounded by

15 line 5: 3-4 mm long were obtainable in

16 line 4: of the atoms in the unit cell

19 line 17: coated with a thermo-

22 line 15: made in the white beam

23 line 4: delete "is truly phenonienological in that one can postulate it on the basis of symmetry" and replace with "can be obtained from phenomenological considerations"

$$W_c = \sum_k \left(\frac{P_k^2}{2m} - \frac{ze^2}{r_k} \right) + \sum \frac{e^2}{r_{kj}}$$

$$W_{ss} = \sum_{jk} \left(\qquad \right) \quad (j \neq k)$$

28 line 7: delete "the total spin operator $\underline{S}$ and replacing" and replace with "$\underline{S}$ (op) and replacing the functions of"

31 Table 1, column 1: $\mathcal{G}_{xy}$ not xy

39 Footnote, line 4: peak to peak height of $3/4\sqrt{3}a^1$ b

41

$$\tan 2\delta \simeq \frac{4\mathcal{G}_{xy}\, g_x g_y}{(B_x - B_y)(g_x^2 + g_y^2) + \frac{h\nu}{m}(g_x^2 - g_y^2)}$$

Page

42 $$\left[H_m(\Theta,\delta)\right]_{\substack{\text{first}\\ \text{order}}} = \frac{h\nu}{g\beta} - \frac{m}{g\beta K}\left\{A^2\frac{g_z^2}{g^2}\cos^2\Theta + B_\perp\frac{g_\perp^2}{g^2}\sin^2\Theta\left[\frac{B_x+B_y}{2} + \frac{B_x-B_y}{2}\left(\frac{g_x^2\cos^2\delta - g_y^2\sin^2\delta}{g_\perp^2}\right) + 2\sigma_{xy}\frac{g_x g_y}{g_\perp^2}\sin\delta\cos\delta\right] + (A+B_\perp)\frac{g_z g_\perp}{g^2}\sin\Theta\cos\Theta\left[\sigma_{xz}\frac{g_x}{g_\perp}\cos\delta + \sigma_{yz}\frac{g_y}{g_\perp}\sin\delta\right]\right\}$$

delete "In fact ... what is observed."

45 line 5: the ionic radii for V^{+4} and O^{-2}

49 Table 4, column 2: 1.9717±5

77 line 5: $$\frac{2M^2}{K}\frac{g_\perp^2}{g^2}B_\perp^2\sin^2\Theta\left\{\qquad\right\}$$

77 line 10: $$\left(1+\frac{A}{K}\frac{g_z^2}{g^2}\cos^2\Theta\right) - \frac{B_x-B_y}{4B_\perp}\left(\quad\times\quad\right)\Big]^2$$

78 line 6: $$I(I+1)\left[Q'\left(\qquad\right) - \frac{Q''}{2}\frac{B_\perp^2}{g^2K^2}\sin^2\Theta\left(\qquad\right)\right]$$

79 bottom term $$\frac{2m^2g_\perp^2}{g^3\beta H}\sin^2\Theta\left\{\qquad\right\}$$

91 line 10: This same expression can be used to compute $\frac{A}{g_z B}$

95 Ref. 5: C. P. Slichter

THE UNIVERSITY OF MICHIGAN

COLLEGE OF ENGINEERING
Department of Nuclear Engineering

Final Report - Part 1

AN EPR INVESTIGATION OF VO^{+2} AND X-RAY PRODUCED V^{+2} IN TUTTON SALT

R. H. Borcherts

ORA Project 04385

under contract with:

NATIONAL SCIENCE FOUNDATION
GRANT NO. G-15912
WASHINGTON, D.C.

administered through:

OFFICE OF RESEARCH ADMINISTRATION ANN ARBOR

June 1963

This report was also a dissertation submitted in partial fulfillment of the requirements for the degree of Doctor of Philosophy in The University of Michigan, 1963.

TABLE OF CONTENTS

TABLE OF CONTENTS (Concluded)

LIST OF TABLES

LIST OF FIGURES

ABSTRACT

In these experiments the Electron Paramagnetic Resonance (EPR) spectrum of the vanadyl ion (VO^{+2}) in single crystals of $Zn(NH_4)_2(SO_4)_2 \cdot 6H_2O$ is studied and comparison of the X-ray irradiated VO^{+2} spectrum to V^{+2} in single crystals of $Zn(NH_4)_2(SO_4)_2 \cdot 6H_2O$ is made.

Investigation, at 9.3 kmc, of the single crystals containing the vanadyl ion, VO^{+2}, showed that the vanadyl ion substitutes for the divalent zinc ion with its V-O axis oriented in one of three directions. The three directions have a population ratio of 20:5:1 with the larger two population positions having their axes at an angle of 77°48' to each other and the third position having its V-O axis inclined an angle of 98° to the other two. The rhombic spin Hamiltonian fits the experimental data well if the x, y principal axes of the g tensor are rotated 23°20' from the x, y principal axes of the A tensor. The z axes of both tensors are assumed to coincide. The rhombic spin Hamiltonian constants (obtained at room temperature) vary slightly for each of the three positions with the larger population position having

$g_z = 1.9331$ $\quad$ $A = 0.018281/cm$

$g_x = 1.9813$ $\quad$ $B_x = 0.007137/cm$

$g_y = 1.9801$ $\quad$ $B_y = 0.007256/cm$

$|Q'| = 0.00024/cm$ $\quad$ $\mathcal{H}_{xy} = -0.0000462/cm$

The constant $\mathcal{H}_{xy} (\equiv F_{xy}+F_{yx})$ results from the noncoincident principal axes of the g and A tensors and arises from the inclusion of off-diagonal terms of the form

$$\sum_{ij}{}' F_{ij}\left(S_i I_j + S_j I_i\right)$$

The constants A, B_x, B_y, and $\mathcal{H}_{xy}$ are related to A_{zz}, A_{xx}, and A_{yy}, the principal axes values of the hyperfine tensor, and were evaluated to be

$$A_{zz} = A$$

$$A_{xx} = 0.0071200/cm$$

$$A_{yy} = 0.0072439/cm$$

The three positions of the V-O axes suggested that the direction of these axes were the (111) directions of the octahedron of water molecules that surround it. Since the octahedron of water molecules is distorted each of the four positions is ordered in energy and thus in population. The lowest population position was not observed. An alternate description in which the vanadyl ion is surrounded by five water molecules (the vanadium is at the center of the octahedron of the five water molecules and the covalent bonded oxygen) is considered a possible description of this complex.

Also observed was a five-line superhyperfine structure on the vanadyl resonances for a specified orientation of the magnetic field. This structure was found to be due to the protons of the surrounding water molecules.

Upon X-ray irradiation of the crystals containing the vanadyl ion it was found that the X-ray, or the subsequent high energy electron it produces, breaks the V-O bond resulting in a V^{+2} EPR spectrum having the same rhombic spin Hamiltonian constants and z axis orientation as crystals grown with V^{+2}. These constants, measured at 24 kmc, were calculated to be

$g_z = 1.9717$	$E = 0.02280/cm$
$g_y = 1.9733$	$A = 0.008263/cm$
$D = 0.15613/cm$	$B = 0.008246/cm$

with A and D having the same sign. Measurements were also made on the V^{+2} (irradiated VO^{+2}) spectra in $Mg(NH_4)_2(SO_4)_2 \cdot 6H_2O$ and $ZnK_2(SO_4)_2 \cdot 6H_2O$.

Although X-ray irradiation, carried out in a white beam from a tungsten target tube operated at 50 KVP, 50 ma, reduced the intensity of the VO^{+2} signal 80-90% in 10 min ($\sim 10^8$ rad) further irradiation failed to reduce the intensity of the remaining vanadyl signals. Also, of reduced vanadyl signal, only 15-20% of it was converted to V^{+2}. An experiment carried out at 4.2°K failed to show any V^{+3}.

CHAPTER I

INTRODUCTION

In recent years the spectroscopy of the solid state has been given a great impetus by the initial successes of such devices as the transistor, the solid state radiation detector, and the ruby maser and laser, as well as by the need for fundamental knowledge of the basic properties of solids in such new areas of application of reactor technology and space exploration.

Magnetic resonance is one branch of solid state spectroscopy that deals with nuclear, ferromagnetic, antiferromagnetic, and paramagnetic resonance. The first, nuclear magnetic resonance, or NMR, is concerned with the magnetic dipoles of nuclei; the other three are concerned with the magnetic dipoles resulting from electrons. In ferromagnetic and antiferromagnetic resonance the electronic dipoles are strongly coupled to each other, while in electron paramagnetic resonance, or EPR, the individual electronic dipoles are considered separate or very loosely coupled.

Paramagnetic substances differ from diamagnetic ones in that the former posses permanent magnetic dipoles arising from the orbital and spin motion of the unpaired electrons. While unpaired electrons occur in the incompleted shells of the four transition series of the periodic table—iron, rare earth, platinum, palladium and uranium—unpaired electrons also occur in some donors, acceptors, and other impurities in

solids, metals, odd electron molecules, such as free radicals and those molecules damaged by radiation, and triplet state molecules, such as O_2. All these may give rise to electron paramagnetic resonance. For texts on EPR one may consult Low,[1] Pake,[2] Ingram,[3,4] and Shlichter,[5] as well as the reviews by Bleaney and Stevens,[6] Bowers and Owen,[7] and Jarrett.[8]

The study of the resonance phenomena of paramagnetic ions began with Zavoisky,[9,10] in 1945. Previously the principal techniques for studying paramagnetic materials had been magnetic susceptibility and paramagnetic rotation. The classic paper by Bethe[11] in 1929, on the prediction of the splitting of the orbitally degenerate ground state of the paramagnetic ion on the basis of the symmetry of the ligands surrounding the ion, and the resulting application by Van Vleck[12] to the explanation of paramagnetism gave rise to the "crystalline field era" in the history of paramagnetism.

Soon after Zavoisky's discovery it became apparent that besides revealing a great deal of information about the paramagnetic ion, EPR could also contribute much to the then meager knowledge of the crystalline field arising from the ligands surrounding the paramagnetic ion. Generally verifying the results of crystal field theory, EPR techniques provided data precise enough that detailed examinations revealed discrepancies between the theoretical energy level scheme and the experimental results. Reconsiderations of the crystalline field theory showed that the more general approach is that of forming a molecular orbital model of the paramagnetic ion and the surrounding

ligands so that covalent bonding is included. In this approach crystalline field theory becomes a limiting case of the molecular orbital treatment.*

A. BACKGROUND TO THE PRESENT INVESTIGATION

One ion of particular interest in EPR investigations is that of vanadium. Almost isotopically pure, vanadium consists of 99.76% V^{51}, nuclear spin 7/2, and 0.24% V^{50}, nuclear spin 6.[14] V^{51} is also an odd proton nucleus—23 protons, 28 neutrons—so that its magnetic moment is expected to be quite large; the result is that the hyperfine structure consisting of eight resonances (2I+1) should be well separated.

The various oxidation states of vanadium have been observed to be +5, +4, +3, and +2. Since the electronic structure of vanadium is $[A]3d^3 4s^2$, where [A] denotes the closed argon shell, the +4, +3, and +2 valence states have $3d^1$, $3d^2$, and $3d^3$ electrons respectively. By Hund's Rule** these valence states +4, +3, and +2, will have electron spins of 1/2, 1, and 3/2; respectively, and orbital angular momentum of 2, 3, and 3, respectively. These electrons are thus unpaired; as a result the EPR signature of each valence state is readily recognized by the number and angular dependence of the fine structure groups, as well as by the separation of the hyperfine structure.

---

*For an excellent introduction to molecular orbital as well as crystal field theory see Ballhausen.[13]

**Hund's Rule applied to vanadium says that the ground state has (a) maximum spin multiplicity and (b) maximum orbital angular momentum consistent with (a). See Heine,[15] p. 97.

B. LITERATURE SURVEY OF V^{51} EPR INVESTIGATIONS

V^{+2}. In 1951 Bleaney, Ingram, and Scovil[16] reported on the EPR spectrum of V^{+2} in $Zn(NH_4)_2(SO_4)_2 \cdot 6H_2O$—the same host crystal used in this investigation. In this crystal six water molecules form a distorted octahedron surrounding the V^{+2} ion, producing a rhombic crystalline field. As a result the 2S+1 degenerate ground state splits into two spin doublets, $M_S = \pm 3/2$ and $M_S = \pm 1/2$, separated by 2D. A magnetic field splits the remaining degeneracy, and application of microwave energy at a frequency ν gives rise to three fine structure groups with $g \simeq 2(1 - \frac{4\lambda}{10Dq})$ corresponding to the selection rule $\Delta M = \pm 1$ (Fig. 1). Because of the 7/2 value of the nuclear spin of V^{51} and its large magnetic moment, each of the fine structure groups are composed of eight resonances (2I+1) with a separation of approximately 90 gauss. Their spin Hamiltonian constants are $g_z = 1.951$, $D = 0.158/cm$, $E = 0.049/cm$, and $A = 0.0088/cm$.

Low[17] investigated V^{+2} substituted in the cubic site of Mg in MgO and found $g = 1.980$ and $A = 0.0074/cm$.

V^{+3}. In 1958 Zverev and Prokhorov[18] and later Lambe, Ager, and Kikuchi[19] reported on V^{+3} in α-Al_2O_3 (corundum or sapphire); their EPR results confirm the magnetic susceptibility measurements of Siegert[20] and van den Handel and Siegert.[21] Pryce and Runciman[22] have performed optical investigations of V^{+3} in sapphire.

In sapphire six oxygens surround each aluminum site in a distorted octahedron, giving rise to a trigonal crystalline electric field. If

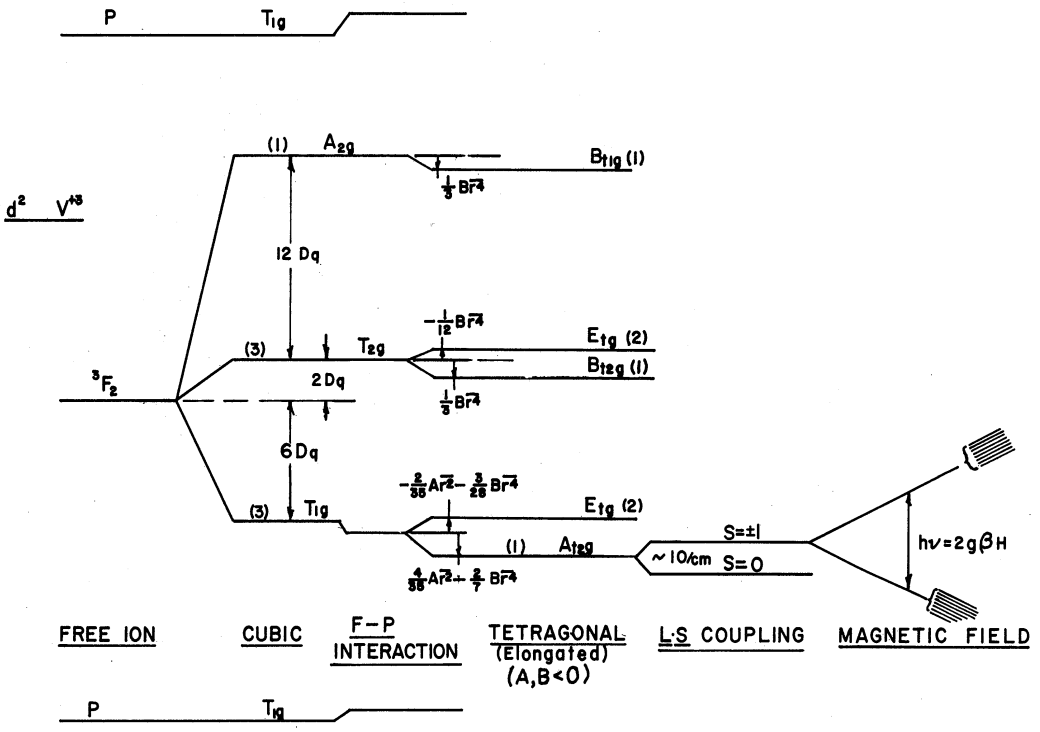

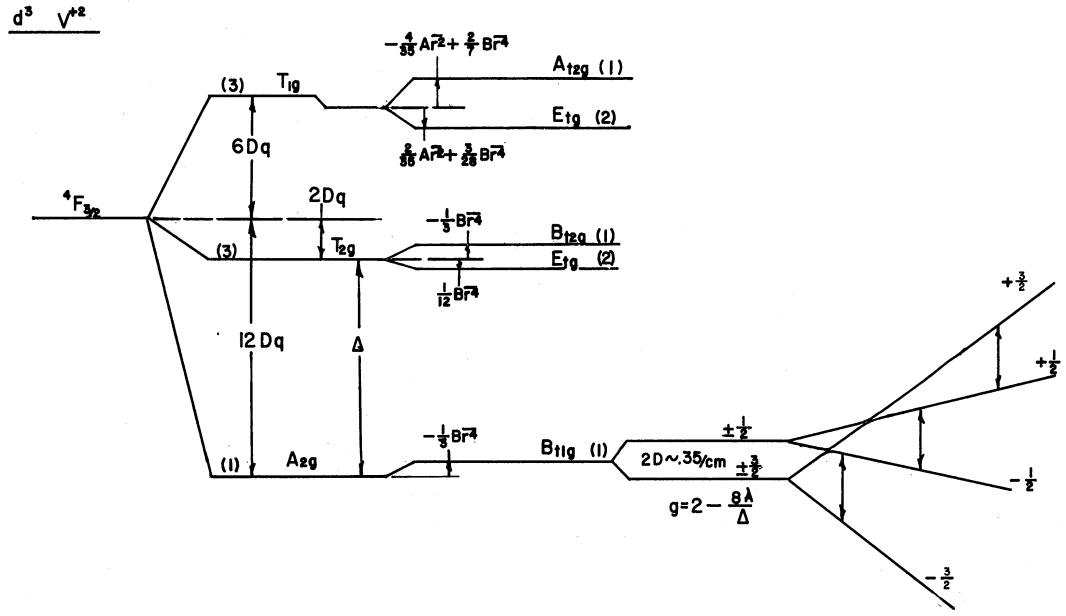

Fig. 1. ^{4}F (V^{+2}) and ^{3}F (V^{+3}) states in crystalline fields.

V^{+3} is substituted for the Al^{+3} ion, the trigonal component splits the T_2 energy level into a doublet E and a singlet B. This splitting acting through the $\underline{L}\cdot\underline{S}$ coupling causes the ground state to split into a lower spin singlet $M_S = 0$ and an upper spin doublet $M_S = \pm 1$ separated by approximately 10/cm (Fig. 1). An applied magnetic field causes the $M_S = \pm 1$ level to split and the application of microwave energy at a frequency ν causes a "forbidden" transition, $\Delta M = \pm 2$, to occur at $H = h\nu/2g\beta$. Since the ground state is separated from the excited state by only a few wave numbers, the relaxation time of this $\Delta M = \pm 2$ transition is so short that the EPR experiment must be performed at very low temperatures, ~4.2°K, in order to observe the spectrum. If the temperature becomes too low, less than 2°K, the $M_S = \pm 1$ state becomes so depopulated that no signal is observed at all. For V^{+3} in α-Al_2O_3, $g = 1.98$, and $A = 0.0102$/cm.

$\underline{V^{+4}}$. In 1960 Lambe and Kikuchi[23] found a small amount of V^{+4} in sapphire having $g \simeq 1.97$ and $|A| \simeq 0.0132$/cm. They were also able to show that by X-ray or gamma irradiation that some V^{+2} is produced from V^{+3}. Also in 1960 Gerritsen and Lewis[24] and Zverev and Prokhorov[25] reported on V^{+4} in TiO_2 (rutile).

In rutile six oxygen atoms surround the Ti^{+4} site, producing a tetragonal field with a small rhombic component. Since V^{+4} has only one 3d electron and thus a spin of 1/2, only one fine structure group corresponding to the $\Delta M = \pm 1$ transition is observed (Fig. 2). Theoretically, the V^{+4} spectrum in rutile has yet to be satisfactorily explained in terms of ordering and separation of energy levels. One notes that vana-

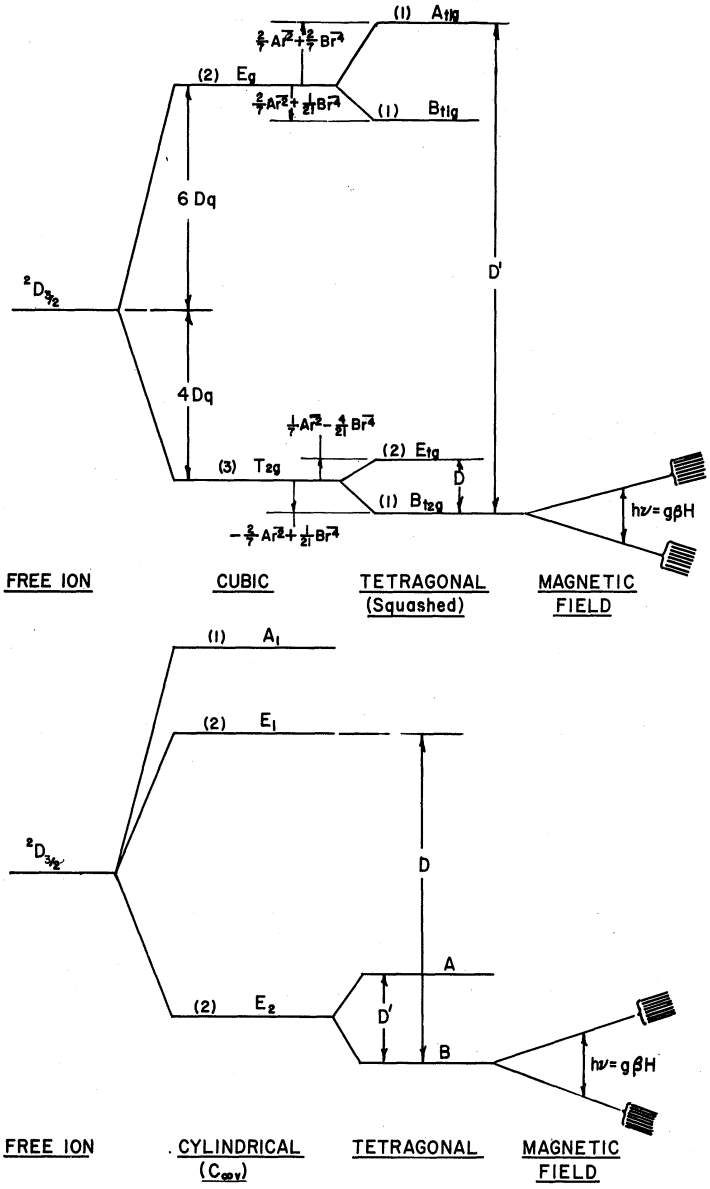

$3d^1$ (V^{+4})

$g_{\parallel} \simeq 2(1 - \frac{4\lambda}{D})$

$g_{\perp} \simeq 2(1 - \frac{\lambda}{D})$

Fig. 2. ^2D (V^{+4} and VO^{+2}) states in crystalline fields.

dium oxide, VO_2, forms a "rutile-like" structure but with one short V-O bond (Andersson[26]). Since V^{+4} tends to form VO^{+2} ions it may well be, as Ballhausen[13] suggests, that in TiO_2 V^{+4} tends to form a strong covalent bond with one of the oxygens. The observed hyperfine spectrum of V^{+4} in rutile is very anisotropic, having a separation of A_z = 0.0142/cm, A_x = 0.0031/cm, and A_y = 0.0043/cm. The g values, g_x = 1.915, g_y = 1.913, and g_z = 1.956 also reflect the rhombic symmetry of the crystalline field.

Although the valence state of vanadium in the vanadyl radical VO^{+2} is also +4, the strong cylindrical field formed by the vanadium and the oxygen produces an energy level structure quite different from that of V^{+4} in a cubic field (Jorgensen[27] and Fig. 2).

The first EPR spectrum of the vanadyl ion VO^{+2} was reported by Garif'ianov and Kozyrev[28] and Kozyrev[29] in both liquid and frozen aqueous and acetone solutions and later by Pake and Sands[30] and Sands[31] in aqueous, acetone, and ether solutions and in glass; by O'Reilly[32] in vanadyl etioporphyrin I dissolved in benzene and high viscosity oil; by Faber and Rogers[33] on various adsorbers (charcoal, Dowex-50, IR-4B, and IR-100); and by Roberts, Koski, and Caughey[34] in some vanadyl porphyrins. As mentioned above, the vanadyl ion carries its own crystalline field so that it matters little what other kind of field surrounds the ion as evidenced by the similar spectra found by these investigators. The results of these investigations are that the g_z and g_1 values are 1.88-1.93 and 1.98-1.99, respectively, and a hyperfine splitting of 0.0147-

0.0184/cm parallel to the z axis and 0.0055-0.0078/cm perpendicular to the z axis. The variation in these values is suggested to be due to the variation of the covalent bonding between the vanadyl ion and the surrounding ligands (Faber and Rogers[33]). Because the samples used in these investigations were either powders or solutions, the resulting EPR spectrum is either an average of the randomly oriented VO^{+2} ions in the frozen or powdered samples (Bleaney,[35] Sands,[31] Searl, Smith and Wyard[36] or Ibers and Swalen[37]) or a time averaged spectrum in solution as a result of the motion of the VO^{+2} ions (McConnell[38] and Rogers and Pake[39]).

Because of the need for EPR information on oriented* VO^{+2} and because of the success of producing the various oxidation states of vanadium by Lambe and Kikuchi[23] and Wertz, Auzins, Griffiths and Orten,[40] this present work was undertaken. Underlying these immediate reasons is perhaps a deeper one—that of a systematic study of the solid state chemistry of vanadium.

*There are brief comments on oriented VO^{+2} in $VOSO_4 \cdot 2H_2O$ by Hutchinson and Singer,[41] as well as some unpublished investigations on VO^{+2} in $ZnK_2(SO_4)_2 \cdot 6H_2O$ by Gager.[42]

CHAPTER II

CONCLUSIONS

A. VO^{+2}

The results of the present EPR experiments on oriented VO^{+2} indicate that the vanadyl ion is substituted for the divalent zinc ion in single crystals of $Zn(NH_4)_2(SO_4)_2 \cdot 6H_2O$ having its V-O axis oriented in one of three directions. The three directions are found to have a population ratio of 40:10:2 with the larger two population positions having their V-O axes at an angle of 77°48' to each other and the least populous position having its V-O axis inclined at 98°1' to the other two. The room temperature spin Hamiltonian constants differ slightly for each position, with the larger population position having:

$g_z = 1.9331 \pm 2$	$B_x = 0.007137 \pm 4/cm$
$g_x = 1.9813 \pm 2$	$B_y = 0.007256 \pm 4/cm$
$g_y = 1.9801 \pm 2$	$\mathscr{F}_{xy} = -0.0000462 \pm 2/cm$
$A = 0.018281 \pm 5/cm$	$\lvert Q' \rvert = 0.00024 \pm 2/cm$

The quantity $\mathscr{F}_{xy}$ ($\mathscr{F}_{xy} \equiv F_{xy}+F_{yx}$) results from the inclusion of terms when the principal axes of the g tensor do not coincide with the principal axes of the A or hyperfine tensor. The experiments indicate that the z axes of the two tensors coincide, but in the xy plane the angle between the x axes of the two tensors is 23°20'. Using the values for $\mathscr{F}_{xy}$, B_x, and B_y, we find the principal axes values of the hyperfine interaction

constants to be A_{xx} = 0.0071200/cm, A_{yy} = 0.0072439/cm, and $A_{zz} \equiv A$.

B. IRRADIATED VO^{+2}

The results of the present EPR experiments on V^{+2} and irradiated VO^{+2} in single crystals of $Zn(NH_4)_2(SO_4)_2 \cdot 6H_2O$ indicate that the X-ray, or the subsequent high energy electron it produces, breaks the V-O bond, resulting in a V^{+2} EPR spectrum having the same spin Hamiltonian constants and z axis orientation as crystals of $Zn(NH_4)_2(SO_4)_2 \cdot 6H_2O$ grown with V^{+2}. The measurements on the irradiated VO^{+2} crystals give the following room temperature spin Hamiltonian constants:

g_z = 1.9717±5	E = 0.02280±3/cm
g_y = 1.9733±5	A = 0.008263±5/cm
D = 0.15613±3/cm	B = 0.008246±5/cm

with A and D having the same sign. Figure 3 depicts these results quite vividly.

In this crystal the VO^{+2} spectrum is reduced in intensity by X-ray irradiation a factor of two for a dose of 5×10^6 rads. Although saturation occurs after 1×10^8 rad, resulting in a 80-90% reduction in the VO^{+2} signal, only 10-20% of the vanadium has been converted to V^{+2}. An EPR experiment carried out at 4.2°K failed to show any of the vanadium in trivalent form.

C. TWO MODELS FOR VO^{+2} IN $Zn(NH_4)_2(SO_4)_2 \cdot 6H_2O$

Ballhausen and Gray[43] have proposed a molecular orbital description

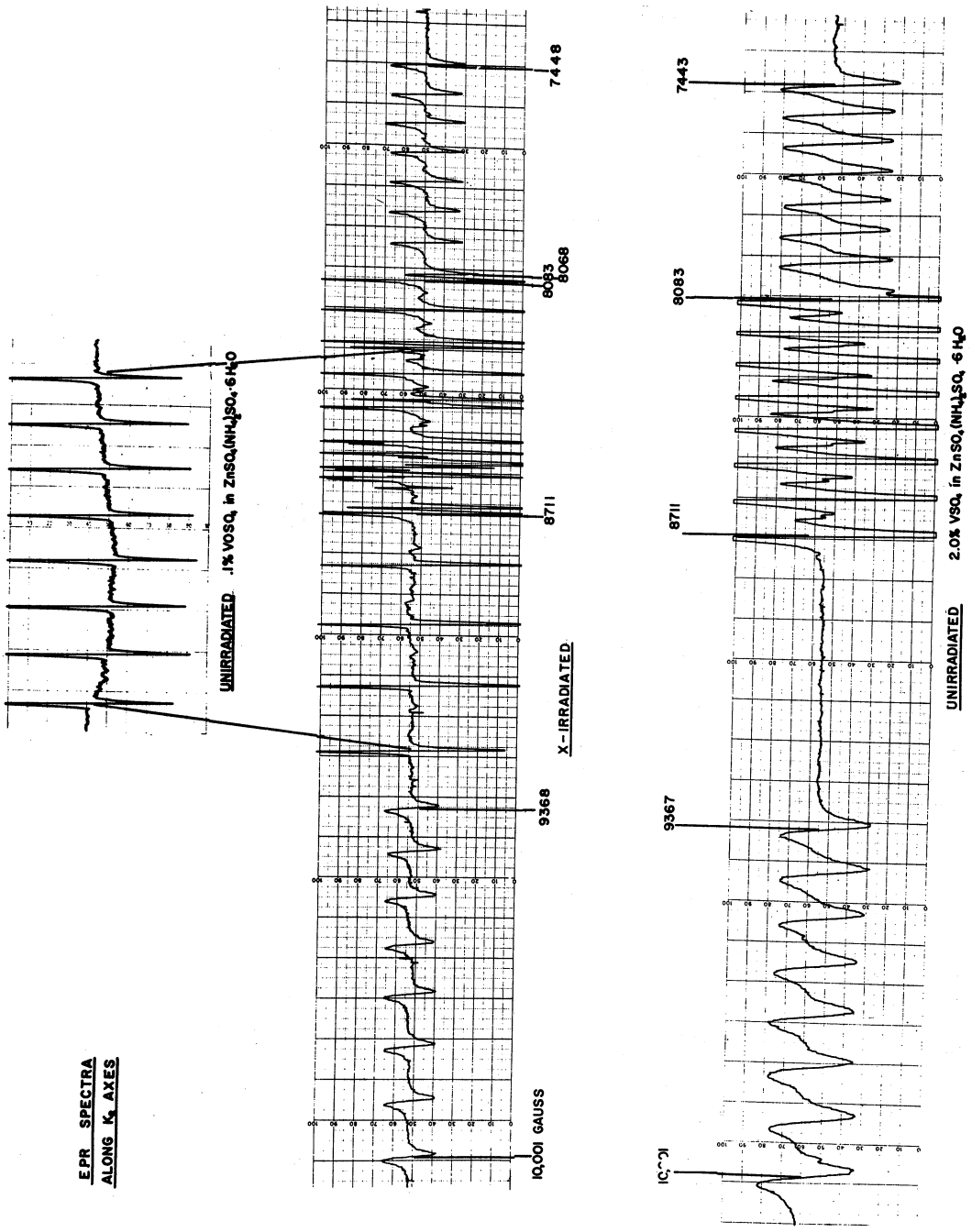

Fig. 3. EPR spectra along K_2 axis.

of the vanadyl ion currounded by five water molecules found for VO^{+2} in solution and VO^{+2} in $VOSO_4 \cdot 2H_2O$ (the vanadium is located at the center and the oxygen and the five water molecules are at the vertices of an octahedron). Their description agrees so well with optical absorption data and the g values reported in the literature as well as the g values found in these experiments, that it should be considered that the VO^{+2} has this pentahydrate environment in the Tutton salt. One other experimental result supporting this pentahydrate model is the three orientations of the V-O axes found in this crystal. If one assumes the validity of the pentahydrate model, the results of the present experiments showing the irradiated VO^{+2} EPR spectrum and the V^{+2} EPR spectrum to be identical imply that the oxygen removed from the VO^{+2} ion takes the place of the missing water molecule of the octahedron, producing a crystalline field identical, as far as EPR can determine, to that for V^{+2} surrounded by six water molecules.

An alternate "model" results if one considers the V-O axis pointing in the (111) direction of the cube where the six water molecules are placed at the centers of the faces. This arrangement predicts four possible directions of the V-O axis, but since the octahedron of water molecules in the Tutton salts is quite distorted, the four directions are ordered in energy and thus in population. The fourth direction, not found experimentally, is then expected to be so energetically unfavorable that it is not detectable by EPR techniques.

D. FURTHER STUDIES

While the major questions of the EPR spectrum of VO^{+2} in $Zn(NH_4)_2(SO_4)_2 \cdot 6H_2O$ and the conversion of VO^{+2} to V^{+2} in this same crystal seem to be answered sufficiently, several unanswered questions suggest further work, such as; (a) an investigation of the superhyperfine structure on the vanadyl resonances that arise from the protons of the surrounding water molecules. That this structure is due to the protons is verified by its absence in crystals grown with D_2O. Replacement of the H_2O by D_2O reduces the line width of the vanadyl resonances by one-half, and the smaller magnetic moment of the deuteron (0.85738 n.m. as contrasted to that of the proton, 2.79275 n.m.) reduces the strength of interaction so that the superhyperfine spectrum due to the deuteron is unable to be resolved. This investigation might be best pursued with ENDOR techniques and might provide information as to the correct model of VO^{+2} in the Tutton salt and a molecular orbital description of the complex; (b) a more accurate measurement of the strength of the quadrupole interaction also best accomplished with ENDOR techniques; (c) an investigation of a vanadyl radiation dosimeter. Vanadium in glass is observed to be in the form of the vanadyl ion and showed a decrease in signal intensity upon X-ray irradiation. Thus, the possibility of a vanadyl glass dosimeter immediately suggests itself.

CHAPTER III

EXPERIMENTAL METHODS

A. CRYSTAL GROWTH

Single crystals of 0.05, 0.1, 0.5, and 1.0% concentrations (vanadyl to zinc) of the Tutton salt $Zn(NH_4)_2(SO_4)_2 \cdot 6H_2O$ were grown by evaporation from a water solution into which $ZnSO_4 \cdot 7H_2O$, $(NH_4)_2SO_4$, and $VOSO_4 \cdot 2H_2O$ were dissolved in the prescribed amounts. Translucent light blue crystals up to 3-4 mm long wer obtainable in 1-2 days. Zinc potassium and magnesium ammonium Tutton salts containing 1.0% VO^{+2} were also grown in this manner.* ** For the crystals containing heavy water, or D_2O, the water of hydration in $ZnSO_4 \cdot 7H_2O$ and $VOSO_4 \cdot 2H_2O$ was first removed by heating, and then the above evaporation technique was employed.***

In contrast to the relative ease of the growing of the vanadyl crystals, the growth of the 1.0% and 2.0% (V^{+2} to Zn) $Zn(NH_4)_2(SO_4)_2 \cdot 6H_2O$ crystals required a greater degree of skill because of the rapidity at which V^{+2} becomes oxidized in solution. Cathodic reduction of the 1.0 and 2.0% (VO^{+2} to Zn) zinc ammonium sulfate solutions, in which the platinum cathode and anode are separated by a porcelain cup, followed by evaporation in a carbon dioxide atmosphere yielded opaque lavender-

*$ZnSO_4 \cdot 7H_2O$—Mallinckrodt, Analytical Reagent; $(NH_4)_2SO_4$—Allied Chemical, Reagent; $VO_2O_4 \cdot 2H_2O$—Fisher, Purified; $MgSO_4$—Allied Chemical, Reagent; and K_2SO_4—Mallinckrodt, Analytical Reagent.

**Activation analysis of the 0.5% VO^{+2} Tutton salt showed a concentration of 0.004% V/Zn. This analysis was performed by Mr. H. Nass of the Radiation Chemistry Group under the supervision of Prof. W. W. Meinke of the Chemistry Department of The University of Michigan.

***The D_2O was obtained from Norsk Hydro (Norway) and is 99.78% pure.

colored crystals 2-3 mm long in 3-4 days.

B. CRYSTAL STRUCTURE AND ORIENTATION

Figure 4 shows the unit cell of a typical Tutton salt. The location of the atoms on the unit cell is taken from the X-ray data listed in Wyckoff,[44] who lists the space group of these double sulfates as $C_{2h}^5 P2_1a$. In this crystal there are two molecules per unit cell and the water molecules surrounding the (0, 1/2, 1/2) position are derived from the (0,0,0) position by a translation to (0,1/2,1/2) followed by a reflection in the ac plane. Although the several views of the octahedron in Fig. 4 show a large deviation from cubic and tetragonal symmetry, suggesting that any EPR results from paramagnetic ions placed in the divalent site will need to be fitted with the rhombic spin Hamiltonian, Wyckoff[44] remarks that because of the closeness of several of the atoms certain distances can only be taken as approximate. Yet EPR results do indicate considerable rhombic symmetry (see Bleaney, Ingram and Scovil[16] as well as the results obtained in Chapter V of this investigation).

As shown in Fig. 5, these double sulfates or Tutton salts grow with well-recognized faces (Tutton[45]), so that orientation of the crystal becomes a task accomplished with relative ease. Figure 5 also shows the two devices for orienting the crystal with respect to the magnetic field. The one device positions a 22-in., 0.25-in.-diam, 0.025-in.-wall quartz rod to the crystal so that when the rod is vertical the desired orientation is in the horizontal plane—the plane of rotation of the magnet.

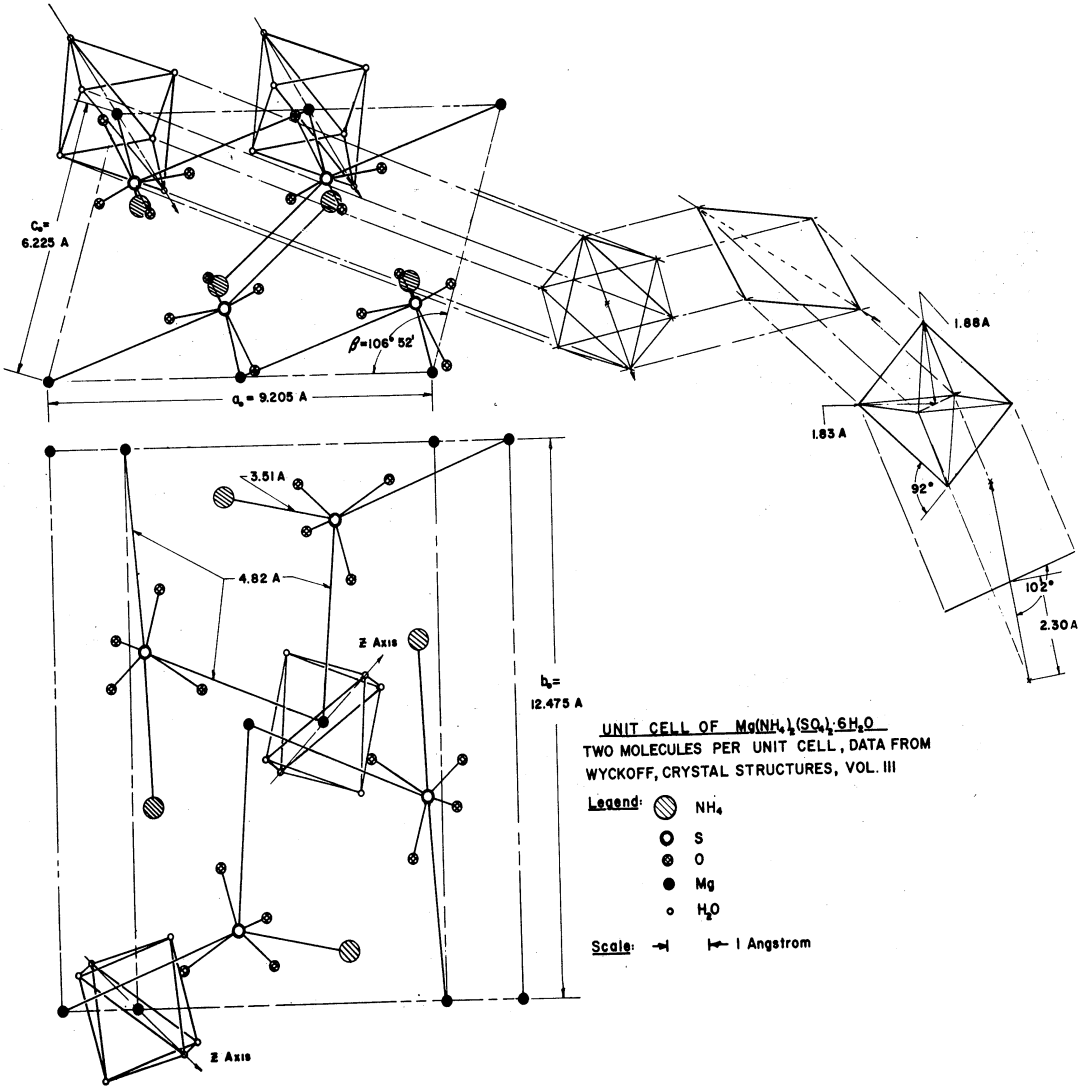

Fig. 4. Unit cell of $Zn(NH_4)_2(SO_4)_2 \cdot 6H_2O$.

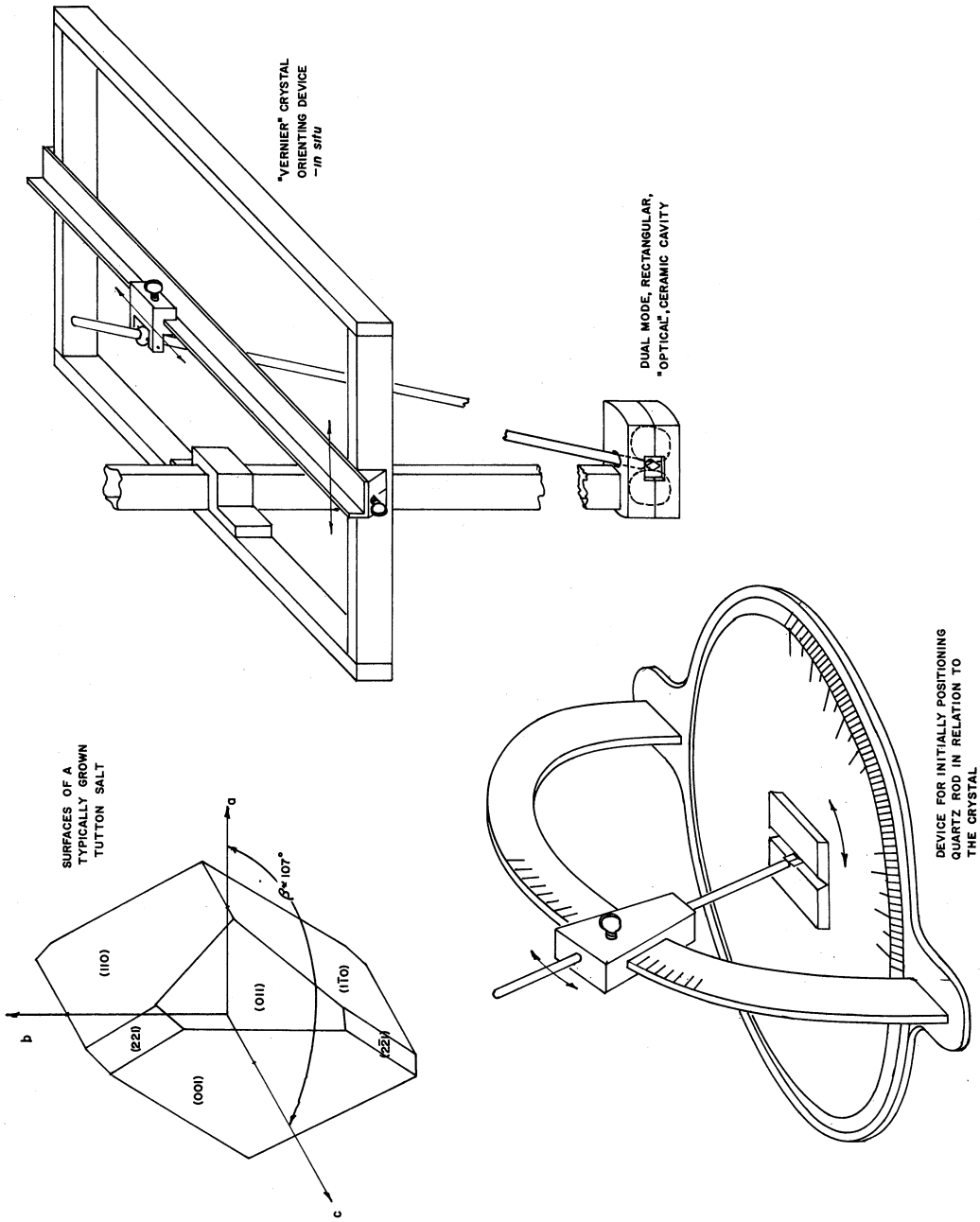

Fig. 5. Faces of Tutton salt, crystal orienting devices.

The position of the crystal is fixed in this device by the grooves that are machined at the same angle as the crystal growth faces. The crystal is attached to the quartz rod with Goodyear Pliobond cement.

After placing the crystal, now fastened at the end of the quartz rod, in the cavity and the other end of the quartz rod in the second orienting device, one makes the final adjustments of the crystal's orientation with respect to the magnetic field by moving the quartz rod in either of the directions indicated in Fig. 5 until the desired EPR spectrum is displayed on the recorder.

C. EPR EXPERIMENTAL ARRANGEMENT

EPR spectra were obtained with a Varian V-4500 EPR Spectrometer, Varian V-4560 100-kc Field Modulation Unit and a Varian 4012-35 12-in. rotating electromagnet. The schematic diagram of the spectrometer system is shown in Fig. 6.

X-Band System. For the VO^{+2} crystal measurements a Varian V-153/6315 Klystron operating at approximately 9.3 kmc was coupled to a dual mode (TE_{011}) rectangular ceramic cavity internally coated with a themosetting silver paint (Hanovia 32A). The thin silvered walls of the cavity allows 100-kc modulation of the magnetic field at the sample crystal. Measurement of the klystron frequency was accomplished by means of tapping a small amount of power from the microwave circuit via a coaxial cable adapter to a Berkeley 7580 Transfer Oscillator and a Berkeley 7370 Universal EPUT and Timer. Such a measurement system is

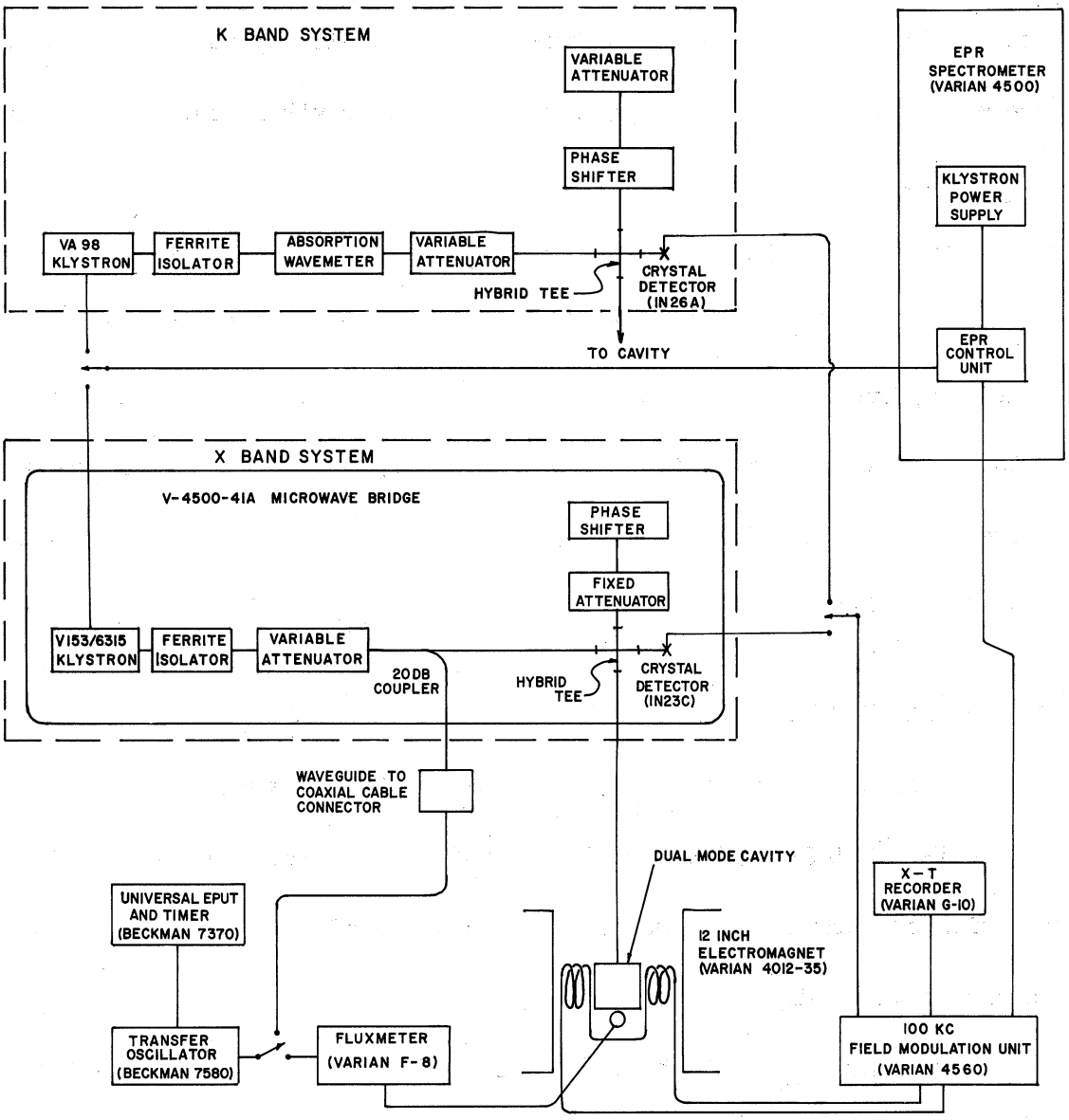

Fig. 6. Schematic diagram of EPR spectrometer system.

accurate to one part in 10^6. The system was operated at room temperature with a magnet gap of 3.25 in.

K-Band System. The V^{+2} and the irradiated VO^{+2} crystals require the use of a higher frequency klystron since the zero field splitting of V^{+2} in the Tutton salts is of the approximate value as the X-band frequency (see Lambe and Kikuchi[23]). A Varian VA-98 Klystron operating at approximately 24-kmc was employed with a 2.0-in. magnet gap. The cavity for these measurements was a dual mode (TE_{011}) cylindrical ceramic cavity. The klystron frequency was measured with a Hewlett-Packard K-532A absorption type wavemeter having a least count of 0.010 kmc and a resettability of 0.002 kmc.

Magnetic Field Measurements. Magnetic field measurements of the individual resonances were made with a Varian Model F-8 Fluxmeter connected to the Berkeley 7580 Transfer Oscillator and the 7380 Universal EPUT and Timer. For magnetic field intensities below 8000 gauss measurement of the proton magnetic resonance frequency is used (42.5776 mc at 10 kilogauss). For higher fields corresponding to the V^{+2} measurements at K-band frequencies the resonant frequency of the deuteron is used, resulting in a slight lowering of the accuracy of the magnetic field (6.536 mc at 10 kilogauss). Measurement of the magnetic field was made directly beneath the cavity, resulting in only a -0.1 and +0.4 gauss difference between the magnetic field intensity at the position of measurement and the position of the sample for 3300 gauss (3.25-in. gap) and 8600 gauss (2.0-in. gap), respectively. For the measurements on the crystals con-

taining D_2O this value was-0.77 gauss.

C Axis Position. For the Tutton salts the relation between the magnetic axes and the crystalline axes was obtained by measuring the angle of the c axis to the zy-plane of the V^{+2} spectrum or the c axis and the K_1K_3 plane of the VO^{+2} spectrum. The measurement was made with a short focal length transit. With the crystal mounted so that the zy-plane was horizontal, as recognized by the EPR spectrum on the recorder, the optical axis of the transit could be aligned along the c axis of the crystal since an intersection of two of the growth planes of the crystal lay parallel to the c axis (Fig. 5). Of course, the length of the intersection of the two planes determines the accuracy with which the angle can be measured, but for a 4-mm length of intersection of the crystal growth planes such a measurement could be made to within ±0.3°.

X-Ray Irradiations. X-ray irradiations of the VO^{+2} crystals were made in the shite beam from a tungsten-target, Machlett AEG-50S tube operated at 50 KVP—40 ma. Using cerrous-cerric dosimetry after Weiss[46] we estimated the dose rate to the crystals to be 7×10^6 rad/min (Appendix A). Although Weiss[46] found the cerrous-cerric yield to be independent of energy from 100 KV X-rays to 2 Mev gamma rays and independent of dose rate from 1/2 Roentgen/sec to 500 Roentgen/sec, and although the above measurement falls out of both ranges, the Machlett tube sheet claims that emission may be more than 2×10^6 Roentgen/min under certain conditions so that the experimental value seems approximately correct.*

*The energy absorbed by the crystal appears to be greater than the tube emission as a result of the higher absorption coefficient of the crystal compared to that of air.

CHAPTER IV

THE HAMILTONIAN

For electron paramagnetic resonance phenomena almost all of the experimental results can be described by a phenomenological Hamiltonian called the "spin Hamiltonian."*

While the spin Hamiltonian is truly phenomenological in that one can postulate it on the basis of symmetry, we shall give an account of the "derivation" as usually seen in the literature. We consider the ion imbedded in a crystalline field produced by the charges or dipoles from the surrounding ligands** and enumerate the interaction terms of the n electron ion in a crystalline electric field subject to an external magnetic field;

	Interaction Energy
$W_c = \sum_{k=1}^{n} \left(\frac{P_k}{2m} - \frac{Ze^2}{r_k} \right) + \sum_{k>j}^{n} \frac{e^2}{r_{kj}}$	$\sim 10^5$/cm
$W_{s.o.} = \sum_{j,k} \left(a_{jk} \underline{\ell}_j \cdot \underline{S}_k + b_{jk} \underline{\ell}_j \cdot \underline{\ell}_k + c_{jk} \underline{S}_j \cdot \underline{S}_k \right)$	$\sim 10^2$/cm (iron group)
$= \lambda \underline{L} \cdot \underline{S}$ (Russell-Saunders coupling)	$\sim 10^3$/cm (rare earth)
$W_{ss} = \sum_{j,k} \left[\frac{\underline{S}_j \cdot \underline{S}_k}{r_{jk}^3} - \frac{3 (\underline{r}_{jk} \cdot \underline{S}_j)(\underline{r}_{jk} \cdot \underline{S}_k)}{r_{jk}^5} \right]$	~ 1/cm

*See Pryce[47] and Abragam and Pryce.[48]

**Recently Lacroix and Emch[49] have generalized the spin Hamiltonian to include the effects of covalent bonding.

Interaction Energy

$$W_N = 2\gamma\beta\beta_N\left[\sum_k\left\{\frac{(\underline{l}_k-\underline{s}_k)\cdot\underline{I}}{r_k^3}+\frac{3(\underline{r}_k\cdot\underline{s}_k)(\underline{r}_k\cdot\underline{I})}{r_k^5}\right\}+\frac{8\pi}{3}\delta(r_k)(\underline{s}_k\cdot\underline{I})\right] \sim 10^{-2}/\text{cm}$$

$$W_Q = \frac{e^2Q}{2I(I+1)}\left[\sum_k\frac{I(I+1)}{r_k^3}-\frac{3(\underline{r}_k\cdot\underline{I})^2}{r_k^5}\right] \sim 10^{-3}/\text{cm}$$

$$W_{mf} = \beta\underline{H}\cdot[\underline{L}+2\underline{S}]+\underline{H}\cdot\underline{\underline{g}}_N\cdot\underline{I}$$

$$W_{cf} = \sum_k^n V_k \quad \text{(crystal field)}$$

The energy of the crystalline field can be noted experimentally to fall into three classifications.

(1) Strong fields ($\sim 10^4$/cm) where there is considerable covalent bonding. Then

$$\sum_{k>f}^n\frac{e^2}{r_{kf}} < W_{cf} < \sum_k^n\frac{ze^2}{r_k}$$

(2) Medium fields ($\sim 10^3$/cm) as in most ions in the iron series and in this work. Then

$$W_{so} < W_{cf} < \sum_k^n\frac{e^2}{r_{kf}}$$

(3) Weak fields ($\sim 10^2$/cm) as in most complexes with the rare earth elements. Then

$$W_{cf} < W_{so}$$

The reason for making the distinction is that our perturbation treatment of the crystalline field on the ion depends on where, in terms of interaction energy, W_{cf} falls in the series of $\mathcal{H} = W_c+W_{so}+W_{ss}+W_n+W_q$.

Since the crystalline field in these experiments falls into classifi-

cation (2), we assume the single electron approximation. That is, the ion is constructed of single electron orbitals such as $(1s)^2(2s)^2(2p)^6(3s)^2(3p)^6(3d)$, which are solutions of the hydrogen-like Hamilton, $P^2/2m-Ze^2/r$. For the closed argon shell, $[A] = (1s)^2(2s)^2(2p)^6(3s)^2(3p)^6$, we note that the mutual repulsion term $\sum_{k>j}^{n} \frac{e^2}{r_{kj}}$ merely adds to the total energy of the shell. However, in our paramagnetic ion with the unpaired 3d electrons this term gives rise to certain configurations of the 3d electrons that are lower in energy than others. Since we need to know the ground state of the "free ion" in our crystalline field one assumes Russell-Saunders coupling of the 3d electrons and constructs antisymmetrized wave functions Ψ to calculate matrix elements of the type $\langle \Psi | W_{cf} | \Psi \rangle$ so that the configurational energy can be computed. The result is a confirmation of Hund's Rule that the ground state has (1) maximum spin multiplicity and (2) maximum orbital degeneracy consistent with maximum spin multiplicity. Thus for $3d^1$, $3d^2$, and $3d^3$ electrons the ground states are ^2D, ^3F, and ^4F.

A. THE CRYSTALLINE FIELD

In order to calculate the splitting of the ground state due to the crystalline field, which is assumed to satisfy Laplace's equation $\nabla^2 V = 0$, we expand V_K in a series of normalized spherical harmonics

$$V_k = \sum_{\ell=0}^{\infty} \sum_{m=-\ell}^{\ell} Y_\ell^m(\theta_k, \varphi_k) A_\ell^m r^\ell$$

and procede to calculate the one electron matrix element for the 3d elec-

trons (Appendix B). We note that (a) if inversion symmetry exists about the paramagnetic ion, all odd terms disappear since V_K must have even parity and Y_ℓ^m has parity $(-)^\ell$, and (b) no terms exist for $\ell > 4$ for 3d electrons since the direct product of two d orbitals span no representation higher than $\ell = 4$.

Also, since V_K must conform to the symmetry of the ligands producing V_K, other terms may be zero. Thus we obtain for cubic fields,

$$V_K = A_4^0 r^4 \left[Y_4^0 + \left(\frac{5}{14}\right)^{1/2} \left(Y_4^4 + Y_4^{-4} \right) \right] + A_0^0$$

or,

$$V_K = A_4^0 \frac{15}{4} \pi^{-\frac{1}{2}} \left[x^4 + y^4 + z^4 - \frac{3}{5} r^4 \right] + A_0^0$$

Calculation of the matrix elements for this cubic field for the ground states ^2D, ^3F, and ^4F results in the splittings shown below where the numbers in parenthesis indicate the orbital dengeneracy and the letters E_g, T_g, and A_g refer to the symmetry of the state wave function. The energy level separation parameter Dq is defined as $Dq = \frac{1}{6} \frac{Q}{a_1^5} \overline{r^4}$ where Q is the charge on the ligand and $\overline{r^4}$ is averaged over the 3d radial function.

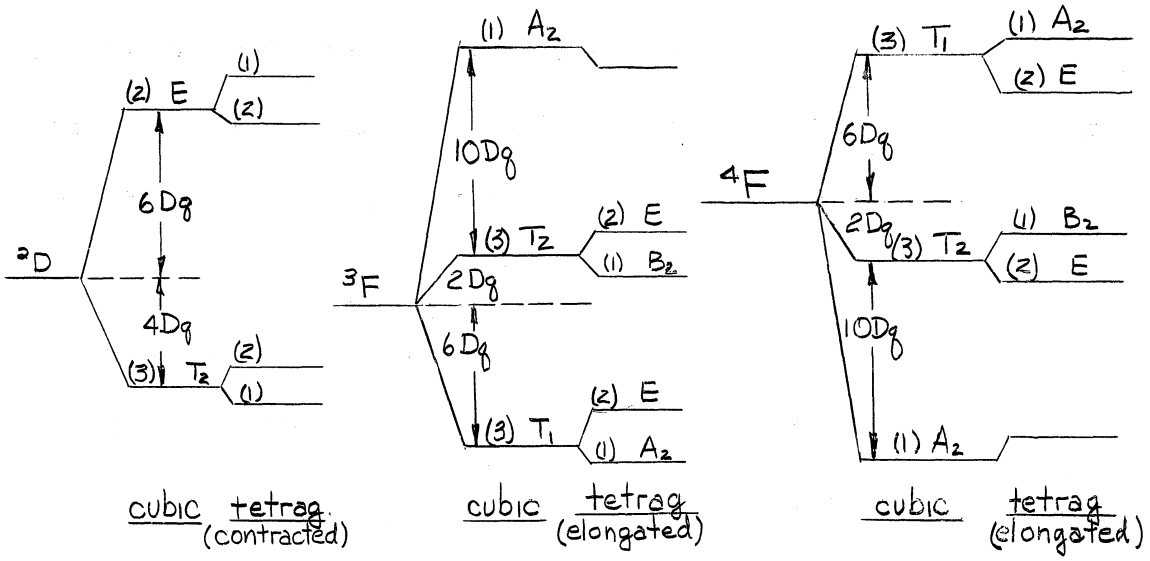

If there is an elongation (contraction) of the charges along the z direction then there is a lowering of the symmetry from O_h(cubic) to D_{4h}(tetragonal). The crystalline field then contains the additional terms $B_2r^2Y_2^0+B_4r^4Y_4^0$ and the degenerate levels split as shown above or in Figs. 1 and 2.

In calculating fields of lower symmetry (rhombic) Ballhausen (Ref. 13, p. 108) points out that it may be necessary to include other terms in the Hamiltonian such as spin orbit coupling or dynamical effects (Jahn-Teller) rather than augmenting the crystalline field potential with a rhombic field component. The important feature one should notice is that the lower symmetry reduces the degeneracy of the ground state to an orbital singlet. In fact, a theorem by Jahn and Teller[50] states that a molecule having orbital degeneracy always distorts to remove the degeneracy. The exceptions are linear molecules and Kramers degeneracy.*

*Kramers theorem states that a system containing an odd number of electrons will have even degeneracy if placed in an external electric field.[51]

B. THE SPIN HAMILTONIAN

The terms in $\mathcal{H}'' = W_{so}+W_n+W_q+W_{mf}$ which are left from the original Hamiltonian are now treated as a perturbation to the system. But instead of calculating the change in energy directly with this perturbation Hamiltonian $\mathcal{H}''$, we use the operator equivalent method of Stevens[52] to obtain a transformed Hamiltonian valid for constant L and constant S. This method consists of replacing the individual electron spin variables, which transform like the components of a vector, by the components of the total spin operator $\underline{S}$ and replacing the position coordinates, which transform like second order spherical harmonics, by the components of $\underline{L}$. This is valid providing that we remain within a manifold of constant L and constant S. With this transformed Hamiltonian the change in energy of the orbital singlet ground state is calculated to second order using only the orbital part of the wave function—now in the L,S representation. The result is the elimination of the orbital operator leaving a Hamiltonian with only spin operators—the spin Hamiltonian.

$$\mathcal{H}_{spin} = \beta \underline{H}\cdot\underline{\underline{g}}\cdot\underline{S} + \underline{S}\cdot\underline{\underline{D}}\cdot\underline{S} + \underline{I}\cdot\underline{\underline{A}}\cdot\underline{S} + \underline{I}\cdot\underline{\underline{Q}}\cdot\underline{I} - \beta_N \underline{H}\cdot\underline{\underline{g}}_N\cdot\underline{I}$$

The first term contains the spectroscopic splitting factor g and differs from 2.0023 as a result of admixing from higher states. D is a measure of the splitting of the ground state in a noncubic field and gives rise to the fine structure, while the third term containing A expresses the hyperfine interaction. The fourth and fifth terms express to first order the quadrupole interaction and the interaction of the magnetic

field with the nuclear moment, respectively. A constant factor has been dropped since it shifts all levels equally.

Since the spin Hamiltonian must conform to the symmetry of the ion in the crystal we note that for axial, cubic, and rhombic symmetry surrounding the paramagnetic ion and providing the principal axes of each of the tensors coincide, we obtain the following spin Hamiltonians for cubic, axial and rhombic environments.

$$\mathcal{H}_{cubic} = g\beta \underline{H}\cdot\underline{S} + A\underline{I}\cdot\underline{S} - g_N\beta_N \underline{H}\cdot\underline{I}$$

$$\mathcal{H}_{axial} = \beta[g_z H_z S_z + g_\perp(H_x S_x + H_y S_y)] + D[S_z^2 - \tfrac{1}{3}S(S+1)] + A I_z S_z$$
$$+ B[S_x I_x + S_y I_y] + Q'[I_z^2 - \tfrac{1}{3}I(I+1)] - \beta_N[g_{N\parallel} H_z I_z + g_{N\perp}(H_x I_x + H_y I_y)]$$

$$\mathcal{H}_{rhombic} = \beta[g_z H_z I_z + g_x H_x I_x + g_y H_y I_y] + D[S_z^2 - \tfrac{1}{3}S(S+1)] + E(S_x^2 - S_y^2)$$
$$+ A I_z S_z + B_x I_x S_x + B_y I_y S_y + Q'[I_z^2 - \tfrac{1}{3}I(I+1)] + Q''[I_x^2 - I_y^2]$$
$$- \beta_N[g_{Nz} H_z I_z + g_{Nx} H_x I_x + g_{Ny} H_y I_y]$$

In general the principal axes of the tensors may not coincide in which case cross terms may appear. For the example of the g and A tensors not having the same principal axes, additional hyperfine terms of the type $\sum_{ij}{}' F_{ij}(S_i I_j + I_i S_j)$ may appear.

The spin Hamiltonian is truly phenomenological in the sense that we could have postulated it from a posteriori arguments on the type of interactions and the symmetry of the environment. In fact for electronic spins higher than 3/2 such as Mn^{+2} (S = 5/2) in cubic environments, one

must include a term quartic in spins (i.e., $a(S_x^4+S_y^4+S_z^4)$. Although higher order terms may also be allowed it can be shown that any monomial in J_x, J_y, and J_z of order more than 2J can be reduced to a linear combination of monomials of order less than or equal to 2J.

Koster and Staatz[53,54] have obtained a more general Hamiltonian that is less restrictive than the spin Hamiltonian. However, the number of constants in their Hamiltonian requires data to be obtained at high and low magnetic fields for a proper evaluation of the constants. Also the difficulty of application of this Hamiltonian increases as the symmetry surrounding the paramagnetic ion decreases.

Because of this difficulty in using the Koster-Staatz Hamiltonion and that of relating the results of this work to that of other investigations, we chose the spin Hamiltonian as the method of evaluating the experimental data. The derivation of the angular variation of the energy levels from the rhombic spin Hamiltonian is done in Appendix C and an "exact" calculation of the fine structure energy level separation for the magnetic field parallel to the x, y, and z axes is carried out in Appendix D. Also, the angular variation of the energy levels for the g and A tensor not coinciding is calculated in Appendices E and F. Finally, Appendices G and H list the equations that were used to reduce the data.

CHAPTER V

EXPERIMENTAL RESULTS

A. VO^{+2}

From the EPR measurements at X-band frequencies of the VO^{+2} ion in $Zn(NH_4)_2(SO_4)_2 \cdot 6H_2O$ crystals, the room temperature rhombic spin Hamiltonian constants with noncoinciding principal axes of the g and A tensor listed in Table 1 were calculated for the three observable locations of the two sites in the unit cell.*

TABLE 1

EXPERIMENTAL RESULTS FOR VO^{+2}

Location 1**	Location 2	Location 3
g_z = 1.9331±2	1.9316±3	1.9299±4
g_x = 1.9813±2	1.9808±4	
g_y = 1.9801±2	1.9797±4	1.9811±10
A = 0.018281±5/cm	0.018275±5/cm	0.018441±10/cm
B_x = 0.007137±4/cm	0.007104±4/cm	0.007250±10/cm
B_y = 0.007256±4/cm	0.007255±4/cm	
A_{xy} = -0.0000462±2/cm		
|Q'| = 0.00024±2/cm	0.00024±5/cm	
Line width (H_2O) 5.0±0.4 gauss	5.0±0.4 gauss	5.0±0.4 gauss
Line width (D_2O) 2.4±0.2 gauss		
Relative intensity 40±10	10±2	2±1

*The errors associated with each of the numbers in the table is the experimental error.

**For this location the constants are listed for the crystals containing D_2O. With the exceptions of reduction of line width and the altering of superhyperfine structure, the presence of D_2O or H_2O produces no detectable difference on the spin Hamiltonian constants.

Figure 7 shows the positions in the crystal of the z axes of the rhombic spin Hamiltonian for the above locations. The positions are referred to the three mutually perpendicular magnetic susceptibility axes, K_1, K_2, and K_3. The K_3 axis coincides with the b axis of the crystal and the other two axes lie in the ac plane. Experimentally, these three axes show the positions of the magnetic field where the spectra from the four most populous sites coincide. These positions can be located with respect to each other within ±0.3°.

B. DISCUSSION OF VO^{+2} RESULTS

Comparison of Spin Hamiltonian Constants. As mentioned in Chapter I, the published spin Hamiltonian constants of the vanadyl ion have been obtained from randomly oriented samples and that this was one reason for attempting single crystal measurements on this ion. The following will show how one can obtain the axial spin Hamiltonian parameters from a powdered spectrum before comparing the constants found in this investigation to that published in the literature.

Since the spin Hamiltonian for VO^{+2} in $Zn(NH_4)_2(SO_4)_2 \cdot 6H_2O$ shows almost axial symmetry, the EPR spectrum of a random orientation of VO^{+2} ions should be able to be explained quite easily from the single crystal spin Hamiltonian constants. With the assumption of axial symmetry we see that for a given magnetic field only those crystals or crystallites whose V-O axes are at an angle θ to the magnetic field are contributing to the resonance—where θ is related to the magnetic field by

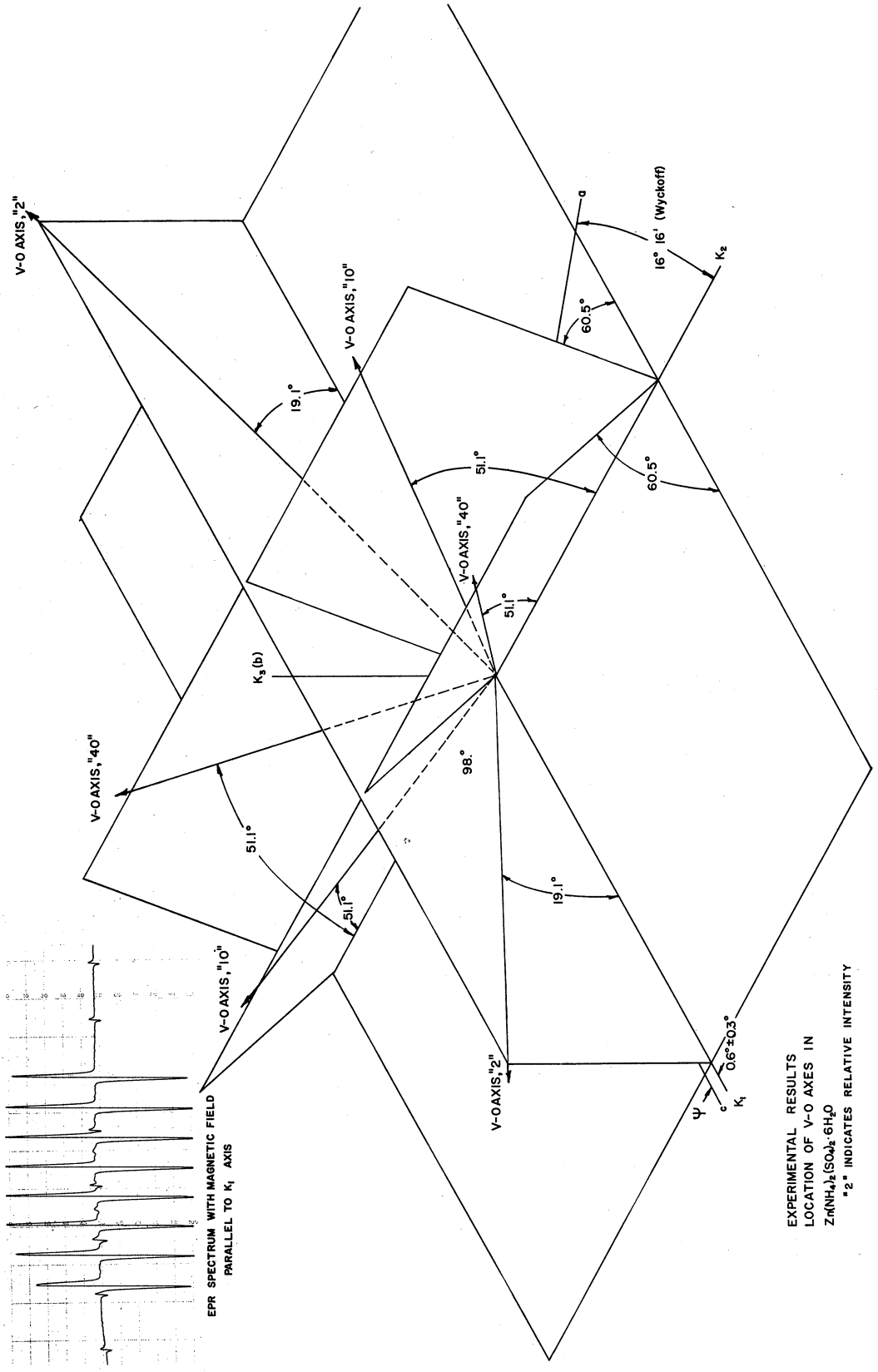

Fig. 7. Position of VO^{+2} axes in $Zn(NH_4)_2(SO_4)_2 \cdot 6H_2O$.

$$H_m(\theta) = \frac{h\nu}{g\beta} - \frac{K}{g\beta} m - \frac{B^2}{4h\nu}\left[1+\left(\frac{A}{K}\right)^2\right]\left[I(I+1)-m^2\right]$$
$$- \frac{g_z^2 g_\perp^2}{g^4}\left[\frac{A^2-B^2}{K}\right]^2 \frac{m^2}{2h\nu}\sin^2\theta\cos^2\theta$$
$$+ 2\frac{(Q')^2 A^2 B^2 g_z^2 g_\perp^2}{K^5 g^5 \beta} m\left[4I(I+1)-8m^2-1\right]\sin^2\theta\cos^2\theta$$
$$- \frac{(Q')^2 B^4 g_\perp^4}{2K^7 g^5 \beta} m\left[2I(I+1)-2m^2-1\right]$$

and where

$$K^2 g^2 = g_z^2 A^2 \cos^2\theta + g_\perp^2 B^2 \sin^2\theta \quad \text{and} \quad g^2 = g_z^2\cos^2\theta + g_\perp^2 \sin^2\theta$$

The number of VO^{+2} axes at this angle is proportional to $\frac{1}{2}\sin\theta\, d\theta$, which is just the probability that a VO^{+2} axis lies at an angle θ to the magnetic field. Thus, the number of VO^{+2} ions contributing to paramagnetic resonance between magnetic field H and H+dH is proportional to

$$\sum_{m=-7/2}^{7/2} \sin\theta \frac{d\theta}{dH_m(\theta)}$$

Figure 8 shows the plot of such an equation evaluated for the single crystal spin Hamiltionian parameters listed in Table 1. Note that the experimental curve in this figure is the first derivative of absorption showing the effect of the finite width of the resonances. The sharp peak-

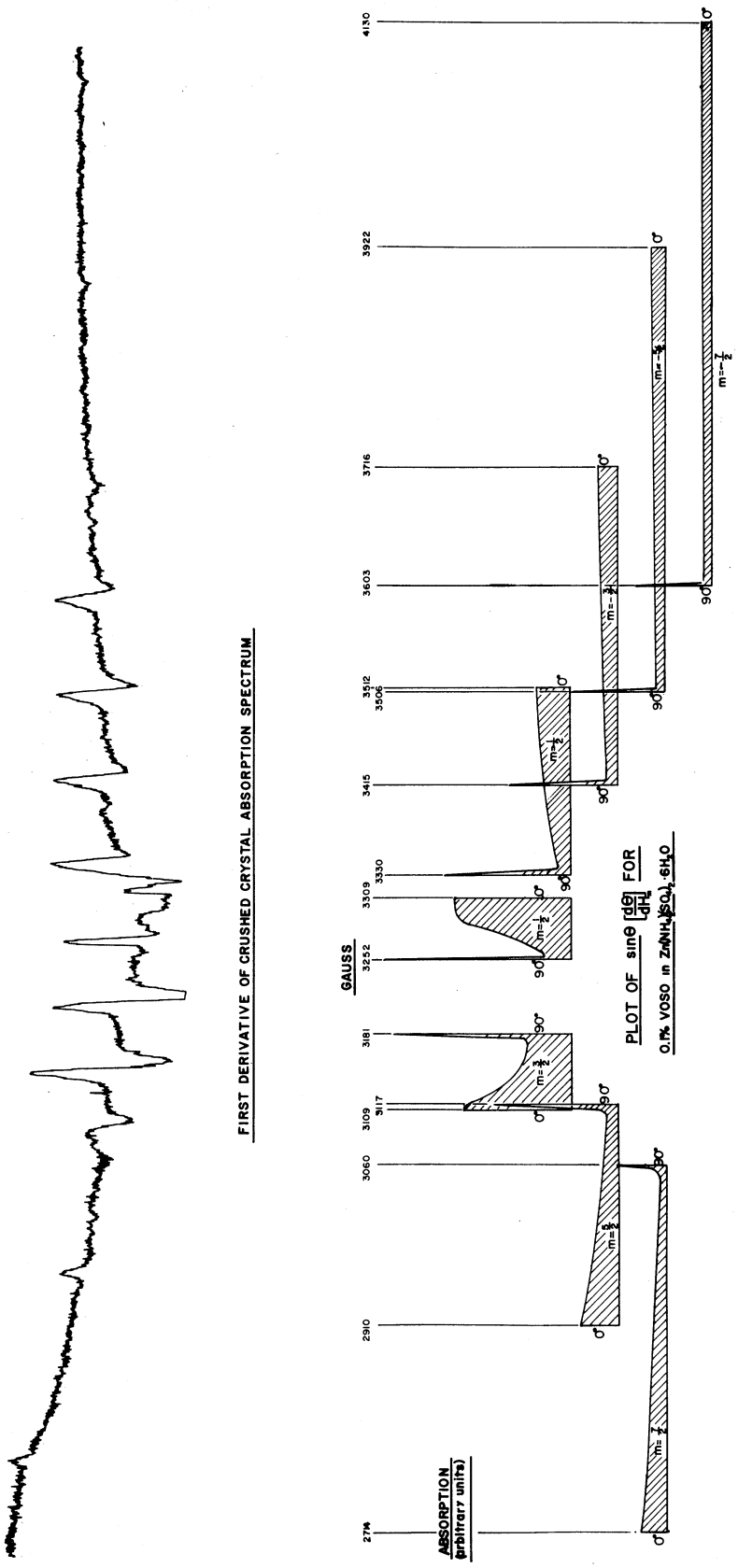

Fig. 8. $\sum_{\pi} \sin\theta \, (d\theta/dH_m)$ curve and VO^{+2} powder spectrum.

ing at the 90° end of the curves is a result of a $[\cos \theta]^{-1}$ dependence of the equation. This can be interpreted as saying that, since there is axial symmetry, more V-O axes are oriented at 90° to the magnetic field than at 0°.

In the powder spectrum the separation of the two extreme peaks corresponds to $7A/g_z\beta$, and if one neglects the quadrupole contribution the separation of the two extreme lines in the central part of the spectrum (if they are distinguishable) is $7\beta/g_\perp\beta$. Thus, if in addition to measuring the frequency of the microwave source, one measures the magnetic field at these four locations, the spin Hamiltonian constants g_z, $g_\perp$, A, and B can be calculated to the accuracy limited by the width of the peaks and the ability to pick out the significant lines in the central part of the spectrum.

Figure 9 compares the spectrum of the crushed VO^{+2} Tutton crystal to that of vanadyl ions adsorbed on IR-4B and V_2O_5 dissolved in glass.* The latter spectrum shows that vanadium in $Na_2O \cdot 3SiO_2$ glass, melted under either oxidizing or reducing conditions, is present as VO^{+2}. The larger width of the peaks in the glass and resin spectra, as contrasted to the sharpness of the peaks in the crushed crystal spectrum, reflects the nonuniformities in the crystalline field from ion to ion.

Table 2 compares the literature values of the axial spin Hamiltonian constants to those found in this investigation.

---

*The glass samples were supplied by Dr. W. Nelson, Owens-Illinois, Toledo, Ohio.

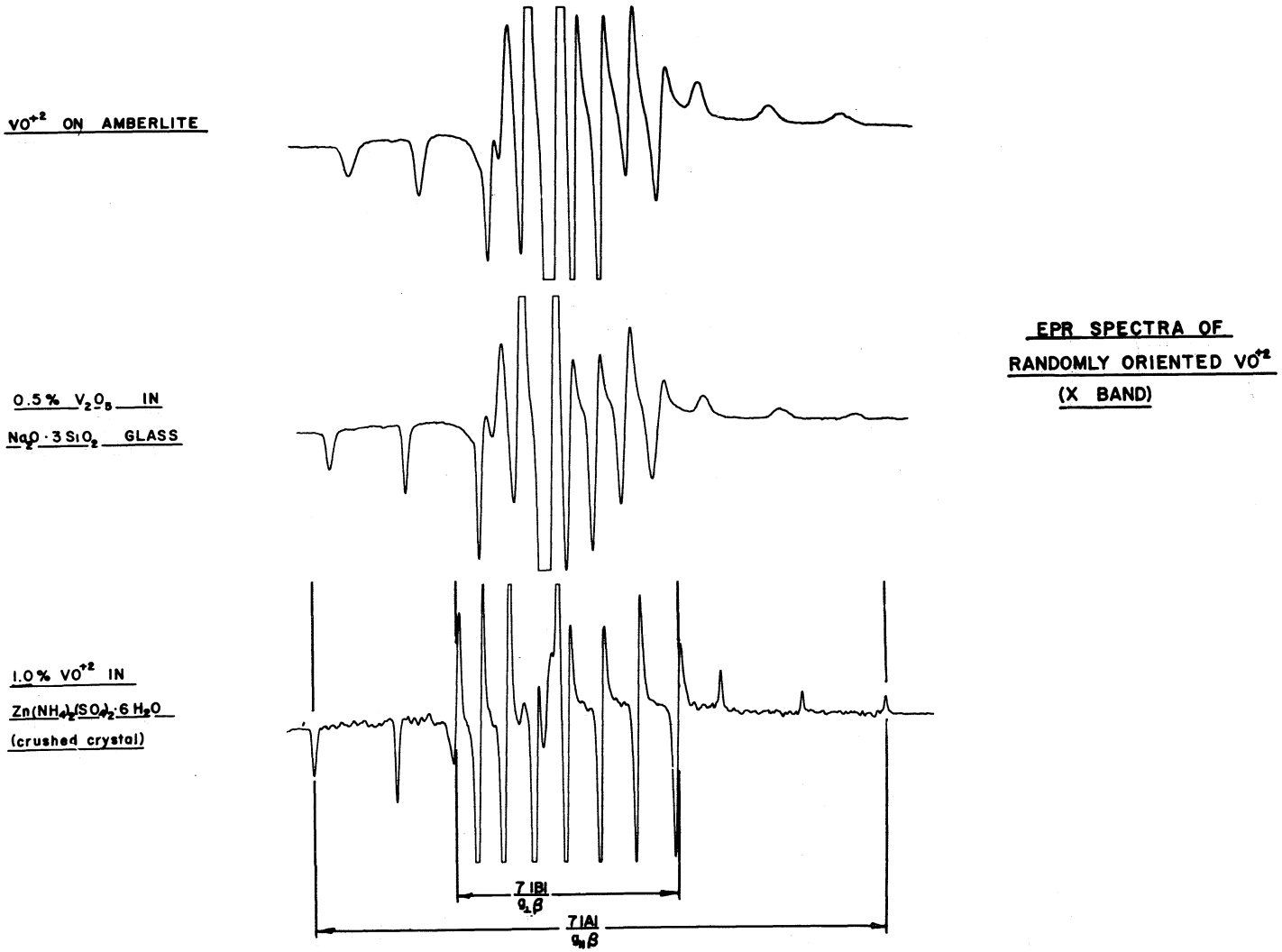

Fig. 9. VO^{+2} in glass, IR-4B, and crushed crystals.

TABLE 2

LITERATURE VALUES OF VO^{+2} SPIN HAMILTONIAN CONSTANTS

	g_z	$g_\perp$	$\|A\| \times 10^2$/cm	$\|B\| \times 10^2$/cm	Material
Present work	1.9331	1.9805	1.828	0.7137	Tutton salt
Faber et al.[33]	1.93	1.983	1.80	0.750	IR-100
	1.88	1.979	1.84	0.740	Dowex-50
	1.983			0.704	Charcoal
	1.93	1.989	1.58	0.612	IR-4B
Roberts et al.[34]	1.947	1.988	1.58	0.54	Vanadyl porphyrins
O'Reilly[32]	1.948	1.987	1.59	0.52	VEP I
Kozyrev[29]	1.92	1.96	1.78	0.7	Frozen solution
Gager[42]	1.950	1.995	1.80	0.75	Tutton salt

Fit To Spin Hamiltonian. That the rhombic spin Hamiltonian with noncoinciding principal axes of the g and A tensors is a good description of the EPR spectra of the vanadyl ion in $Zn(NH_4)_2(SO_4)_2 \cdot 6H_2O$ is illustrated in Fig. 10. The curves in this figure are predicted from the spin Hamiltonian with the values listed in Column 1, Table 1, and the circles represent the experimental values of the magnetic field. The crystal for these measurements was grown from heavy water, reducing the line width of the resonances and enabling one to make more accurate measurements of the magnetic field.*

Noncoinciding Principal Axes of the g and A Tensors. One of the unusual results of this set of experiments is that the x and y principal axes of the g and A tensors do not coincide but in fact are separated by 23°20'.

If one uses the first order expression for the magnetic field in the xy plane

* of spin systems a reduction of 2 in the line width increases the slope of the derivative curve at x = 0 by a factor of $4\sqrt{2}$, increasing the accuracy with which one can measure the magnetic field at resonance. Since the magnetic moments of the surrounding nuclei produce inhomogeneities in the magnetic field at the paramagnetic ion and the deuteron has a magnetic moment less than one-third that of the proton, the line width of the resonances can be reduced by growing the crystals with heavy water. Experimentally the width is found to be reduced by a factor of 2.

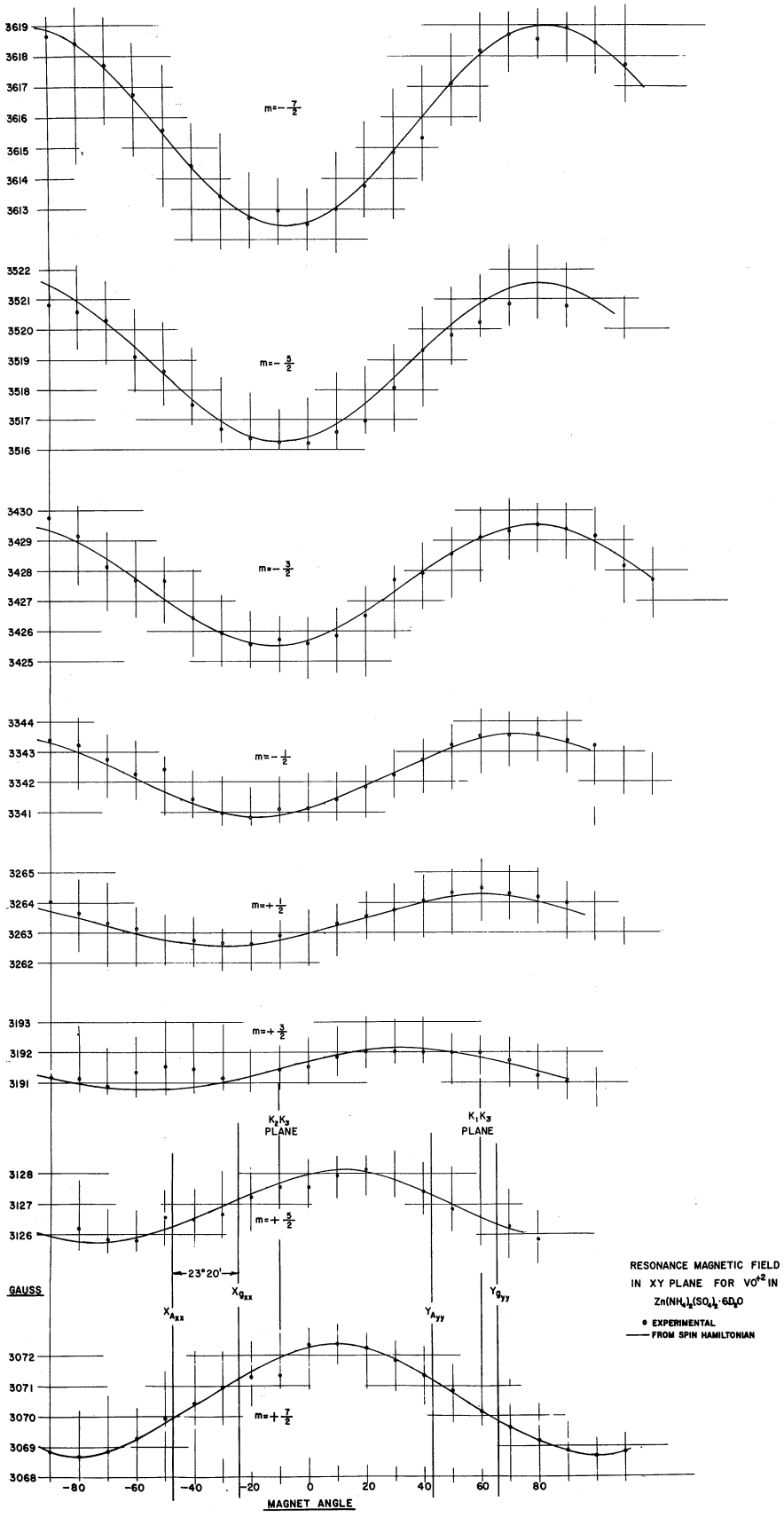

Fig. 10. X-Y plane phase shift.

$$\left[H_m(\delta)\right]_{\substack{\text{first}\\ \text{order}}} = \frac{h\nu}{g_\perp \beta} - \frac{m}{g_\perp \beta}\left[\frac{B_x+B_y}{2} + \frac{B_x-B_y}{2}\frac{(g_x^2\cos^2\delta - g_y^2\sin^2\delta)}{g_\perp^2} + 2\mathcal{A}_{xy}\frac{g_x g_y}{g_\perp^2}\sin\delta\cos\delta\right]$$

where

$$\mathcal{A}_{xy} \equiv F_{xy} + F_{yx} \quad \text{and} \quad g_\perp^2 \equiv g_x^2\cos^2\delta + g_y^2\sin^2\delta$$

and δ is the angle between the magnetic field and the x axis, as the major contribution to the angular variation of the magnetic field, then it can be easily shown that the maxima and minima of the resonance magnetic field occurs when

$$\tan 2\delta = \frac{2\mathcal{A}_{xy} g_x g_y}{(B_x-B_y)(g_x^2+g_y^2) + \frac{1}{m}\frac{h\nu}{g_\perp \beta}(g_y^2-g_x^2)}$$

$$\simeq \frac{1}{1+\frac{2}{m}}$$

for this experiment.*

From this result one notices that if the principal axes of the two tensors coincide then $\mathcal{A}_{xy} = 0$ and the maxima and minima occur at $\delta = 0$ and 90° for all values of m. This is the usual result encountered in EPR experiments.

If one assumes that the z axes of the g and A tensors coincide but the x axes do not, then it can be shown (Appendix E) that the principal values of the hyperfine tensor, A_{xx} and A_{yy} are related to $\mathcal{A}_{xy}$, B_x, and B_y by the following expressions

*Second order terms such as $(B_x-B_y)(g_y^2-g_x^2)$ are ignored.

$$B_x = A_{xx}\cos^2\theta + A_{yy}\sin^2\theta$$

$$B_y = A_{xx}\sin^2\theta + A_{yy}\cos^2\theta$$

$$\mathcal{H}_{xy} = (A_{yy} - A_{xx})\sin\theta\cos\theta$$

where θ is the angle between the x axes of the g and A tensor. Using the experimental values for $\mathcal{H}_{xy}$, B_x, and B_y listed in Table 1, the principal axes values of the A tensor are found to be

$$A_{xx} = 0.0071200/cm \quad (B_x = 0.0071367/cm)$$

$$A_{yy} = 0.0072439/cm \quad (B_y = 0.0072564/cm)$$

and the angle between the x axes of the two tensors to be, θ = -23.3 °.

The assumption that the z axes of the two tensors coincide may not be a valid assumption since the first order terms involving $\mathcal{H}_{xz}$ and $\mathcal{H}_{yz}$ appearing in the expression

$$\left[H_m(\Theta,\delta)\right]_{\substack{\text{first}\\ \text{order}}} = \frac{h\nu}{g\beta} - \frac{m}{K}\left\{A^2\frac{g_z^2}{g^2}\cos^2\Theta + B_\perp\frac{g_\perp^2}{g^2}\sin^2\Theta\left[\frac{B_x+B_y}{2} + \right.\right.$$

$$\left.\frac{B_x - B_y}{2}\left(\frac{g_x^2\cos^2\delta - g_y^2\sin^2\delta}{g_\perp^2}\right)\right] + (A + B_\perp)\frac{g_z g_\perp}{g^2}\sin^2\Theta\cos^2\Theta \times$$

$$\left.\left[\frac{\mathcal{H}_{xz}}{g_z}\frac{g_x}{g_z}\cos\delta + \frac{\mathcal{H}_{yz}}{g_\perp}\frac{g_y}{g_\perp}\sin\delta\right] + 2\frac{g_\perp^2}{g^2}\mathcal{H}_{xy}\sin^2\Theta\sin\delta\cos\delta\right\}$$

disappear when Θ = 0. In fact,

$$\frac{\partial H_m(\Theta,\delta)}{\partial\Theta} = \sin\Theta\cos\Theta\,[\text{non-zero}]$$

showing that the maxima and minima occur at $\Theta = 0$ and 90° for all values of m—exactly what is observed.* However, one may argue why the z axes of these tensors should be expected to coincide. If one first considers an isolated vanadyl ion, the V-O axis will be the z axis of axial spin Hamiltonian and the z axes of both the g and the A tensor since the charges on the vanadium and oxygen are the only physical reasons for producing a preferential direction. Then, for example, if one places the vanadyl ion in a weak crystalline field produced by an octahedral arrangement of water molecules, the surrounding ligands may destroy the pure axial field of the vanadyl ion, setting up an x direction for the g tensor and the A tensor. The z axes of these two tensors will remain coincident or almost coincident is to be expected since the z axis of the ligand field is weak in comparison with the cylindrical field of the vanadyl ion. That the vanadyl crystalline field is very strong is evidenced by the similar spectra found in the investigations (28) to (33), indicating that the vanadyl ion carries along its own crystalline field. Also the fact that $g_\perp > g_z$ can be explained if one assumes the vanadyl ion to have a very strong cylindrical field (Ref. 44 and Appendix B).

*Other than including second order terms, which does not appear practical, the only way to detect the possible noncoinciding z axes of the g and A tensors would be to look for an asymmetry in the resonance magnetic field for positive and negative values of Θ. In this manner the term involving $\mathcal{H}_{xz}$, $\mathcal{H}_{yz}$ changes sign as Θ goes through 0°. However, since Θ can be measured to only ±0.1°, this error can produce a ±0.7 gauss error in the measurement of magnetic field which might mask the observed asymmetry. Table 3 lists the experimental and calculated values of the magnetic field for Θ between 0 and 90°. The calculated values are obtained from the axial spin Hamiltonian.

TABLE 3

VO^{+2} MAGNETIC FIELD RESONANCE VALUES

Degree	Magnetic Field	7/2	5/2	3/2	1/2	-1/2	-3/2	-5/2	-7/2
0	Calculated	2714.0	2910.8	3109.5	3309.5	3512.3	3716.5	3922.6	4130.5
	Experimental	2714.1	2910.9	3110.0	3310.1	3512.7	3716.8	3922.8	4130.2
	Difference	-.1	.1	-.5	.6	.4	.3	.2	.3
10	Calculated	2720.0	2914.7	3111.0	3308.8	3508.2	3709.3	3911.9	4116.1
	Experimental	2719.4						3911.9	
	Difference	-.6						.0	
20	Calculated	2733.3	2922.8	3113.0	3304.1	3496.0	3688.9	3882.9	4077.9
	Experimental	2736.3	2925.0	3114.8	3305.8	3496.0	3688.0	3880.8	
	Difference	3.0	2.2	1.8	1.7	-.0	-.9	-2.1	
30	Calculated	2766.2	2944.2	3121.8	3299.3	3476.7	3654.3	3832.3	4010.8
	Experimental	2764.6							4010.5
	Difference	-1.6							-.3
40	Calculated	2805.1	2967.2	3131.6	3292.5	3452.3	3611.4	3770.1	3929.0
	Experimental	2803.8	2968.2	2130.9	3291.9	3452.2	3611.7	3769.6	3929.0
	Difference	1.3	-1.0	.7	.6	.1	-.3	.5	.0
50	Calculated	2854.4	3000.9	3144.2	3285.2	3424.5	3562.7	3700.7	3839.0
	Experimental	2854.2	3000.5	3144.9	3283.3	3422.9	3561.7	3699.4	3837.8
	Difference	.2	.4	-.7	1.9	1.6	1.0	1.3	1.2
60	Calculated	2912.0	3037.2	3158.7	3277.6	3395.0	3512.2	3630.2	3750.3
	Experimental	2911.3							3749.2
	Difference	.7							1.1
70	Calculated	2974.2	3074.4	3172.1	3268.8	3365.8	3464.8	3567.2	3674.5
	Experimental	2973.1	3073.7		3268.1	3365.4		3567.6	3673.4
	Difference	1.0	.7		.7	.4		-.4	1.1
80	Calculated	3032.7	3104.4	3179.4	3258.1	3341.2	3429.2	3522.7	3622.2
	Experimental	3030.7		3179.8	3257.8			3523.0	3622.2
	Difference	2.0		-.4	-.2			-.3	.0
90	Calculated	3059.2	3115.7	3179.1	3251.9	3330.7	3416.0	3507.3	3604.2
	Experimental	3059.2	3115.5	3180.1	3252.0	3330.8	3415.8	3507.1	3604.1
	Difference	.0	.2	-1.0	-.1	-.1	.2	.2	.1

C. TWO MODELS OF VO^{+2} IN $Zn(NH_4)_2(SO_4)_2 \cdot 6H_2O$

Model 1. If one considers a regular octahedron of water molecules located at the center of the faces of a cube whose dimension is approximately 4Å (the Tutton salts) the length of the V-O bond, 1.67Å,[55] and the ionic radii for V^{+4} and O^{+2}, 0.60Å and 1.3Å, respectively,[56] require the direction of the V-O axis to be along the body diagonal of the cube. If this is true, there are four equivalent positions of the V-O axis in a regular or elongated octahedron of water molecules. In the Tutton salts the six water molecules do not form a regular octahedron but rather one with considerable rhombic symmetry. This is borne out by the X-ray data, Wyckoff,[44] and the V^{+2} EPR data presented in the following section. This rhombic distortion of the water molecules makes the four positions of the V-O axes nonequivalent and ordered in energy and thus in population. Experimentally, there are only three positions with a population ratio 40:10:2. The fourth position might be expected to be so energetically unfavorable that its low population makes it unobservable.

One check on this model would be a comparison of the angle between (111) and $(\bar{1}11)$ directions in a cube, 70°33', with that of the angles that the three V-O axes make with each other. Figure 7 shows the angle between the z axes of the two most populous positions to be 77°48' and that between these two axes and that of the least populous position to be 98°.

Model 2. Ballhausen and Gray[43] have constructed a molecular orbital description of the vanadyl ion in which the vanadyl ion is surrounded by five water molecules in the form of a pyramid—the vanadium at the center of the base and the covalent bonded oxygen sticking out perpendicular to the base a distance of 1.67Å.

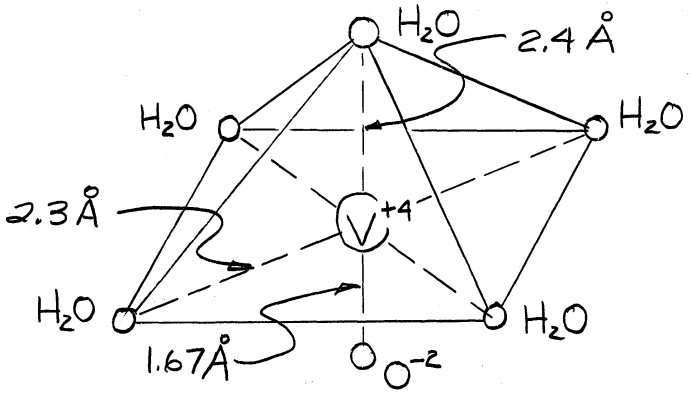

Such a description is found in $VO_2O_4 \cdot 2H_2O$ and is also supposed to be the description of the vanadyl ion in solution—see Ballhausen and Gray.[43] With this molecular orbital description of this model they found $g_z = 1.940$, $g_\perp = 1.983$ and $< g > = 1.969$. They also obtained good agreement with optical absorption spectra and magnetic susceptibility measurements.

Although the g values found in this work differ slightly (this work: $g_z = 1.9330$, $g_\perp = 1.9805$ and $< g > = 1.9647$) from that of Ballhausen and Gray[43] it should be considered possible that their pentahydrate model of VO^{+2} may be that found in the Tutton crystal, particularly since this pentahydrate model will show only three orientations of the V-O axis when the model is viewed as an octahedron. However, if

this model is to be correct, the result of producing a V^{+2} spectrum from VO^{+2} by X-rays identical to that of V^{+2} surrounded by six water molecules implies that the oxygen released from the vanadyl ion by X-ray irradiation must take the place of the missing water molecule producing a crystalline field identical to that of V^{+2} surrounded by six water molecules.

Vanadyl Superhyperfine Structure. An interesting experimental result is the additional structure found on the resonances of the vanadyl ion for a particular orientation of the magnetic field (Fig. 11). The five resonances are each separated by approximately four gauss and result from overlap of the wave function onto the protons of the surrounding water molecules (i.e., superhyperfine structure). That these additional resonances arise from the protons is verified by the fact that they are unobservable in the crystals grown with heavy water.

Since these additional resonances are superhyperfine structure a measurement of the strength of this interaction may provide some information on the molecular orbital description of the vanadyl ion and the surrounding water molecules and the validity of one model or the other.

D. V^{+2} AND IRRADIATED VO^{+2} CRYSTALS

From the EPR measurements at K-band frequencies (~24 kmc) of the vanadous ion in $Zn(NH_4)_2(SO_4)_2 \cdot 6H_2O$ crystals, the room temperature rhombic spin Hamiltonian constants shown in Table 3 were calculated

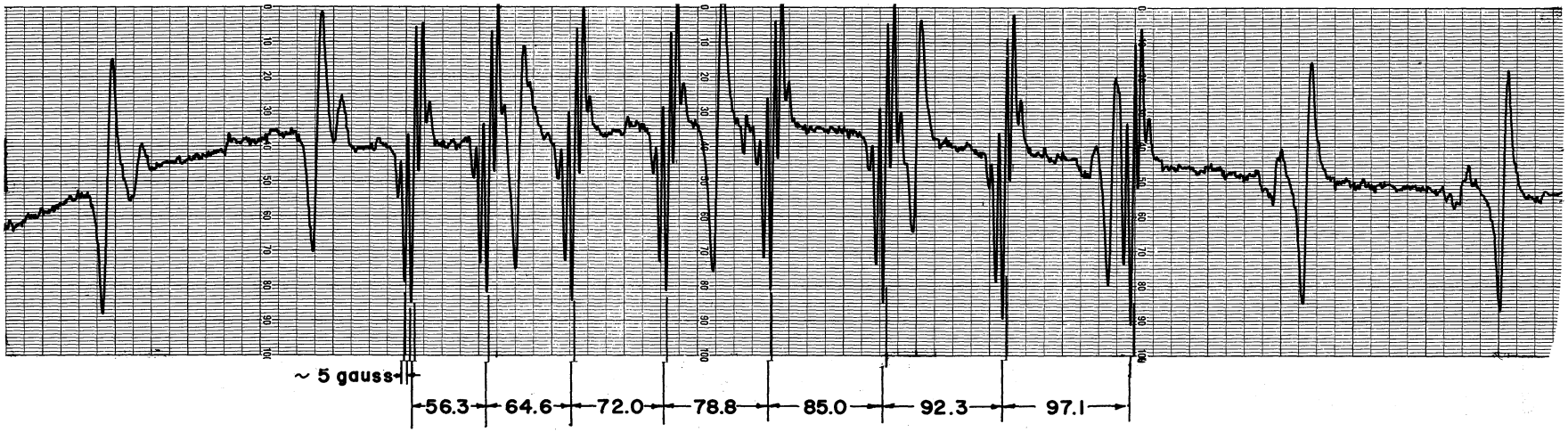

EPR SPECTRUM OF .1% $VOSO_4$ in $Zn(NH_4)_2(SO_4)_2 \cdot 6H_2O$ WITH MAGNETIC FIELD ALONG "TETRAGONAL" AXIS

Fig. 11. Vanadyl superhyperfine structure.

by means of the method in Appendix H.

TABLE 4

EXPERIMENTAL RESULTS FOR V^{+2}

	V^{+2} (Grown)	V^{+2} (Irradiated VO^{+2})	V^{+2} (Bleaney[16])
g_z	1.9717±*	1.9718±5	1.951
g_y	1.9733±5	1.9733±5	
$\|D\|$	0.15613±3/cm	0.15609±3/cm	0.158/cm
$\|E\|$	0.02290±3/cm	0.02297±3/cm	0.049/cm
$\|A\|$	0.008263±5/cm	0.008267±5/cm	0.0088/cm
$\|B\|$	0.008246±5/cm	0.008249±5/cm	
α**	20.5°±0.5°	20.5°±0.5°	22°
Ψ	2°±5°	3°±1°	2°
Line width	6.0±0.6 gauss	6.0±0.6 gauss	6.0±0.6 gauss

*The errors associated with the values in Tables 4 and 5 are the experimental errors and do not include the 0.08% error on the wave meter calibration.

**α and Ψ locate the z axis of the spin Hamiltonian with respect to the ac plane and the c axis.

For the V^{+2} produced by X-ray irradiation in the three different vanadyl Tutton salts, the following room temperature rhombic spin Hamiltonian constants in Table 5 were calculated.

TABLE 5

EXPERIMENTAL RESULTS FOR V^{+2} (IRRADIATED VO^{+2})

	$Zn(NH_4)_2(SO_4)_2 \cdot 6H_2O$	$Mg(NH_4)_2(SO_4)_2 \cdot 6H_2O$	$ZnK_2(SO_4)_2 \cdot 6H_2O$
g_z	1.9718	1.9720	1.9722
g_y	1.9733	1.9723	1.9741
$\|D\|$	0.15609	0.15793 (1.2%)	0.15244 (-2.3%)
$\|E\|$	0.02297	0.02452 (+6.6%)	0.02742 (19.2%)
$\|A\|$	0.008267	0.008262	0.008253
$\|B\|$	0.008249	0.008253	0.008212
ψ	3°±1°	1°±1°	11°±2°
α	20.5°±0.5°	20.0°±0.5°	14.7°±0.5°

E. DISCUSSION OF V^{+2} RESULTS

As seen by the close agreement of the V^{+2} (grown) and V^{+2} (irradiated VO^{+2}), spin Hamiltonian constants and the identical (within experimental error) location of the z axes for both cases leads to the following conclusions. Either, (1) the VO^{+2} ion existing in the Tutton salt before irradiation is surrounded by six water molecules, and after irradiation the released oxygen moves far enough away from the divalent site so that its influence on the crystalline field is no longer felt; or, (2) the vanadyl ion in the Tutton salts is the pentahydrate model of Ballhausen and Gray,[43] and after irradiation the released oxygen takes the place of the missing water molecule, completing the octahe-

dron and producing a crystalline field identical to the one with the V^{+2} surrounded by six water molecules. That the crystalline field must be identical for V^{+2} and irradiated VO^{+2} is also supported by comparing the spin Hamiltonian constants and z axis positions for V^{+2} (irradiated VO^{+2}) in the three Tutton salts listed in Table 5. These results indicate that the substitution of different host ions in the monovalent and divalent positions distort the octahedron an amount that is measured by the changes of D, E, α, and Ψ .*

Note that the value of E reported by Bleaney, Ingram and Scovil,[16] and listed in Table 4, is almost twice the value found in these experiments. Since they used the EPR data along the z direction to evaluate both D and E, and since E enters the equation in this direction as a second order correction (Appendix H), we expect that their value is not as correct.

Fit to Spin Hamiltonian. Table 6 compares the experimental and calculated values of the resonance magnetic field for the z and y axes for each of the eight resonances in the three fine structure groups. Note that although the spin Hamiltonian is fitted to an average of the magnetic field values in a fine structure group (Appendix H) the individual values of the calculated resonances deviate in a consistent

*The result that changes in the monovalent ion influence the position of the z axis in the crystal to a great extent was noticed by Bleaney, Penrose, and Plumpton[57] in their EPR investigations of Cu^{+2}. They also noticed large changes in the g values, ~1%, which were not observed in this work.

TABLE 6

V^{+2} MAGNETIC FIELD RESONANCE VALUES (GAUSS)

Z Axis (ν = 24.118 kmc)			Y Axis (ν = 24.112 kmc)		
Calc.	Diff.	Exper.	Calc.	Diff.	Exper.
12439.6	(- .7)	12440.3	11468.1	(-4.3)	11472.4
12348.5	(.9)	12347.6	11376.8	(- .6)	11377.4
12258.1	(1.8)	12256.3	11285.0	(.9)	11284.1
12168.3	(1.9)	12166.4	11194.1	(2.1)	11192.0
12079.2	(1.3)	12077.9	11103.9	(2.7)	11101.2
11990.8	(- .1)	11990.9	11014.4	(2.4)	11012.0
11903.0	(-2.2)	11905.2	10925.0	(1.4)	10924.2
11815.9	(-5.1)	11821.0	10837.5	(- .1)	10827.6
9029.6	(1.7)	9027.9	8854.9	(1.3)	8853.6
8937.0	(- .3)	8936.7	8762.6	(.3)	8762.3
8845.4	(- .6)	8846.0	8671.2	(- .6)	8671.8
8754.7	(-1.0)	8755.7	8580.0	(-1.0)	8581.8
8665.0	(-1.4)	8666.4	8491.3	(-1.0)	8492.3
8576.2	(- .7)	8576.9	8402.7	(- .7)	8403.4
8488.2	(.2)	8488.0	8315.1	(.1)	8315.0
8401.3	(1.7)	8399.6	8228.4	(1.5)	8226.9
5676.0	(7.3)	5668.7	6644.2	(2.0)	6642.2
5580.2	(1.5)	5578.7	6552.2	(- .6)	6552.8
5486.0	(-2.3)	5488.3	6461.4	(-1.4)	6462.8
5393.2	(-5.2)	5398.4	6371.9	(-2.0)	6373.9
5301.9	(-5.7)	5307.6	6283.7	(-1.4)	6285.1
5212.2	(-4.6)	5216.8	6196.7	(.3)	6196.4
5123.9	(-2.0)	5125.9	6111.0	(2.9)	6108.1
5037.2	(2.5)	5034.7	6026.5	(6.2)	6020.3

manner that corresponds to second-order hyperfine correction that is too large by a factor of two or three. No explanation suggests itself unless it is that the experiment is performed at a microwave frequency insufficiently removed from the energy level crossover which mixes the levels M, m-1 and M-1, m (Lambe and Kikuchi[23]). It should also be noted

that, if the experiment is performed at a frequency too close to the zero field splitting value 2D, the measured value for 2D will be smaller than the correct value.

X Axis Data. If one performs a general coordinate rotation on the rhombic spin Hamiltonian in order to diagonalize the Zeeman term (Appendix C), only when the magnetic field is along the x, y, or z axes do the cross terms become zero, simplifying the spectrum and thus enabling one to make precise measurements for the spin Hamiltonian constants. The effect of this mixing is illustrated in Fig. 12, which shows the EPR spectrum with the magnetic field parallel to the z axis of one of the two sites in the crystal. Note that, as a result of this mixing, the spectrum from the second site is so spread as to make it almost unobservable.

Figure 12 shows the effect of not having the magnetic field precisely parallel to either the x, y, or z axes. In this figure the magnetic field bisects the angle made by the x axes of each of the two sites—approximately 10°. Since the spectrum from the one site could not be differentiated from that of the second site, the magnetic field measurements for the x direction could not be made to any precision; hence, no g_x value is listed in Tables 4 and 5.

F. CONVERSION OF VO^{+2} TO V^{+2}

Because irradiation of the vanadyl crystal results in the breaking of the V-O bond and the production of V^{+2}, it might be expected that all the vanadyl ions might be able to be converted to V^{+2} in accordance with

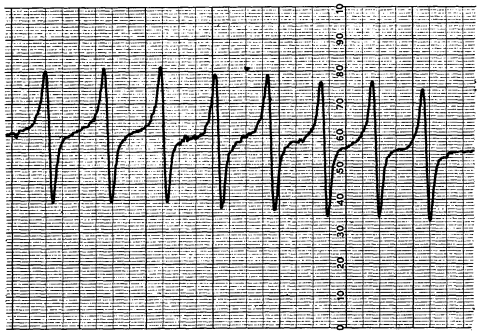

LOW FIELD

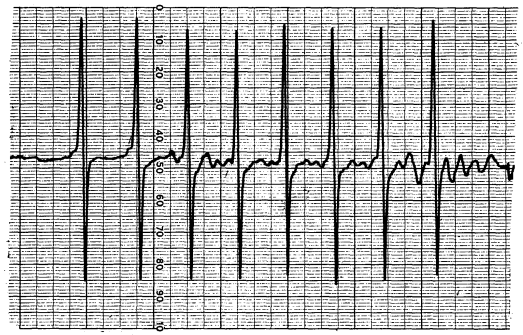

CENTER FIELD

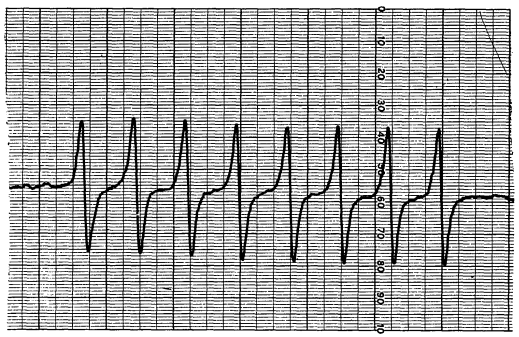

HIGH FIELD

MAGNETIC FIELD PARALLEL TO Z AXIS

1% V^{+2} in $ZnSO_4(NH_4)SO_4 \cdot 6H_2O$, $\nu = 24$ KMc

Fig. 12. V^{+2} spectrum along Z axis.

the exponential relation $N(V^{+2}) = N_o(VO^{+2})(1-e^{-\lambda R})$, where $N_o(VO^{+2})$ is the number of VO^{+2} ions originally present in the crystal and R is the energy dose absorbed by the crystal. While the initial conversion of VO^{+2} to V^{+2} by irradiation may follow such a law, some mechanism interferes to prevent more than a reduction of 80-90% in the vanadyl signal intensity and only 10-20% of this amount is converted to V^{+2}. These results are illustrated in Fig. 13, which shows the conversion of VO^{+2} to V^{+2} as a function of irradiation time.*

The degree of saturation appeared to vary slightly for the three different host crystals with the same initial concentration of VO^{+2}, but remained constant for different sizes of the same host crystal, grown from the same solution, indicating that the X-rays penetrated the entire crystal. Also a slight annealing affect was noticed. These same effects, saturation, variation in saturation for "different" crystals, slight annealing, and loss of the reduced signal were also observed in the experiments by Lambe and Kikuchi[23] and Sturge[58] in the conversion of V^{+3} to V^{+2} in sapphire.

*While a graph of the absolute intensity of V^{+2} and VO^{+2} versus dose might be more meaningful in light of the observation that the decrease in VO^{+2} signal intensity is not entirely accounted for in the increase of the V^{+2} signal, such measurements were a practical impossibility with the apparatus used in this set of experiments. Also, comparison to a standard such as hydrazyl was impossible since an irradiation center was produced in the crystal masking the hydrazyl resonance.

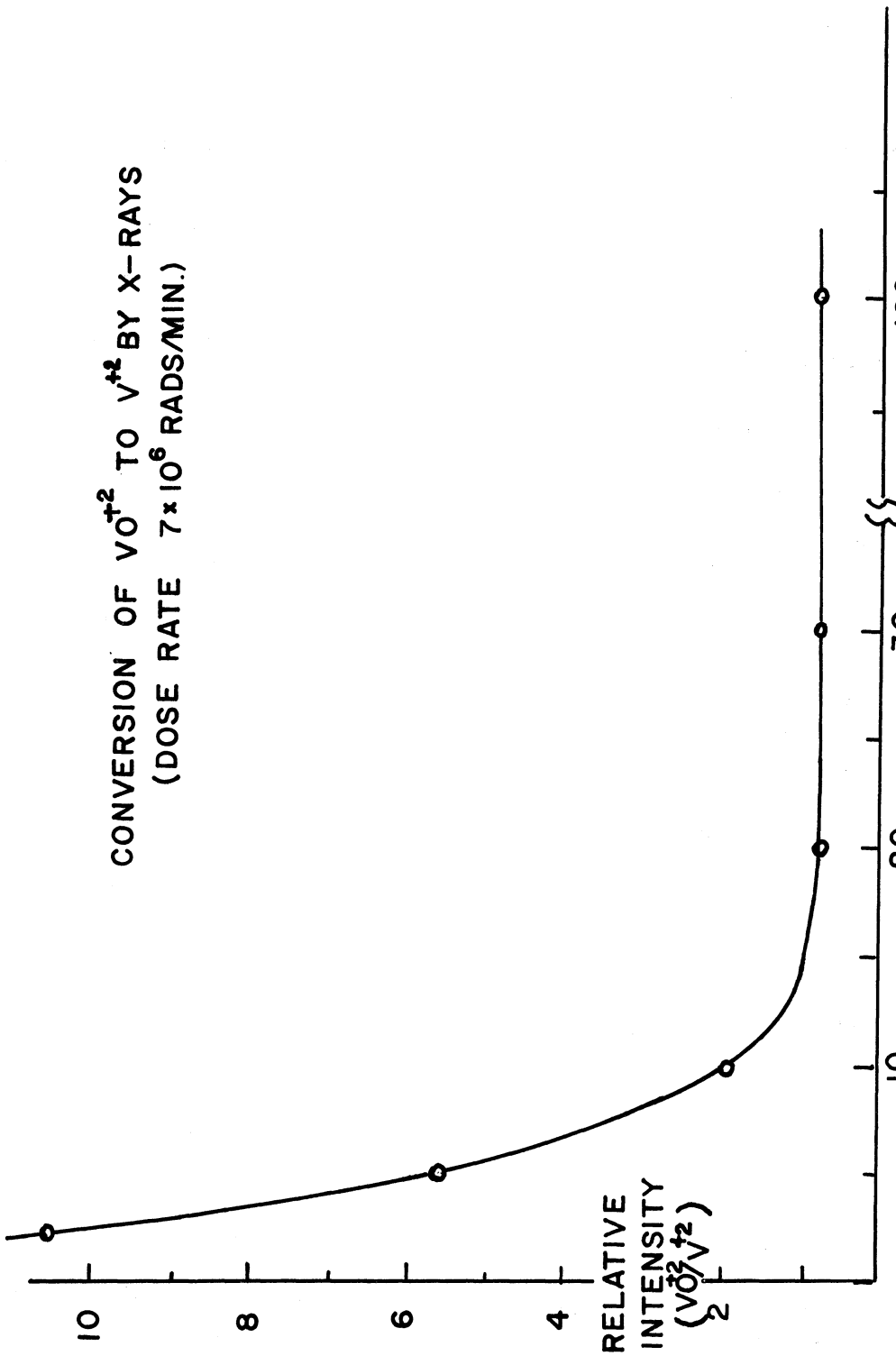

Fig. 13. Conversion of VO^{+2} to V^{+2}.

APPENDIX A

X-RAY-DOSE CALCULATIONS

In this appendix we wish to compute the X-ray dose given to the crystals, using the data obtained from the cerric-cerrous sulfate dosimetry of the Machlelett AEG-50S operated at 50 KVP 40 ma.

The experimental setup for the irradiations is shown below

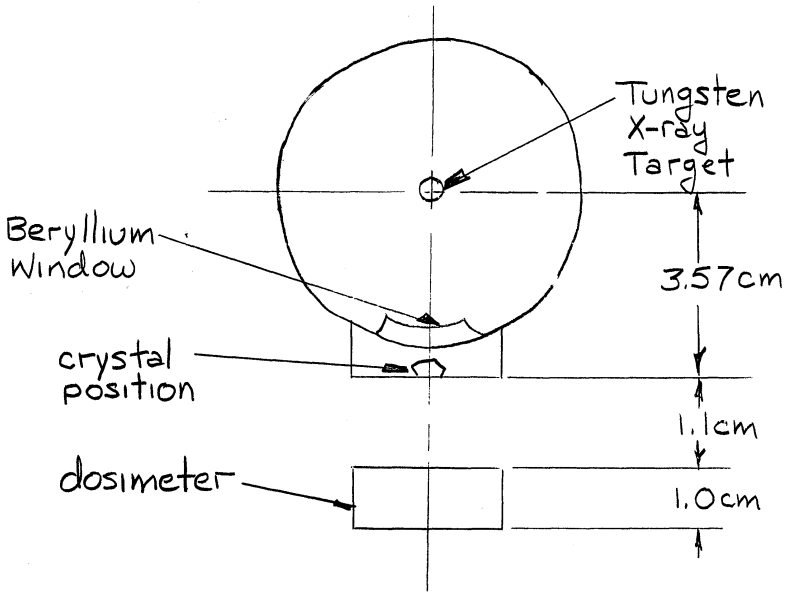

The dose rate measured by the dosimeter is 0.73×10^6 rep/min. If we can assume that the X-rays are monoenergetic at an energy of their maximum intensity* (33 KV for 50 KVP), and that the absorption coefficient of the crystal is that of aluminum, then the dose rate absorbed by the crystal is

*Kulenkampff lists an empirical law for the white beam of an X-ray tube to be $I(\lambda) = CZ(1/\lambda^2)(1/\lambda_o - 1/\lambda) + BZ^2(1/\lambda^2)$ where $B \ll C$ and can be ignored for practical purposes.[59] Z is the atomic number of the target, λ the wavelength, and λ_o the cutoff wavelength.

$$0.73 \times 10^6 \frac{\text{rep}}{\text{min}} \times \frac{93 \text{ ergs/gm}}{1 \text{ Rep}} \times \frac{1 \text{ Rad}}{100 \text{ ergs}} \times \left(\frac{4.67 \text{ cm}}{3.57 \text{ cm}}\right)^2 \times \frac{0.66 \text{ cm}^2/\text{gm (Al)}}{0.11 \text{ cm}^2/\text{gm } (H_2O)} *$$

$$= 7.0 \times 10^6 \text{ rad/min}$$

*These absorption coefficients are from Evans (Ref. 60, p. 714).

APPENDIX B

CRYSTAL FIELD CALCULATIONS

In this appendix we wish to calculate the splitting of the ground state ^2D, ^3F, and ^4F in cubic and tetragonal fields and then calculate the effective g values for such environments.

We assume that the paramagnetic ion is surrounded by point charges and that there is no overlap of charges of the paramagnetic ion and the surrounding ligands. Then the crystalline electric field in this region has a potential satisfying Laplace's equation

$$\nabla^2 V = 0$$

which has the general solution

$$V(\vec{r}_i) = \sum_{n=0}^{\infty} \sum_{m=-n}^{n} A_n^m r_i^n Y_n^m(\theta_i, \varphi_i) \qquad \text{(B-1)}$$

Assuming that we have a point charge Q on each of the j surrounding ligands leads us to express $V(\vec{r}_i)$ as

$$V(\vec{r}_i) = \sum_j \frac{Q}{|\vec{r}_{ij}|}$$

where the vectors $\vec{r}_i$, $\vec{r}_j$, and $\vec{r}_{ij}$ form the triangle shown below.

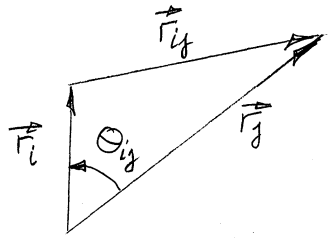

From the law of cosines we may express $V(\vec{r}_i)$ as

$$V(\vec{r}_i) = \sum_j \frac{Q}{[r_i^2 + r_j^2 - 2\vec{r}_i \cdot \vec{r}_j]^{1/2}}$$

$$= \sum_j \frac{Q}{r_j} \sum_{n=0}^{\infty} \left(\frac{r_i}{r_j}\right)^n P_n(\cos\theta_{ij})$$

By expanding $P_n(\cos\theta_{ij})$ by the spherical harmonic addition theorem, $V(\vec{r}_i)$ becomes

$$V(\vec{r}_i) = \sum_{n=0}^{\infty} \sum_{m=-n}^{n} \left\{ \sum_j \frac{Q}{r_j^{n+1}} \left(\frac{4\pi}{2n+1}\right) (-1)^m Y_n^{-m}(\theta_j, \varphi_j) \right\} r_i^n Y_n^m(\theta_i, \varphi_i) \quad \text{(B-2)}$$

Then, comparing like terms in Eqs. (B-1) and (B-2), we find

$$A_n^m = \sum_j \frac{Q}{r_j^{n+1}} (-1)^m Y_n^{-m}(\theta_j, \varphi_j) \quad \text{(B-3)}$$

1. SYMMETRY CONSIDERATIONS

By exploiting the symmetry of the locations of the ligands surrounding the paramagnetic ion, we can find that many of the A_n^m vanish. For example:

(a) If the polar axis (z axis) possesses p-fold symmetry, the coefficients A_n^m vanish unless m is zero or an integral multiple of 2π. That is,

$$V(\varphi_i) = V\left(\varphi_i + \frac{2\pi}{p}\right)$$

so that

$$e^{im\varphi_i} = e^{im\left(\varphi_i + \frac{2\pi}{p}\right)}$$

which is satisfied only when m = 0, ±p, ±2p,... .

(b) Since $V(\vec{r}_i)$ is to be real, $[V(\vec{r}_i)]^* = V(\vec{r}_i)$ implies

$$(A_n^{-m})^* = A_n^m$$

(c) If there is a reflection plane through the polar axis, and if this plane is the x-0-z plane, then $V(\varphi_i) = V(-\varphi_i)$ which implies

$$A_n^m = A_n^{-m}$$

This together with (b) gives the result that the A_n^m are real.

(d) If there is inversion symmetry about the paramagnetic ion, then

$$V(\theta_i, \varphi_i) = V(\pi - \theta_i, \pi + \varphi_i)$$

and

$$\sum_n \sum_{m=-n}^{n} A_n^m r_i^n Y_n^m(\theta_i, \varphi_i) = \sum_n \sum_{m=-n}^{n} A_n^m r_i^n (-)^n Y_n^m(\theta_i, \varphi_i)$$

Since the Y_n^m have parity $(-1)^n$ we obtain the result

$$A_n^m = 0 \quad \text{for } n \text{ odd}$$

(e) For d electrons we see that the matrix elements $\langle \psi \mid V(\vec{r}_i) \mid \psi \rangle$ will span no A_n^m with $n > 4$. Thus for 4-fold symmetry about the z axis we need to consider only those terms involving

$$A_0^0, A_2^0, A_4^0, A_4^4 = A_4^{-4}$$

Cubic Fields. For cubic fields we see that from Eq. (B-3)

$$A_2^0 = \frac{4\pi}{5} \sum_j \frac{Q}{r_j^3} \frac{1}{2} \left(3\cos^2\theta_j - 1\right) \left(\frac{5}{4\pi}\right)^{1/2}$$

Performing the summation for the ligands located at $\pm a_1$ along each of

the coordinate axes, we find that

$$A_2^0 = 0$$

Now dropping the term involving A_0^0 since it shifts all levels equally and dropping the subscript i, we find that $V(\vec{r_i})$ becomes

$$r^4\left[A_4^0 Y_4^0 + A_4^4\left(Y_4^4 + Y_4^{-4}\right)\right]$$

Note that

$$V(r,0,0) = V\left(r,\tfrac{\pi}{2},0\right)$$

so that A_4^0 is related to A_4^4 by the following

$$A_4^0 = \sqrt{\tfrac{14}{5}}\, A_4^4$$

Thus, for cubic fields

$$V_{cubic} = A_4^0 r^4\left[Y_4^0 + \left(\tfrac{5}{14}\right)^{\frac{1}{2}}\left(Y_4^4 + Y_4^{-4}\right)\right]$$

or,

$$V_{cubic} = A_4^0 \pi^{-\frac{1}{2}} \tfrac{15}{4}\left[x^4 + y^4 + z^4 - \tfrac{3}{5} r^4\right]$$

where from (B-3)

$$A_4^0 = \frac{Q}{a_1^5}\pi^{\frac{1}{2}}\frac{7}{3}$$

Tetragonal Fields. If we lengthen (shorten) the distance along the z axis so that the charges are located at a distance $\pm a_2$ along the z axis and $\pm a_1$ along the x and y axes, then

$$V(\vec{r}_i) \equiv V_{tetrag} = V_{cubic} + V'_{tetrag}$$

where $$V'_{tetrag} = \left[2Q\left(\frac{4\pi}{5}\right)^{\frac{1}{2}}\left(\frac{1}{a_2^3} - \frac{1}{a_1^3}\right)\right] r^2 Y_2^0 + \left[2Q\left(\frac{4\pi}{9}\right)^{\frac{1}{2}}\left(\frac{1}{a_2^5} - \frac{1}{a_1^5}\right)\right] r^4 Y_4^0$$

where in V_{cubic}

$$A_4^0 = \frac{Q}{a_1^5}\,\pi^{\frac{1}{2}}\,\frac{7}{3}$$

as before.

2. $^2D(3d^1)$

Cubic Field. Group theoretical considerations can show that the ^2D state splits into a three-fold degenerate level, T_{2g}, and a two-fold level, E_g, for cubic fields. If we anticipate the results and write the orbital parts of the wave function of the five-fold degenerate level as

$$|T_2\xi\rangle = \frac{i}{\sqrt{2}}\left(Y_2^1 + Y_2^{-1}\right) = \left(\frac{5}{4\pi}\right)^{\frac{1}{2}}\sqrt{3}\,\frac{yz}{r^2}$$

$$|T_2\eta\rangle = \frac{1}{\sqrt{2}}\left(-Y_2^1 + Y_2^{-1}\right) = \left(\frac{5}{4\pi}\right)^{\frac{1}{2}}\sqrt{3}\,\frac{xz}{r^2}$$

$$|T_2\zeta\rangle = \frac{1}{i\sqrt{2}}\left(Y_2^2 - Y_2^{-2}\right) = \left(\frac{5}{4\pi}\right)^{\frac{1}{2}}\sqrt{3}\,\frac{xy}{r^2}$$

$$|E\,u\rangle = Y_2^0 = \left(\frac{5}{4\pi}\right)^{\frac{1}{2}}\frac{1}{2}\,(3z^2 - r^2)/r^2$$

$$|E\,v\rangle = \frac{1}{\sqrt{2}}\left(Y_2^2 + Y_2^{-2}\right) = \left(\frac{5}{4\pi}\right)^{\frac{1}{2}}\frac{\sqrt{3}}{2}\,(x^2 - y^2)/r^2$$

then the matrix elements $\langle \psi_{2D} | V_{cubic} | \psi_{2D} \rangle$ become diagonal in this "cubic harmonic" representation. The results are that the three-fold T_{2g} level is depressed by an amount $4Dq$ and the two-fold E_{2g} level is raised $6Dq$, where $Dq \equiv \frac{Q}{6a_1^5}\overline{r^4}$ and $\overline{r4}$ is averaged over the 3d radial function.

Tetragonal Field. Since the cubic part of the tetragonal field has already been evaluated above, we need only to calculate the matrix elements of

$$V'_{tetrag} = 2Q\left(\frac{4\pi}{5}\right)^{\frac{1}{2}}\left(\frac{1}{a_2^3} - \frac{1}{a_1^3}\right) r^2 Y_2^0 + 2Q\left(\frac{4\pi}{9}\right)^{\frac{1}{2}}\left(\frac{1}{a_2^5} - \frac{1}{a_1^5}\right) r^4 Y_4^0$$

$$= A \cdot \frac{1}{2}(3z^2 - r^2) + B \cdot \frac{1}{8}(35z^4 - 30r^2z^2 + 3r^4)$$

where

$$A \equiv 2Q\left(\frac{1}{a_2^3} - \frac{1}{a_1^3}\right)$$

$$B \equiv 2Q\left(\frac{1}{a_2^5} - \frac{1}{a_1^5}\right)$$

Note that both A and B have the same sign and are negative (positive) if the octahedron is lengthened (shortened) along the z axis. Also $A \simeq \frac{3}{5}a_2^2 B$ for $\left|1 - \frac{a_2}{a_1}\right| \ll 1$. Since it is easier to calculate the matrix elements in the operator equivalent form,[52] we write

$$V'_{tetrag}(O_p) = \alpha A \frac{\overline{r^2}}{2}\left[3L_z^2 - L(L+1)\right] + \beta B \frac{\overline{r^4}}{8}\left[35L_z^4 - 30L_z^2 L(L+1)\right.$$

$$\left. + 25L_z^2 - 6L(L+1) + 3L^2(L+1)^2\right]$$

where $\alpha = -\frac{2}{21}$ and $\beta = \frac{2}{63}$ are found by evaluating a matrix element of V'_{tetrag} and $V'_{tetrag}(OP)$ for ^2D. Using this operator to calculate the matrix elements of the tetragonal crystal field yields the following energy level changes*

$$\Delta E(\xi) = \tfrac{1}{7}A\bar{r}^2 - \tfrac{4}{21}B\bar{r}^4$$

$$\Delta E(\eta) = \tfrac{1}{7}A\bar{r}^2 - \tfrac{4}{21}B\bar{r}^4$$

$$\Delta E(\zeta) = -\tfrac{2}{7}A\bar{r}^2 + \tfrac{1}{21}B\bar{r}^4$$

$$\Delta E(u) = \tfrac{2}{7}A\bar{r}^2 + \tfrac{6}{21}B\bar{r}^4$$

$$\Delta E(v) = -\tfrac{2}{7}A\bar{r}^2 + \tfrac{1}{21}B\bar{r}^4$$

which are shown graphically below.

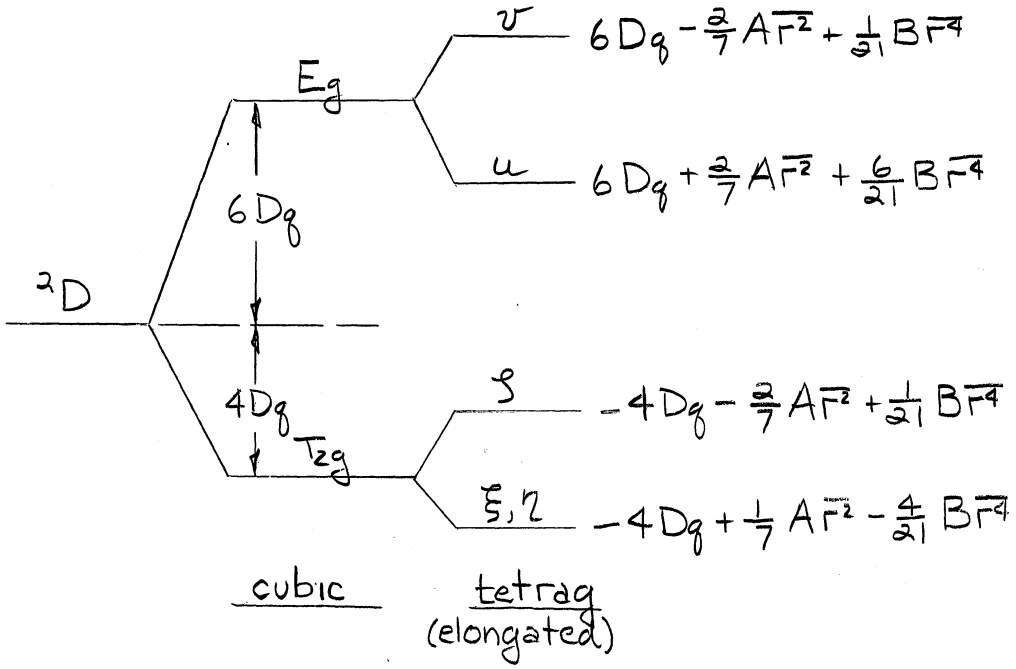

*Ballhausen[13] defines $\frac{A}{7}\bar{r}^2 = Ds$ and $\frac{B}{21}\bar{r}^4 = Dt$.

3. $3d^2$ (^3F)

Cubic Field. Group theoretical methods can shown that the sevenfold orbitally degenerate F state splits into two orbital triplets and one singlet. Again, we anticipate the results and write down the linear combination of state functions that diagonalize the matrix elements of the cubic field

$$A_2: \frac{1}{\sqrt{2}}(\Psi_2 - \Psi_{-2})$$

$$T_2: \frac{1}{\sqrt{2}}(\Psi_2 + \Psi_{-2})$$

$$\sqrt{\frac{5}{8}}\Psi_1 - \sqrt{\frac{3}{8}}\Psi_{-3}$$

$$\sqrt{\frac{5}{8}}\Psi_{-1} - \sqrt{\frac{3}{8}}\Psi_3$$

$$T_1: \Psi_0$$

$$\sqrt{\frac{3}{8}}\Psi_1 + \sqrt{\frac{5}{8}}\Psi_{-3}$$

$$\sqrt{\frac{3}{8}}\Psi_{-1} + \sqrt{\frac{5}{8}}\Psi_3$$

where the Ψ_i are antisymmetrized linear combinations of the two electron orbitals and are written below for the $M_S = 1$ spin state

$$\Psi_3 = (\overset{+}{2}, \overset{+}{1}) \equiv \frac{1}{\sqrt{2}} \begin{vmatrix} Y_2^2(1) & Y_2^1(1) \\ Y_2^2(2) & Y_2^1(2) \end{vmatrix} \alpha \, R_{3d}(r)$$

$$\Psi_2 = (\overset{+}{2}, \overset{+}{0})$$

$$\Psi_1 = \sqrt{\frac{3}{5}}(\overset{+}{2}, \overset{+}{-1}) + \sqrt{\frac{2}{5}}(\overset{+}{1}, \overset{+}{0})$$

$$\Psi_0 = \sqrt{\tfrac{1}{5}}\left(2^+,-2^+\right) + \sqrt{\tfrac{4}{5}}\left(1^+,-1^+\right)$$

$$\Psi_{-1} = \sqrt{\tfrac{3}{5}}\left(1^+,-2^+\right) + \sqrt{\tfrac{2}{5}}\left(0^+,-1^+\right)$$

$$\Psi_{-2} = \left(0^+,-2^+\right)$$

$$\Psi_{-3} = \left(-1^+,-2^+\right)$$

If we use the operator equivalent form for the cubic field

$$V_{cubic}(O_p) = \frac{7}{16}\frac{Q}{a_1^5}\overline{r^4}\beta\left[35L_z^4 - 30L(L+1)L_z^2 + 25L_z^2 - 6L(L+1) + 3L^2(L+1)^2 + \frac{5}{2}\left(L_+^4 + L_-^4\right)\right]$$

where β can be evaluated to be - 2/315 for $3d^2(^3F)$, it is found that the seven-fold degenerate level splitting is

$$A_2\ (+12D_q)$$
$$T_2\ (+2D_q)$$
$$T_1\ (-6D_q)$$

Tetragonal Field. From the operator equivalent form for V'_{tetrag}

$$V'_{tetrag}(O_p) = \alpha A\frac{\overline{r^2}}{2}\left[3L_z^2 - L(L-1)\right] + \beta B\frac{\overline{r^4}}{8}\left[35L_z^4 - 30L_z^2L(L+1) + 25L_z^2 - 6L(L+1) + 3L^2(L+1)^2\right]$$

where α = - 2/105, β = - 2/315 for $3d^2(^3F)$, we find the following energy-level splittings for the A^2, T_2, and T_1 levels due to a tetragonal

field:

$$A_2: \quad \Delta E\left(\frac{1}{\sqrt{2}}[\Psi_2 - \Psi_{-2}]\right) = \frac{1}{3}Br^4$$

$$T_2: \quad \Delta E\left(\frac{1}{\sqrt{2}}[\Psi_2 + \Psi_{-2}]\right) = \frac{1}{3}Br^4$$

$$\Delta E\left(\sqrt{\frac{5}{8}}\Psi_1 - \sqrt{\frac{3}{8}}\Psi_{-3}\right) = -\frac{1}{12}Br^4$$

$$\Delta E\left(\sqrt{\frac{5}{8}}\Psi_{-1} - \sqrt{\frac{3}{8}}\Psi_3\right) = -\frac{1}{12}Br^4$$

$$T_1: \quad \Delta E(\Psi_0) = \frac{4}{35}Ar^2 - \frac{2}{7}Br^4$$

$$\Delta E\left(\sqrt{\frac{3}{8}}\Psi_1 + \sqrt{\frac{5}{8}}\Psi_{-3}\right) = -\frac{2}{35}Ar^2 - \frac{3}{28}Br^4$$

$$\Delta E\left(\sqrt{\frac{3}{8}}\Psi_{-1} + \sqrt{\frac{5}{8}}\Psi_3\right) = -\frac{2}{35}Ar^2 - \frac{3}{28}Br^4$$

These results are shown graphically below:

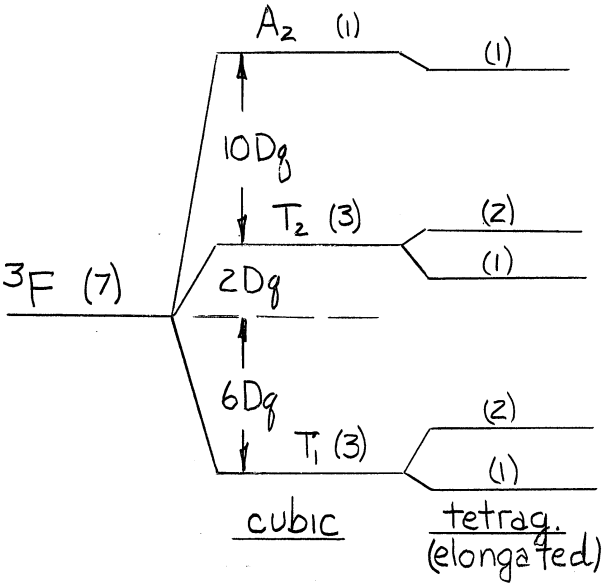

4. $3d^3$ (^4F)

Cubic Field; Tetragonal Field. For the $3d^3(^4F)$ ground state it can be shown that $\alpha = +2/105$, $\beta = 2/315$, in contrast to $\alpha = -2/105$, $\beta = -2/315$ for the $3d^2(^3F)$ state. Thus the energy-level splitting for

this ^4F state, including the tetragonal field, is obtained by inverting the ^3F levels. This results in the energy diagram below:*

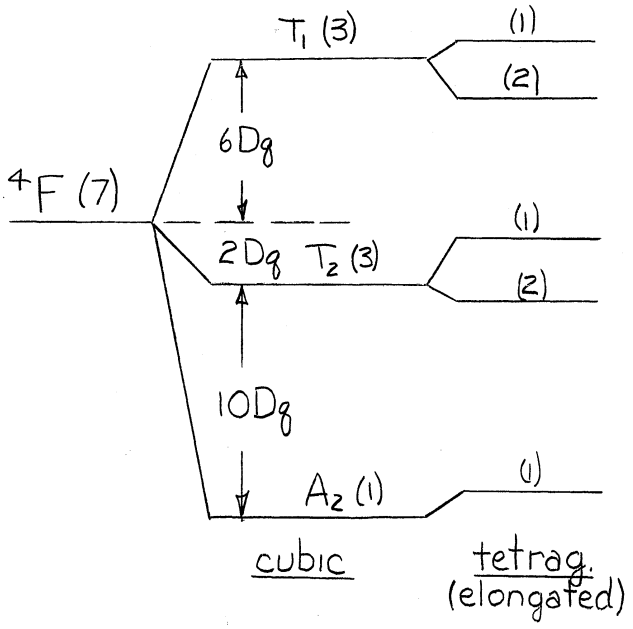

5. ^2D g VALUES

The results from crystal field calculations of the ^2D state in a squashed tetragonal field is summarized below:

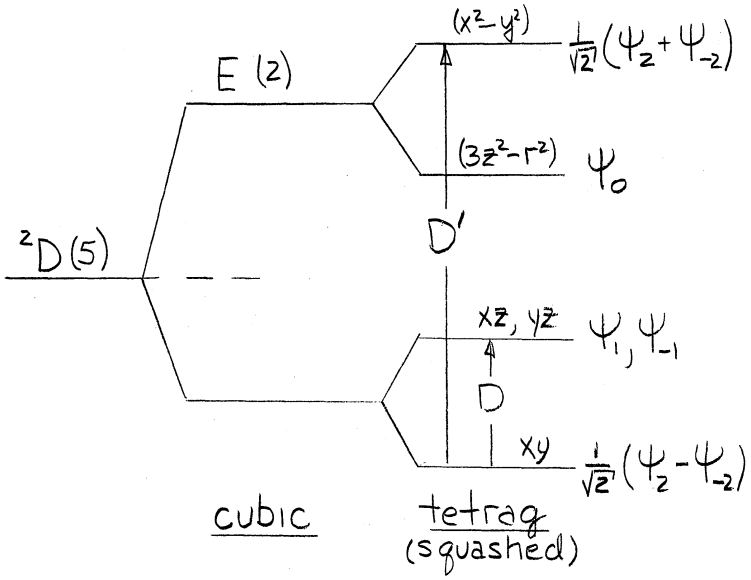

*If the octahedron is squashed, the tetragonal levels are inverted since A and B change signs.

However, if we consider the vanadyl ion to produce a strong cylindrical crystal field as a result of the covalent bond between the oxygen and the vanadium, the ^2D state splits in the following manner:

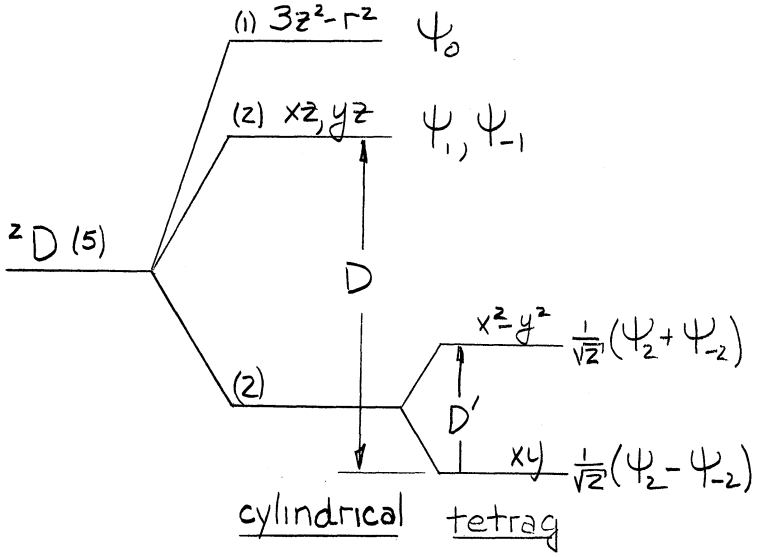

To compute the g values, we first calculate the correct wave functions for the ground state when the spin orbit interaction $\lambda \underline{L}\cdot\underline{S}$ is included. The corrected wave functions, to first order, become

$$\Phi_\alpha \equiv \frac{1}{\sqrt{2}}(\psi_2-\psi_{-2})\alpha - \frac{\lambda}{\sqrt{2}D'}(\psi_2+\psi_{-2})\alpha + \frac{\lambda}{\sqrt{2}D}\psi_1\beta$$

$$\Phi_\beta \equiv \frac{1}{\sqrt{2}}(\psi_2-\psi_{-2})\beta + \frac{\lambda}{\sqrt{2}D'}(\psi_2+\psi_{-2})\beta - \frac{\lambda}{\sqrt{2}D}\psi_1\alpha$$

where α, β are the spin parts of the product wave functions such that

$$S_-\alpha = \beta \qquad S_+\alpha = 0$$
$$S_+\beta = \alpha \qquad S_-\beta = 0$$
$$S_z\alpha = \tfrac{1}{2}\alpha \qquad S_z\beta = -\tfrac{1}{2}\beta$$
$$S^2\begin{pmatrix}\alpha\\ \beta\end{pmatrix} = \frac{3}{4}\begin{pmatrix}\alpha\\ \beta\end{pmatrix}$$

The ground state is still degenerate but lowered an amount

$$\lambda^2\left[\frac{1}{(D')^2}+\frac{1}{4D^2}\right]$$

Applying a magnetic field results in an interaction of the form

$$\underline{H}\cdot(\underline{L}+2\underline{S})$$

causing the energy levels to separate by an amount

$$\Delta E = g\beta H$$

Using degenerate perturbation theory to first order, first with $\underline{H}$ parallel to z, and then with $\underline{H}$ parallel to the x axis results in

$$g_{\parallel} = 2\left(1-\frac{4\lambda}{D'}\right)$$

$$g_x = 2\left(1-\frac{\lambda}{D}\right)$$

Now if $g_{\perp} > g_{\parallel}$, which happens to be the case for the vanadyl ion, then $4D > D'$, which is very easily satisfied when the crystal field is assumed to have strong cylindrical symmetry.

$^4\underline{F}$ g Values. For the 3 electrons in the ^4F ground state in cubic or tetragonal field the first order g value is calculated in a similar manner and is found to be

$$g = 2\left(1-\frac{4\lambda}{10Dq}\right)$$

APPENDIX C

ANGULAR VARIATION OF ENERGY LEVELS OF THE RHOMBIC SPIN HAMILTONIAN

We start with the rhombic spin Hamiltonian with the principal axes of the several tensors coincident (Chapter III)

$$\begin{aligned}\mathcal{H} = {} & \beta[g_z H_z S_z + g_x H_x S_x + g_y H_y S_y] + D[S_z^2 - \tfrac{1}{3}S(S+1)] + E(S_x^2 - S_y^2) \\ & + A I_z S_z + B_x I_x S_x + B_y I_y S_y + Q'[I_z^2 - \tfrac{1}{3}I(I+1)] \\ & + Q''[I_x^2 - I_y^2] + \beta_N[g_{Nx} H_x I_x + g_{Ny} H_y I_y + g_{Nz} H_z I_z]\end{aligned} \tag{C-1}$$

1. ZEEMAN TERM

Since the Zeeman term, $\sum_i \beta g_i H_i S_i$, has the largest interaction by at least one order of magnitude, we proceed to make a coordinate transformation in order to diagonalize this term and then treat the additional terms by perturbation theory.

The coordinate system x', y', z' in which the Zeeman term is diagonal is related to the x, y, z coordinate system by the Eulerian angles θ, φ and ψ as shown below:

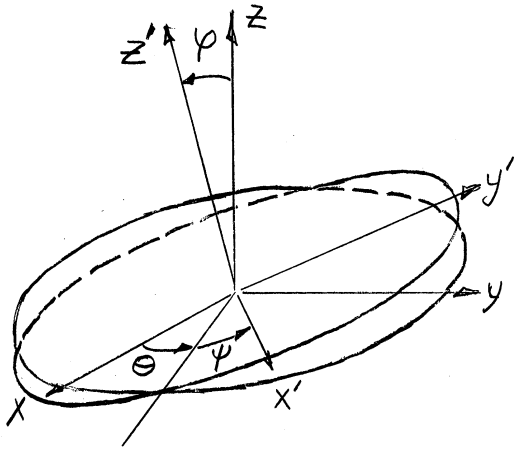

Then, since

$$\underline{S} = (\hat{e}_1 \cdot \underline{S})\hat{e}_1 + (\hat{e}_2 \cdot \underline{S})\hat{e}_2 + (\hat{e}_3 \cdot \underline{S})\hat{e}_3$$

$$= (\hat{e}_1' \cdot \underline{S})\hat{e}_1' + (\hat{e}_2' \cdot \underline{S})\hat{e}_2' + (\hat{e}_3' \cdot \underline{S})\hat{e}_3'$$

where $\hat{e}_1$, $\hat{e}_2$, $\hat{e}_3$ are unit vectors in the x, y, z directions respectively, we find that the components of $\underline{S}$ in the x, y, z coordinate system are related to those in the x', y', z' coordinate system by the following equations:

$$S_x = S_x'(\cos\theta\cos\psi - \sin\theta\cos\varphi\sin\psi) + S_y'(-\cos\theta\sin\psi - \sin\theta\cos\varphi\cos\psi) + S_z' \sin\theta\sin\varphi$$

$$S_y = S_x'(\sin\theta\cos\psi + \cos\theta\cos\varphi\sin\psi) + S_y'(-\sin\theta\sin\psi + \cos\theta\cos\varphi\cos\psi) + S_z'(-\cos\theta\sin\varphi)$$

$$S_z = S_x' \sin\varphi\sin\psi + S_y' \sin\varphi\cos\psi + S_z' \cos\varphi \qquad \text{(C-2)}$$

Now, if

$$H_x = H \sin\Theta \cos\delta$$
$$H_y = H \sin\Theta \sin\delta$$
$$H_z = H \cos\Theta$$

and we require

$$\cos\Theta = -\frac{g_y}{g_\perp}\sin\delta$$
$$\sin\Theta = \frac{g_x}{g_\perp}\cos\delta$$
$$\sin\varphi = \frac{g_\perp}{g}\sin\Theta$$
$$\cos\varphi = \frac{g_z}{g}\cos\Theta$$

where

$$g_\perp^2 \equiv g_x^2\cos^2\delta + g_y^2\sin^2\delta$$

and

$$g^2 \equiv g_z^2\cos^2\Theta + g_\perp^2\sin^2\Theta \qquad \text{(C-3)}$$

then

$$g_z H_z S_z + g_x H_x S_x + g_y H_y S_y \Rightarrow g H S_z'$$

(i.e., the Zeeman term is diagonalized).

2. FINE STRUCTURE TERMS

With this transformation the axial and rhombic fine structure terms become

$$D\left[S_z^2-\tfrac{1}{3}S(S+1)\right] \Rightarrow D\Big\{\left(\frac{g_z}{g}\right)^2\cos^2\Theta\,(S_z')^2+\frac{g_\perp^2}{4g^2}\sin^2\Theta\,(S_+'S_-'+S_-'S_+')$$

$$-\frac{g_\perp^2}{4g^2}\sin^2\Theta\left[(S_+')^2e^{2i\Psi}+(S_-')^2e^{-2i\Psi}\right]+i\,\frac{g_\perp g_z}{2g^2}\sin\Theta\cos\Theta\,e^{i\Psi}(S_z'S_-'+S_-'S_z')$$

$$-\tfrac{1}{3}S(S+1)\Big\}$$

$$E\left(S_x^2-S_y^2\right)\Rightarrow E\Big\{\frac{\sin^2\Theta}{g^2}\left(g_x^2\cos^2\delta-g_y^2\sin^2\delta\right)\left[(S_z')^2-\tfrac{1}{4}(S_+'S_-'+S_-'S_+')\right]$$

$$+(S_+'S_z'+S_z'S_+')e^{i\Psi}\left[-\frac{g_xg_y}{g\,g_\perp}\sin\Theta\sin\delta\cos\delta+\frac{i}{2}\frac{g_z}{g^2g_\perp}\sin\Theta\cos\Theta\left(g_x^2\cos^2\delta\right.\right.$$

$$\left.\left.-g_y^2\sin^2\delta\right)\right] \qquad \text{(C-4)}$$

$$+(S_-'S_z'+S_z'S_-')e^{-i\Psi}\left[\ \text{"}\qquad\qquad\text{"}\ \text{(complex conjugate)}\ \right]$$

$$+(S_+')^2e^{2i\Psi}\left[-\frac{1}{4g_\perp^2}\left(1-\frac{g_z^2}{g^2}\cos^2\Theta\right)\left(g_x^2\cos^2\delta-g_y^2\sin^2\delta\right)\right.$$

$$\left.-i\,\frac{g_xg_yg_z}{g\,g_\perp^2}\cos\Theta\sin\delta\cos\delta\right]$$

$$+(S_-')^2e^{-2i\Psi}\left[\ \text{"}\qquad\qquad\text{"}\ \text{(complex conjugate}\ \right]$$

which give the following contributions to the energy level $|SM\rangle$

$$+\frac{M^2}{2}\left[D\left(3\,\frac{g_z^2}{g^2}\cos^2\Theta-1\right)+3E\,\frac{\sin^2\Theta}{g^2}\left(g_x^2\cos^2\delta-g_y^2\sin^2\delta\right)\right]$$

$$+S(S+1)\left[D\left(\frac{g_\perp^2}{2g^2}\sin^2\Theta-\frac{1}{3}\right)-\frac{E}{2}\,\frac{\sin^2\Theta}{g^2}\left(g_x^2\cos^2\delta-g_y^2\sin^2\delta\right)\right]$$

$$+\frac{2MS(S+1)-M(2M^2+1)}{8g\beta H}\Big\{\Big[D\,\frac{g_\perp^2}{g^2}\sin^2\Theta+\frac{E}{g_\perp^2}\left(g_x^2\cos^2\delta-g_y^2\sin^2\delta\right)\left(1+\frac{g_z^2}{g^2}\cos^2\Theta\right)\Big]^2 \qquad \text{(C-5)}$$

$$+16E^2\,\frac{g_x^2g_y^2g_z^2}{g_\perp^4g^2}\cos^2\Theta\sin^2\delta\cos^2\delta\Big\}$$

$$+\frac{M(8M^2+1)-4MS(S+1)}{2g\beta H}\Big\{\Big[D-\frac{E}{g_\perp^2}\left(g_x^2\cos^2\delta-g_y^2\sin^2\delta\right)\Big]^2\frac{g_\perp^2g_z^2}{g^2}\sin^2\Theta\cos^2\Theta$$

$$+4E^2\,\frac{g_x^2g_y^2}{g_\perp^2g^2}\sin^2\Theta\sin^2\delta\cos^2\delta\Big\}$$

the first being the diagonal contribution, the latter two resulting from second order contributions.

3. HYPERFINE TERM

For the hyperfine term $AI_zS_z+B_xI_xS_x+B_yI_yS_y$ the coordinate rotation matrix for the spin operators I_x, I_y, I_z is

$$\begin{pmatrix} \frac{B_x}{B_\perp}\cos\psi & \frac{B_y}{B_\perp}\sin\psi & 0 \\ -\frac{B_y}{B_\perp}\sin\psi & \frac{B_x}{B_\perp}\cos\psi & 0 \\ 0 & 0 & 1 \end{pmatrix} \begin{pmatrix} 1 & 0 & 0 \\ 0 & \frac{A}{K}\cos\varphi & \frac{B_\perp}{K}\sin\varphi \\ 0 & -\frac{B_\perp}{K}\sin\varphi & \frac{A}{K}\cos\varphi \end{pmatrix} \begin{pmatrix} \cos\theta & \sin\theta & 0 \\ -\sin\theta & \cos\theta & 0 \\ 0 & 0 & 1 \end{pmatrix}$$

where the determinant of each matrix set equal to unity defines $B_\perp$ and K; that is

$$A^2\cos^2\varphi + B_\perp^2\sin^2\varphi = K^2$$

$$B_x^2\cos^2\psi + B_y^2\sin^2\psi = B_\perp^2$$

The resulting equations for I_z, I_+, and I_- become

$$I_z = \frac{A}{K}\cos\varphi I_z' - i\frac{\sin\varphi}{2K}(B_x\cos\psi+iB_y\sin\psi)I_+' + i\frac{\sin\varphi}{2K}(B_x\cos\psi-iB_y\sin\psi)I_-'$$

$$I_+ = \frac{e^{i\theta}}{2}\frac{(B_x\cos\psi+iB_y\sin\psi)}{B_\perp}\left(1+\frac{A}{K}\cos\varphi\right)I_+' - ie^{i\theta}\sin\varphi\frac{B_\perp}{K}I_z' + \frac{e^{i\theta}}{2}\frac{(B_x\cos\psi-iB_y\sin\psi)}{B_\perp}\left(1-\frac{A}{K}\cos\varphi\right)I_-' \qquad \text{(C-6)}$$

$$I_- = \frac{e^{-i\theta}}{2}\frac{(B_x\cos\psi+iB_y\sin\psi)}{B_\perp}\left(1-\frac{A}{K}\cos\varphi\right)I_+' + ie^{-i\theta}\sin\varphi\frac{B_\perp}{K}I_z' + \frac{e^{i\theta}}{2}\frac{(B_x\cos\psi-iB_y\sin\psi)}{B_\perp}\left(1+\frac{A}{K}\cos\varphi\right)I_-'$$

Putting these equations, as well as those for S_x, S_y, and S_z (C-2), in the hyperfine term and evaluating the resulting expression for the state $|SMIm\rangle$ yields the following addition to the energy level

$$
\begin{aligned}
&+Mm\left\{\frac{A^2}{K}\frac{g_z^2}{g^2}\cos^2\Theta+\frac{B_\perp}{K}\frac{g_\perp^2}{g^2}\sin^2\Theta\left[\frac{B_x+B_y}{2}+\frac{B_x-B_y}{2g_\perp^2}\left(g_x^2\cos^2\delta-g_y^2\sin^2\delta\right)\right]\right\}\\
&+\frac{2M^2}{K}\frac{g_\perp^2}{g^2}B_\perp^2\left\{\left[\frac{A}{2K}\left(1-\frac{B_x+B_y}{2B_\perp}\right)-\frac{B_x-B_y}{4B_\perp g_\perp^2}\left(g_x^2\cos^2\delta-g_y^2\sin^2\delta\right)\right]^2\frac{g_z^2}{g^2}\cos^2\Theta\right.\\
&\qquad\left.+\frac{g_x^2g_y^2}{g_\perp^4}\sin^2\delta\cos^2\delta\,\frac{(B_x-B_y)^2}{4B_\perp^2}\right\}\\
&+\frac{2Mm^2}{g\beta H}\frac{g_\perp^2}{g^2}\sin^2\Theta\left\{\frac{g_z^2}{g^2}\cos^2\Theta\left[\frac{1}{2K}\left(A^2-B_\perp\frac{(B_x+B_y)}{2}\right)-\frac{B_\perp(B_x-B_y)}{4K}\times\right.\right.\\
&\qquad\left.\left.\left(\frac{g_x^2\cos^2\delta-g_y^2\sin^2\delta}{g_\perp^2}\right)\right]^2+\frac{g_x^2g_y^2}{g_\perp^4}\sin^2\delta\cos^2\delta\,\frac{(B_x-B_y)^2B_\perp^2}{4K^2}\right\}\\
&+\frac{I(I+1)M-mS(S+1)+mM(M-m)}{g\beta H}\frac{B_\perp^2}{2}\left\{\left[\frac{A}{2K}\frac{g_\perp^2}{g^2}\sin^2\Theta+\frac{B_x+B_y}{4B_\perp}\times\right.\right.\\
&\qquad\left.\left(1+\frac{A}{K}\cos^2\Theta\right)-\frac{B_x-B_y}{4B_\perp}\left(1-\frac{A}{K}\frac{g_z^2}{g^2}\cos^2\Theta\right)\left(\frac{g_x^2\cos^2\delta-g_y^2\sin^2\delta}{g_\perp^2}\right)\right]^2\\
&\qquad\left.+\frac{g_z^2g_x^2g_y^2}{g^2g_\perp^4}\cos^2\Theta\sin^2\delta\cos^2\delta\,\frac{(B_x-B_y)^2}{4B_\perp^2}\left(1-\frac{A}{K}\right)^2\right\}\\
&+\frac{I(I+1)M+mS(S+1)-mM(m+M)}{g\beta H}\frac{B_\perp^2}{2}\left\{\left[\frac{A}{2K}\frac{g_\perp^2}{g^2}\sin^2\Theta-\frac{B_x+B_y}{4B_\perp}\times\right.\right.\\
&\qquad\left.\left(1-\frac{A}{K}\frac{g_z^2}{g^2}\cos^2\Theta\right)+\frac{B_x-B_y}{4B_\perp}\left(1+\frac{A}{K}\frac{g_z^2}{g^2}\cos^2\Theta\right)\left(\frac{g_x^2\cos^2\delta-g_y^2\sin^2\delta}{g_\perp^2}\right)\right]^2\\
&\qquad\left.+\frac{g_z^2g_x^2g_y^2}{g^2g_\perp^4}\cos^2\Theta\sin^2\delta\cos^2\delta\,\frac{(B_x-B_y)^2}{4B_\perp^2}\left(1+\frac{A}{K}\right)^2\right\}
\end{aligned}
\qquad \text{(C-7)}
$$

where the first term is the diagonal contribution and the other terms are evaluated from second order corrections.

4. QUADRUPOLE TERMS

The quadrupole term $Q'\left[I_z^2-\frac{1}{3}I(I+1)\right]+Q''\left[I_x^2-I_y^2\right]$ rotates like the fine structure term so that its contribution to the energy level can be written immediately as

$$+m^2\left[Q'\left(1-\frac{3}{2}\frac{B_\perp^2}{K}\frac{g_\perp^2}{g^2}\sin^2\Theta\right)+\frac{3}{2}Q''\frac{B_\perp^2}{g^2K^2}\sin^2\Theta\left(g_x^2\cos^2\delta-g_y^2\sin^2\delta\right)\right]$$

$$+I(I+1)\left[Q'\left(\frac{B_\perp^2}{2K^2}\frac{g_\perp^2}{g^2}\sin^2\Theta-\frac{1}{3}\right)-\frac{Q''}{2}\frac{B_\perp^2}{g^2}\sin^2\Theta\left(g_x^2\cos^2\delta-g_y^2\sin^2\delta\right)\right]$$

$$+\frac{4mI(I+1)-2m(2m^2+1)}{KM}\left\{\left[Q'\frac{g_z^2B_\perp^2}{4g^2K^2}\sin^2\Theta+\frac{Q''}{4g_\perp^2}\left(g_x^2\cos^2\delta-g_y^2\sin^2\delta\right)\times\right.\right.$$

$$\left.\left.\left(1+\frac{A^2g_z^2}{K^2g^2}\cos^2\Theta\right)\right]^2+(Q'')^2\frac{A^2g_z^2g_x^2g_y^2}{K^2g^2g_\perp^4}\cos^2\Theta\sin^2\delta\cos^2\delta\right\} \qquad \text{(C-8)}$$

$$+\frac{2m(8m^2+1)-8mI(I+1)}{KM}\left\{\left[Q'-Q''\left(g_x^2\cos^2\delta-g_y^2\sin^2\delta\right)\right]^2\times\right.$$

$$\left.\frac{A^2}{4K^4}\frac{g_z^2g_\perp^2}{g^4}\sin^2\Theta\cos^2\Theta+\frac{(Q'')^2}{K^2}\frac{g_x^2g_y^2}{g^2g_\perp^2}\sin^2\Theta\cos^2\delta\sin^2\delta\right\}$$

5. NUCLEAR INTERACTION TERM

For the term involving the interaction of the magnetic field with the nucleus $\beta_N\left[g_{Nx}H_xI_x+g_{Ny}H_yI_y+g_{Nz}H_zI_z\right]$ the same straightforward procedure yields the following contribution to the energy levels,

$$+\beta_N Hm\left\{\frac{A}{K}g_{Nz}\frac{g_z}{g}\cos^2\Theta+\frac{B_\perp}{Kg}\sin^2\Theta\left[g_{Ny}g_y\sin^2\delta+g_{Nx}g_x\cos^2\delta\right]\right\}$$

$$+\beta_N^2\frac{H^2m}{2KM}\left\{\left[\frac{Ag_z}{Kgg_\perp}\sin\Theta\cos\Theta\left(g_{Ny}g_y\sin^2\delta+g_{Nx}g_x\cos^2\delta\right)\right.\right. \qquad \text{(C-9)}$$

$$\left.\left.-\frac{B_\perp g+g_{Nz}}{Kg}\sin\Theta\cos\Theta\right]^2+\frac{\sin^2\Theta\sin^2\delta\cos^2\delta}{g_\perp^2}\left(g_{Nx}g_y-g_{Ny}g_x\right)^2\right\}$$

Thus, to second order the angular variation in the energy level E_{M_m} from the rhombic spin Hamiltonian is given by

$$E_{M_m} = g\beta HM + (C-5) + (C-7) + (C-8) + (C-9)$$

In EPR work the energy for resonance is given by the selection rule $\Delta M \pm 1$, $\Delta m = 0$. Evaluating the expression E_{M_m} for this transition we obtain:

$$\begin{aligned}
E_{M,m} - E_{M-1,m} = h\nu = {} & g\beta H + (M-\tfrac{1}{2})\left[D\left(3\frac{g_z^2}{g^2}\cos^2\Theta - 1\right)\right. \\
& \left. + 3E\frac{\sin^2\Theta}{g^2}(g_x^2\cos^2\delta - g_y^2\sin^2\delta)\right] \\
& + \frac{2S(S+1)-6M(M-1)-3}{8g\beta H}\left\{\left[D\frac{g_\perp^2}{g^2}\sin^2\Theta + \frac{E^2}{g_\perp^2}(g_x^2\cos^2\delta - g_y^2\sin^2\delta)\times\right.\right. \\
& \left.\left.(1+\frac{g_z^2}{g^2}\cos^2\Theta)\right]^2 + 16E^2\frac{g_x^2g_y^2g_z^2}{g_\perp^4 g^2}\cos^2\Theta\sin^2\delta\cos^2\delta\right\} \\
& + \frac{24M(M-1)-4S(S+1)+9}{2g\beta H}\left\{\left[D - E\frac{(g_x^2\cos^2\delta - g_y^2\sin^2\delta)}{g_\perp^2}\right]^2\frac{g_\perp^2 g_z^2}{g^4}\sin^2\Theta\cos^2\Theta\right. \\
& \left. + 4E^2\frac{g_x^2g_y^2}{g_\perp^2 g^2}\sin^2\Theta\sin^2\delta\cos^2\delta\right\} \\
& + m\left\{\frac{A^2}{K}\frac{g_z^2}{g^2}\cos^2\Theta + \frac{B_\perp}{K}\frac{g_z^2}{g^2}\sin^2\Theta\left[\frac{B_x+B_y}{2} + \frac{B_x-B_y}{2}\frac{(g_x^2\cos^2\delta - g_y^2\sin^2\delta)}{g_\perp^2}\right]\right\} \\
& + 4(M-\tfrac{1}{2})\frac{g_\perp^2 B_\perp^2}{g^2 K}\sin^2\Theta\left\{\left[\frac{A}{K}\left(\frac{1}{2} - \frac{B_x+B_y}{4B_\perp}\right) - \frac{B_x-B_y}{4B_\perp}\frac{(g_x^2\cos^2\delta - g_y^2\sin^2\delta)}{g_\perp^2}\right]^2\frac{g_z^2}{g^2}\cos^2\Theta\right. \\
& \left. + \frac{g_x^2g_y^2}{g_\perp^4}\sin^2\delta\cos^2\delta\frac{(B_x-B_y)^2}{4B_\perp^2}\right\} \\
& + \frac{2m^2g_\perp^2}{g\beta H}\sin^2\Theta\left\{\left[\frac{1}{2K}\left(A^2 - B_\perp\frac{B_x+B_y}{2}\right) - \frac{B_\perp(B_x-B_y)}{4K}\frac{(g_x^2\cos^2\delta - g_y^2\sin^2\delta)}{g_\perp^2}\right]^2\frac{g_z^2}{g^2}\cos^2\Theta\right. \\
& \left. + \frac{g_x^2g_y^2}{g_\perp^4}\cos^2\delta\sin^2\delta\frac{B_\perp^2(B_x-B_y)^2}{4K^2}\right\} \\
& +
\end{aligned}$$

$$+\frac{I(I+1)-m^2+2m(M-\frac{1}{2})}{2g\beta H}B_\perp^2\left\{\left[\frac{A}{2K}\frac{g_\perp^2}{g^2}\sin^2\Theta+\frac{B_x+B_y}{4B_\perp}\left(1+\frac{A}{K}\frac{g_z^2}{g^2}\cos^2\Theta\right)-\frac{B_x-B_y}{4g_\perp^2B_\perp}\left(1-\frac{A}{K}\frac{g_z^2}{g^2}\cos^2\Theta\right)\times\right.\right.$$
$$\left.\left.(g_x^2\cos^2\delta-g_y^2\sin^2\delta)\right]^2+\frac{g_z^2}{g^2}\cos^2\Theta\,\frac{(B_x-B_y)^2}{4B_\perp^2}\left(1-\frac{A}{K}\right)^2\frac{g_x^2g_y^2}{g_\perp^2}\sin^2\delta\cos^2\delta\right\}$$

$$+\frac{I(I+1)-m^2-2m(M-\frac{1}{2})}{2g\beta H}B_\perp^2\left\{\left[\frac{A}{2K}\frac{g_\perp^2}{g^2}\sin^2\Theta-\frac{B_x+B_y}{4B_\perp}\left(1-\frac{A}{K}\frac{g_z^2}{g^2}\cos^2\Theta\right)+\frac{B_x-B_y}{4g_\perp^2B_\perp}\left(1+\frac{A}{K}\frac{g_z^2}{g^2}\cos^2\Theta\right)\times\right.\right.$$
$$\left.\left.(g_x^2\cos^2\delta-g_y^2\sin^2\delta)\right]^2+\frac{g_z^2}{g^2}\cos^2\Theta\,\frac{(B_x-B_y)^2}{4B_\perp^2}\left(1+\frac{A}{K}\right)^2\frac{g_x^2g_y^2}{g_\perp^4}\sin^2\delta\cos^2\delta\right\}$$

$$+\frac{m(2m^2+1)-2mI(I+1)}{8KM(M-1)}\left\{Q'\frac{B_\perp^2}{K^2}\frac{g_\perp^2}{g^2}\sin^2\Theta+\frac{Q''}{g_\perp^2}\left(1+\frac{A^2}{K^2}\frac{g_z^2}{g^2}\cos^2\Theta\right)(g_x^2\cos^2\delta-g_y^2\sin^2\delta)\right]^2$$
$$\left.+16(Q'')^2\frac{A^2}{K^2}\frac{g_x^2g_y^2g_z^2}{g_\perp^2g^2}\cos^2\Theta\sin^2\delta\cos^2\delta\right\}$$

$$+\frac{4mI(I+1)-m(8m^2+1)}{2KM(M-1)}\left\{\left[Q'-\frac{Q''}{g_\perp^2}(g_x^2\cos^2\delta-g_y^2\sin^2\delta)\right]^2\frac{g_\perp^2g_z^2}{g^4K^4}A^2\sin^2\Theta\cos^2\Theta+4\frac{(Q'')^2}{K^2}\frac{g_x^2g_y^2}{g_\perp^2g^2}\sin^2\Theta\sin^2\delta\cos^2\delta\right\}$$

$$-\frac{mH^2\beta_N^2}{2KM(M-1)}\left\{\left[\frac{g_{NZ}B_\perp g_\perp}{Kg}\sin\Theta\cos\Theta-\frac{Ag_z}{Kgg_\perp}\sin\Theta\cos\Theta(g_{NY}g_y\sin^2\delta+g_{NX}g_x\cos^2\delta)\right]^2\right.$$
$$\left.+\sin^2\Theta\sin^2\delta\cos^2\delta\,\frac{(g_{NX}g_y-g_{NY}g_X)}{g_\perp^2}\right\}$$

APPENDIX D

FINE STRUCTURE ENERGY LEVELS (RHOMBIC)

Given the rhombic spin Hamiltonian we wish to calculate the energy levels for the magnetic field in the x, y, and z directions for only the Zeeman and fine structure terms.

1. H PARALLEL TO z AXIS

$$\mathcal{H}_z = g_z \beta H S_z + D\left[S_z^2 - \tfrac{1}{3}S(S+1)\right] + \frac{E}{2}\left[S_+^2 + S_-^2\right]$$

Degenerate perturbation calculations leads to the following secular determinant:

	$-\frac{3}{2}$	$-\frac{1}{2}$	$\frac{1}{2}$	$\frac{3}{2}$
$-\frac{3}{2}$	$-\frac{3}{2}g_z\beta H + D - \lambda$		$\sqrt{3}E$	
$-\frac{1}{2}$		$-\frac{1}{2}g_z\beta H - D - \lambda$		$\sqrt{3}E$
$\frac{1}{2}$	$\sqrt{3}E$		$\frac{1}{2}g_z\beta H - D - \lambda$	
$\frac{3}{2}$		$\sqrt{3}E$		$\frac{3}{2}g_z\beta H + D - \lambda$

which may be solved for the following energy levels

$$\tfrac{3}{2}: \quad \lambda_2^+ = \tfrac{1}{2}g_z\beta H + \sqrt{3E^2 + (g_z\beta H + D)^2}$$

$$\tfrac{1}{2}: \quad \lambda_1^+ = -\tfrac{1}{2}g_z\beta H + \sqrt{3E^2 + (g_z\beta H - D)^2}$$

$$-\tfrac{1}{2}: \quad \lambda_2^- = \tfrac{1}{2} g_z \beta H - \sqrt{3E^2 + (g_z \beta H + D)^2}$$

$$-\tfrac{3}{2}: \quad \lambda_1^- = -\tfrac{1}{2} g_z \beta H - \sqrt{3E^2 + (g_z \beta H - D)^2}$$

For the transitions $\Delta M = \pm 1$ the change in energy is

$$E_{3/2,\,1/2} = \lambda_2^+ - \lambda_1^+ = g_z \beta H_{3/2} + \sqrt{3E^2 + (g_z \beta H_{3/2} + D)^2} - \sqrt{3E^2 + (g_z \beta H_{3/2} - D)^2}$$

$$E_{1/2,-1/2} = \lambda_1^+ - \lambda_2^+ = -g_z \beta H_{1/2} + \sqrt{3E^2 + (g_z \beta H_{1/2} - D)^2} + \sqrt{3E^2 + (g_z \beta H_{1/2} + D)^2}$$

$$E_{-1/2,-3/2} = \lambda_2^- - \lambda_1^- = g_z \beta H_{-1/2} - \sqrt{3E^2 + (g_z \beta H_{-1/2} + D)^2} + \sqrt{3E^2 + (g_z \beta H_{-1/2} - D)^2}$$

Making use of a Taylors expansion for each of the square roots and solving for the magnetic field (in the major term) yields the following equation (to fourth order):

$$(A) \quad H_{3/2} \simeq \frac{h\nu}{g_z \beta} - 2\frac{D}{g_z \beta} + \frac{3E^2 D}{g_z^3 \beta^3 H_{3/2}^2}\left[\frac{1}{1 - \left(\frac{D}{g_z \beta H_{3/2}}\right)^2}\right] - \frac{27}{4}\frac{E^4 D}{g_z^5 \beta^5}\frac{1}{H_{3/2}^4}$$

$$(B) \quad H_{1/2} \simeq \frac{h\nu}{g_z \beta} - \frac{3E^2}{g_z^2 \beta^2 H_{1/2}}\left[\frac{1}{1 - \left(\frac{D}{g_z \beta H_{1/2}}\right)^2}\right] + \frac{9}{4}\frac{E^4 D}{g_z^5 \beta^5 H_{1/2}^4}\left[1 + \frac{3D}{g_z \beta H}\right]$$

$$(C) \quad H_{-1/2} \simeq \frac{h\nu}{g_z \beta} + 2\frac{D}{g_z \beta} - \frac{3E^2 D}{g_z^3 \beta^3 H_{-1/2}^2}\left[\frac{1}{1 - \left(\frac{D}{g_z \beta H_{-1/2}}\right)^2}\right] + \frac{27}{4}\frac{E^4 D}{g_z^5 \beta^5}\frac{1}{H_{-1/2}^4}$$

For the magnetic field parallel to the x direction, the Zeeman term is not diagonal. To diagonalize, a coordinate rotation about the y axis by 90° is performed, resulting in the following fine structure spin Hamiltonian

$$\mathcal{H}_x' = g_x\beta H S_z' + \frac{D}{4}\left[(S_+')^2 + (S_-')^2 + S_+S_- + S_-S_+ - \frac{5}{4}\right] + E\left\{(S_z')^2 + \frac{1}{4}\left[(S_+')^2 + (S_-')^2 - S_-S_+ - S_+S_-\right]\right\}$$

which leads to the following secular determinant:

	$-\frac{3}{2}$	$-\frac{1}{2}$	$\frac{1}{2}$	$\frac{3}{2}$
$-\frac{3}{2}$	$-\frac{3}{2}g_x\beta H - \lambda - \frac{1}{2}(D-3E)$		$\frac{\sqrt{3}}{2}(D+E)$	
$-\frac{1}{2}$		$-\frac{1}{2}g_x\beta H - \lambda + \frac{1}{2}(D-3E)$		$\frac{\sqrt{3}}{2}(D+E)$
$\frac{1}{2}$	$\frac{\sqrt{3}}{2}(D+E)$		$\frac{1}{2}g_x\beta H - \lambda + \frac{1}{2}(D-3E)$	
$\frac{3}{2}$		$\frac{\sqrt{3}}{2}(D+E)$		$\frac{3}{2}g_x\beta H - \lambda - \frac{1}{2}(D-3E)$

which is the same secular determinant for H parallel to the z axis with $g_x \rightarrow g_z$; $-\frac{D-3E}{2} \rightarrow D$ and $\frac{D+E}{2} \rightarrow E$; thus, with these changes, Eqs. (A), (B), and (C) also hold for the x axis. Similarly for the magnetic field parallel to the y axis the following substitutions are made:

$g_y \rightarrow g_z$; $-\frac{D+3E}{2} \rightarrow D$ and $\frac{D-E}{2} \rightarrow E$.

APPENDIX E

g AND A TENSOR PRINCIPAL AXES NOT COINCIDENT

In this section we would like to note the effect on the hyperfine term $\underline{I}\cdot\underline{\underline{A}}\cdot\underline{S}$ when the principal axes of the A tensor do not coincide with the principal axes of the g tensor.

We denote by x, y, and z and x', y', and z' the principal axes of the g and A tensors, respectively. Then, performing a coordinate rotation R on the term $\underline{I}\cdot\underline{\underline{A}}\cdot\underline{S}$, we obtain in the unprimed coordinate system

$$\underline{I}\cdot\underline{\underline{A}}\cdot\underline{S} \Rightarrow IR^{-1}RAR^{-1}RS$$

where

$$A=\begin{pmatrix} A_{x'x'} & 0 & \\ & A_{y'y'} & \\ 0 & & A_{z'z'} \end{pmatrix}\ ;\ IR^{-1}=(I_x, I_y, I_z)\ ;\ RS=\begin{pmatrix} S_x \\ S_y \\ S_z \end{pmatrix}$$

and

$$R=\begin{pmatrix} \cos\psi & \sin\psi & 0 \\ -\sin\psi & \cos\psi & 0 \\ 0 & 0 & 1 \end{pmatrix}\begin{pmatrix} 1 & 0 & 0 \\ 0 & \cos\varphi & \sin\varphi \\ 0 & -\sin\varphi & \cos\varphi \end{pmatrix}\begin{pmatrix} \cos\theta & \sin\theta & 0 \\ -\sin\theta & \cos\theta & 0 \\ 0 & 0 & 1 \end{pmatrix}$$

where θ, φ, ψ are the Eulerian angles relating the primed to the unprimed coordinate system as shown below.

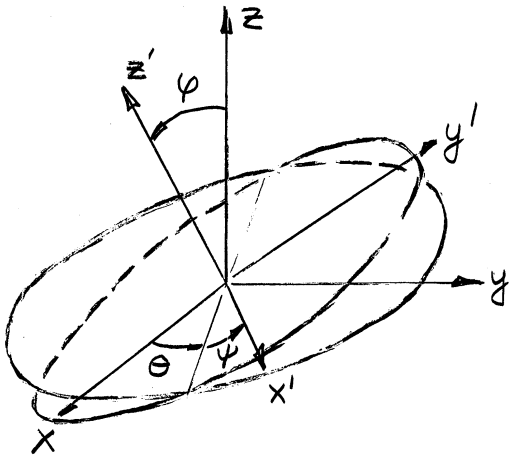

For the special case when the z axes of the two tensors are coincident, $\varphi = 0$, and we may choose $\Psi = 0$ also. Then $IR^{-1}\,RAR^{-1}\,RS$ becomes, dropping the primes on the $A_{i'i'}$;

$$(I_x, I_y, I_z)\begin{pmatrix} A_{xx}\cos^2\theta + A_{yy}\sin^2\theta & \sin\theta\cos\theta(A_{yy}-A_{xx}) & 0 \\ \sin\theta\cos\theta(A_{yy}-A_{xx}) & A_{xx}\sin^2\theta + A_{yy}\cos^2\theta & 0 \\ 0 & 0 & A_{zz} \end{pmatrix}\begin{pmatrix} S_x \\ S_y \\ S_z \end{pmatrix}$$

$$= S_x I_x (A_{xx}\cos^2\theta + A_{yy}\sin^2\theta) + S_y I_y (A_{xx}\sin^2\theta + A_{yy}\cos^2\theta)$$

$$+ A_{zz} I_z S_z + S_x I_y (A_{yy}-A_{xx})\sin\theta\cos\theta + S_y I_x (A_{yy}-A_{xx})\sin\theta\cos\theta$$

APPENDIX F

ANGULAR VARIATION OF ENERGY LEVELS FOR APPENDIX E

As shown in Appendix E, when the principal axes of the g and A tensor do not coincide, cross terms arise so that the hyperfine interaction term in the spin Hamiltonian

$$AI_zS_z + B_xI_xS_x + B_yI_yS_y \tag{E-1}$$

has to be supplemented with terms of the form

$$\sum_{ij}{}' F_{ij}(S_iI_j+S_jI_i) + \sum_{ij}{}' G_{ij}(S_iI_j - S_jI_i) \tag{E-2}$$

where the prime on the sum denotes $i\neq j$ and we have written the off-diagonal terms in a symmetric and antisymmetric form. However, the hyperfine tensor may be written in a diagonal form (E-1) so that any orthogonal transformation will leave the A tensor symmetric—thus $G_{ij} \equiv 0$.

Writing $\mathcal{H}_{ij} \equiv F_{ij}+F_{ji}$, we obtain for the form (E-2) the following terms:

$$\frac{\mathcal{H}_{xy}}{2i}(S_+I_+ - S_-I_-) + \frac{1}{2}\left[\mathcal{H}_{xz} - i\mathcal{H}_{yz}\right](S_zI_+ + S_+I_z) + \frac{1}{2}\left[\mathcal{H}_{xz} + i\mathcal{H}_{yz}\right](S_zI_- + S_-I_z) \tag{E-3}$$

Since we want the angular variation of the energy levels due to the hyperfine term, we perform a coordinate rotation on the spin operators as in Appendix C and obtain for the transformed equation of (E-3)

$$(E\text{-}3) \Rightarrow I_z' S_z' \frac{\sin\varphi}{K}\left[-\mathscr{H}_{xy} B_\perp \sin\varphi \sin 2\theta + (A+B_\perp)\cos\varphi(\mathscr{H}_{xz}\sin\theta - \mathscr{H}_{yz}\cos\theta)\right]$$

$$+ I_z' S_+' \frac{e^{i\psi}}{2K}\left[-\mathscr{H}_{xy} B_\perp \sin\varphi(\cos 2\theta + i\cos\varphi\sin 2\theta) + (\mathscr{H}_{xz}\cos\theta + \mathscr{H}_{yz}\sin\theta)A\cos\varphi + i(\mathscr{H}_{xz}\sin\theta - \mathscr{H}_{yz}\cos\theta)(A\cos^2\varphi - B_\perp\sin^2\varphi)\right]$$

$$+ I_z' S_-' \frac{e^{-i\psi}}{2K}\Big[\quad \text{complex conjugate} \quad \Big]$$

$$+ S_z' I_+' \frac{(B_x\cos\psi + iB_y\sin\psi)}{2B_\perp}\left[-\mathscr{H}_{xy}\sin\varphi(\cos 2\theta + i\frac{A}{K}\cos\varphi\sin 2\theta) + (\mathscr{H}_{xz}\cos\theta + \mathscr{H}_{yz}\sin\theta)\cos\varphi + i(\mathscr{H}_{xz}\sin\theta - \mathscr{H}_{yz}\cos\theta)(\frac{A}{K}\cos^2\varphi - \frac{B_\perp}{K}\sin^2\varphi)\right]$$

$$+ S_z' I_-' \frac{(B_x\cos\psi - iB_y\sin\psi)}{2B_\perp}\Big[\quad \text{complex conjugate} \quad \Big]$$

$$- iS_+' I_+' \frac{(B_x\cos\psi + iB_y\sin\psi)}{4B_\perp} e^{i\psi}\left\{\mathscr{H}_{xy}\left[(1+\frac{A}{K})\cos\varphi\cos 2\theta + i(1+\frac{A}{K}\cos^2\varphi)\sin 2\theta\right] + \sin\varphi(\mathscr{H}_{xz}\cos\theta + \mathscr{H}_{yz}\sin\theta)(1+\frac{B_\perp}{K}) + i\sin\varphi\cos\varphi(\frac{A+B_\perp}{K})(\mathscr{H}_{xz}\sin\theta - \mathscr{H}_{yz}\cos\theta)\right\}$$

$$+ iS_-' I_-' \frac{(B_x\cos\psi - iB_y\sin\psi)}{4B_\perp} e^{i\psi}\Big\{ \quad \text{complex conjugate} \quad \Big\}$$

$$- iS_+' I_-' \frac{(B_x\cos\psi - iB_y\sin\psi)}{4B_\perp} e^{i\psi}\left\{\mathscr{H}_{xy}\left[(1-\frac{A}{K})\cos\varphi\cos 2\theta + i(1-\frac{A}{K}\cos^2\varphi)\sin 2\theta\right] + \sin\varphi(\mathscr{H}_{xz}\cos\theta + \mathscr{H}_{yz}\sin\theta)(1-\frac{B_\perp}{K}) - i\sin\varphi\cos\varphi(\mathscr{H}_{xz}\sin\theta - \mathscr{H}_{yz}\cos\theta)(\frac{A+B_\perp}{K})\right\}$$

$$+ iS_-' I_+' \frac{(B_x\cos\psi + iB_y\sin\psi)}{4B_\perp} e^{-i\psi}\Big\{ \quad \text{complex conjugate} \quad \Big\} \qquad (E\text{-}4)$$

These terms arising from the off-diagonal contributions of $\underline{I}\cdot\underline{\underline{A}}\cdot\underline{S}$ when the principal axes of g and A do not coincide must be added to the diagonal contributions of Appendix C before matrix elements of this part of the Hamiltonian can be evaluated for the state $|SM,Im>$.

Since the resulting equation would be extremely complicated in general, and since we are primarily interested in this approach where the phase shift is the largest, i.e., the xy plane, we set $\varphi = 0$. The hyperfine terms then become:

$$
\begin{aligned}
&A I_z S_z + B_x I_x S_x + B_y I_y S_y + \sum_{ij}{}' F_{ij}(S_i I_j + S_j I_i)\Big|_{\varphi=0} \Rightarrow \\
&I_z' S_z' \left[\frac{B_x+B_y}{2} - \frac{B_x-B_y}{2}\cos 2\theta - \mathcal{F}_{xy}\sin 2\theta\right] \\
&+S_z' I_+' \frac{(B_x\cos\psi + iB_y\sin\psi)}{2B_\perp}\left[\frac{B_x-B_y}{2}\sin 2\theta - \mathcal{F}_{xy}\cos 2\theta - i(\mathcal{F}_{xz}\sin\theta - \mathcal{F}_{yz}\cos\theta)\right] \\
&+S_z' I_-' \frac{(B_x\cos\psi - iB_y\sin\psi)}{2B_\perp}\left[\quad \text{complex conjugate} \quad\right] \\
&+I_z' S_+' \frac{e^{i\psi}}{2}\left[\frac{B_x-B_y}{2}\sin 2\theta - \mathcal{F}_{xy}\cos 2\theta - i(\mathcal{F}_{xz}\sin\theta - \mathcal{F}_{yz}\cos\theta)\right] \\
&+I_z' S_-' \frac{e^{-i\psi}}{2}\left[\quad \text{complex conjugate} \quad\right] \\
&-I_+' S_\perp' e^{i\psi}\frac{B_x\cos\psi + iB_y\sin\psi}{4B_\perp}\left[A - \frac{B_x+B_y}{2} - \frac{B_x-B_y}{2}\cos 2\theta - \mathcal{F}_{xy}\sin 2\theta\right. \\
&\qquad\qquad \left. + 2i(\mathcal{F}_{xz}\cos\theta - \mathcal{F}_{yz}\sin\theta)\right] \\
&-I_-' S_-' e^{-i\psi}\frac{B_x\cos\psi - iB_y\sin\psi}{4B_\perp}\left[\quad \text{complex conjugate} \quad\right] \\
&+I_+' S_-' e^{-i\psi}\frac{B_x\cos\psi + iB_y\sin\psi}{4B_\perp}\left[A + \frac{B_x+B_y}{2} + \frac{B_x-B_y}{2}\cos 2\theta + \mathcal{F}_{xy}\sin 2\theta\right] \\
&+I_-' S_+' e^{i\psi}\frac{B_x\cos\psi - iB_y\sin\psi}{4B_\perp}\left[\quad " \quad " \quad " \quad "\right]
\end{aligned}
\qquad (E-5)
$$

Applying perturbation theory to second order on (E-5) gives the variation of the energy levels in the xy plane. Using the selection rules $\Delta M = \pm 1$, $\Delta m = 0$ and solving for the magnetic field as in Appendix C results in the following equation describing the variation of the resonance magnetic field for $S = \frac{1}{2}$ — if we neglect the quadrupole terms:

$$H_m(\delta) = \frac{h\nu}{g_\perp \beta} - \frac{m}{g_\perp \beta}\left[\frac{B_x+B_y}{2} + \frac{B_x-B_y}{2}\left(\frac{g_x^2\cos^2\delta - g_y^2\sin^2\delta}{g_\perp^2}\right) + 2\mathscr{A}_{xy}\frac{g_x g_y}{g_\perp^2}\sin\delta\cos\delta\right]$$

$$- \frac{m^2}{2g_\perp^2\beta^2 H}\left\{\left[-(B_x-B_y)\frac{g_x g_y}{g_\perp^2}\sin\delta\cos\delta + \mathscr{A}_{xy}\left(\frac{g_x^2\cos^2\delta - g_y^2\sin^2\delta}{g_\perp^2}\right)\right]^2 + \left[\mathscr{A}_{xz}\frac{g_x}{g_\perp}\cos\delta + \mathscr{A}_{yz}\frac{g_y}{g_\perp}\sin\delta\right]^2\right\}$$

$$- \frac{I(I+1)-m^2}{8g_\perp^2\beta^2 H}\left\{A + \frac{B_x+B_y}{2} - \frac{B_x-B_y}{2}\left(\frac{g_x^2\cos^2\delta - g_y^2\sin^2\delta}{g_\perp^2}\right) - 2\mathscr{A}_{xy}\frac{g_x g_y}{g_\perp^2}\sin\delta\cos\delta\right\}^2$$

$$- \frac{I(I+1)-m^2}{8g_\perp^2\beta^2 H}\left\{\left[A - \frac{B_x+B_y}{2} + \frac{B_x-B_y}{2}\left(\frac{g_x^2\cos^2\delta - g_y^2\sin^2\delta}{g_\perp^2}\right) + 2\mathscr{A}_{xy}\frac{g_x g_y}{g_\perp^2}\sin\delta\cos\delta\right]^2 + 4\left[\mathscr{A}_{xz}\frac{g_y}{g_\perp}\sin\delta + \mathscr{A}_{yz}\frac{g_x}{g_\perp}\cos\delta\right]^2\right\}$$

APPENDIX G

DATA REDUCTION FOR VO^{+2} CRYSTALS

From Appendices C and F the resonance magnetic field can be evaluated along the x($\Theta = \pi/2$, $\delta = 0$), y($\Theta = \pi/2$, $\delta = \pi/2$), and z($\Theta = 0$) axes to give the following equations:

$$H_z = \frac{h\nu}{g_z\beta} - 2\frac{D}{g_z\beta}\left(M-\tfrac{1}{2}\right) - \frac{2S(S+1)-6M(M-1)-3}{2g_z^2\beta^2 H}E^2 - \left[\frac{A}{g_z\beta} + \frac{B_x B_y}{g_z^2\beta^2 H}\left(M-\tfrac{1}{2}\right)\right]m$$
$$- \frac{I(I+1)-m^2}{4g_z^2\beta^2 H}\left(B_x^2+B_y^2\right) - \frac{m(2m^2+1)-2mI(I+1)}{2AM(M-1)g_z\beta}(Q'')^2$$

$$H_x = \frac{h\nu}{g_x\beta} + \frac{D-3E}{g_x\beta}\left(M-\tfrac{1}{2}\right) - \frac{2S(S+1)-6M(M-1)-3}{8g_x^2\beta^2 H}(D+E)^2$$
$$- \left[\frac{B_x}{g_x\beta} + \frac{AB_y}{g_x^2\beta^2 H}\left(M-\tfrac{1}{2}\right)\right]m - \frac{I(I+1)-m^2}{4g_x^2\beta^2 H}\left(A^2+B_y^2\right) - \frac{m(2m^2+1)-2mI(I+1)}{8g_x\beta B_x M(M-1)}(Q'+Q'')^2$$

$$H_y = \frac{h\nu}{g_y\beta} + \frac{D+3E}{g_y\beta}\left(M-\tfrac{1}{2}\right) - \frac{2S(S+1)-6M(M-1)-3}{8g_y^2\beta^2 H}(D-E)^2$$
$$- \left[\frac{B_y}{g_y\beta} + \frac{AB_x}{g_y^2\beta^2 H}\left(M-\tfrac{1}{2}\right)\right]m - \frac{I(I+1)-m^2}{4g_y^2\beta^2 H}\left(A^2+B_x\right)^2 - \frac{m(2m^2+1)-2mI(I+1)}{8g_y\beta B_y M(M-1)}(Q'-Q'')^2$$

(G-1)

Since the magnetic field for each of the 2I+1 resonances is measured, we choose to evaluate the spin Hamiltonian constants in the following manner.

Z Axis. For S = 1/2, I = 7/2, the above equation for H_Z reduces to

$$H_z = \frac{h\nu}{g\beta} - \frac{A}{g_z\beta}m - \frac{B_x^2+B_y^2}{4g_z^2\beta^2 H}\left[\frac{63}{4}-m^2\right] - 4\frac{(Q'')^2}{Ag_z\beta}m\left[\frac{61}{4}-m^2\right] \qquad (G\text{-}2)$$

|A| and |Q"|. To evaluate |Q"| one can look at

$$\frac{1}{2m}\left[H_z(-m)-H_z(m)\right] = \frac{A}{g_z\beta} + 4\frac{(Q'')^2}{Ag_z\beta}\left[\frac{61}{4}-m^2\right] \qquad (G\text{-}3)$$

for the various values of m.

This same expression can also be used to compute $H/g_z\beta$.

g_z. To evaluate g_z we use

$$\frac{1}{8}\sum_m H_z(m) = \frac{h\nu}{g_z\beta} - \frac{21}{32}\frac{B_x^2+B_y^2}{g_z^2\beta^2 H} \qquad (G\text{-}4)$$

X Axis. Similarly, for the x axis H_x in (G-1) reduces to the following for S = 1/2, I = 7/2:

$$H_x = \frac{h\nu}{g_x\beta} - \frac{B_x}{g_x\beta} - \frac{A^2+B_y^2}{4g_x^2\beta^2 H}\left[\frac{63}{4}-m^2\right] - \frac{(Q'+Q'')^2}{B_x g_x\beta}m\left[\frac{61}{4}-m^2\right] \qquad (G\text{-}5)$$

Forming 1/2m $[H_x(-m)-H_x(m)]$ one can evaluate $B_x/g_x\beta$ and $(Q'+Q'')^2$. And with 1/8 $[\sum_m H_x(m)]$, g_x can be computed.

Y Axis. For the y axis a similar treatment on the data is performed by using

$$H_y = \frac{h\nu}{g_y\beta} - \frac{B_y}{g_y\beta}m - \frac{A^2+B_x^2}{4g_y^2\beta^2 H}\left[\frac{63}{4} - m^2\right] - \frac{[Q'-Q'']^2}{B_x g_x \beta}m\left[\frac{61}{4} - m^2\right] \quad \text{(G-6)}$$

$\underline{\mathcal{H}_{xy}}$. In the xy plane the term involving the quantity $\mathcal{H}_{xy}$ was evaluated at $\delta \simeq 45°$. At this angle

$$H_{\frac{\pi}{4}} \simeq \frac{h\nu}{g_\perp\beta} - \frac{m}{g_\perp\beta}\left[\frac{B_x+B_y}{2} + \mathcal{H}_{xy}\right] - \frac{(Q')^2}{B_\perp g_\perp \beta}m\left(\frac{61}{4} - m^2\right)$$

$$- \frac{I(I+1)-m^2}{4g_\perp^2\beta^2 H}\left[A^2 + \left(\frac{B_x+B_y}{2} - \mathcal{H}_{xy}\right)^2\right]$$

APPENDIX H

DATA REDUCTION FOR V^{+2} CRYSTALS

From Appendix D the rhombic spin Hamiltonian gives the following equation for the fine structure part with the magnetic field parallel to the z axis (we also add the hyperfine terms evaluated by perturbation theory from Appendix C):

$$H_{3/2,m} = \frac{h\nu}{g_z\beta} - 2\frac{D}{g_z\beta} + 3\left(\frac{E}{g_z\beta}\right)^2 \frac{D}{g_z\beta H_{3/2}^2}\left[\frac{1}{1-\left(\frac{D}{g_z\beta H_{3/2}}\right)^2}\right] - \left[\frac{A}{g_z\beta} + \frac{B^2}{g_z^2\beta^2}\frac{1}{H_{3/2}}\right]m - \frac{I(I+1)-m^2}{2H_{3/2}}\left(\frac{B}{g_z\beta}\right)^2$$

$$H_{1/2,m} = \frac{h\nu}{g_z\beta} - 3\left(\frac{E}{g_z\beta}\right)^2 \frac{1}{H_{1/2}}\left[\frac{1}{1-\left(\frac{D}{g_z\beta H_{1/2}}\right)^2}\right] - \frac{A}{g_z\beta}m - \frac{I(I+1)-m^2}{2H_{1/2}}\left(\frac{B}{g_z\beta}\right)^2$$

$$H_{-\frac{1}{2},m} = \frac{h\nu}{g_z\beta} + 2\frac{D}{g_z\beta} - 3\left(\frac{E}{g_z\beta}\right)^2 \frac{D}{g_z\beta H_{-1/2}^2}\left[\frac{1}{1-\left(\frac{D}{g_z\beta H_{-\frac{1}{2}}}\right)^2}\right] - \left[\frac{A}{g_z\beta} - \left(\frac{B}{g_z\beta}\right)^2\frac{1}{H_{-\frac{1}{2}}}\right]m - \frac{I(I+1)-m^2}{2H_{-\frac{1}{2}}}\left(\frac{B}{g_z\beta}\right)^2$$

Similarly for the magnetic field along the y axis:

$$H_{3/2,m} = \frac{h\nu}{g_y\beta} + \frac{D+3E}{g_y\beta} - \frac{3}{8}\left(\frac{D-E}{g_y\beta}\right)^2\left(\frac{D+3E}{g_y\beta}\right)\frac{1}{H_{3/2}^2}\left[\frac{1}{1-\left(\frac{D+3E}{2g_y\beta H_{3/2}}\right)^2}\right] - \frac{I(I+1)-m^2}{2H_{3/2}}\left(\frac{A}{g_y\beta}\right)^2 + \frac{27}{128}\left(\frac{D-E}{g_y\beta H_{3/2}}\right)^4\left(\frac{D+3E}{g_y\beta}\right)\left[1+\frac{10}{3}\left(\frac{D+3E}{2g_y\beta H_{3/2}}\right)^3\right] - \left[\frac{B}{g_y\beta} + \left(\frac{A}{g_y\beta}\right)^2\frac{1}{H_{3/2}}\right]m$$

$$H_{1/2,m} = \frac{h\nu}{g_y\beta} - \frac{3}{4}\left(\frac{D-E}{g_y\beta}\right)^2\frac{1}{H_{1/2}}\left[\frac{1}{1-\left(\frac{D+3E}{2g_y\beta H_{1/2}}\right)^2}\right] + \frac{9}{64}\frac{1}{H_{1/2}^3}\left(\frac{D-E}{g_y\beta}\right)^4 - \frac{B}{g_y\beta}m - \frac{I(I+1)-m^2}{2H_{1/2}}\left(\frac{A}{g_y\beta}\right)^2$$

$$H_{-1/2,m} = \frac{h\nu}{g_y\beta} - \frac{D+3E}{g_y\beta} + \frac{3}{8}\left(\frac{D-E}{g_y\beta}\right)^2\left(\frac{D+3E}{g_y\beta}\right)\frac{1}{H_{-1/2}^2}\left[\frac{1}{1-\left(\frac{D+3E}{2g_y\beta H_{-1/2}}\right)^2}\right] - \frac{27}{128}\left(\frac{D-E}{g_y\beta H_{-1/2}}\right)^4\left(\frac{D+3E}{g_y\beta}\right)\left[1+\frac{10}{3}\left(\frac{D+3E}{2g_y\beta H_{-1/2}}\right)^3\right] - \left[\frac{B}{g_y\beta} - \left(\frac{A}{g_y\beta}\right)^2\frac{1}{H_{-1/2}}\right]m - \frac{I(I+1)-m^2}{2H_{-1/2}}\left(\frac{A}{g_y\beta}\right)^2$$

Since the magnetic field for each of the 2I+1 resonances is measured, we choose to evaluate the data in the following manner: for the z axis and the value for D,

$$\sum_{m=-7/2}^{7/2} \frac{H_{-1/2,m} - H_{3/2,m}}{8} = \frac{4D}{g_z\beta} - 3\left(\frac{E}{g_z\beta}\right)^2\left(\frac{D}{g_z\beta}\right)\left\{\frac{1}{H_{-1/2}^2}\left[\frac{1}{1-\left(\frac{D}{g_z\beta H_{-1/2}}\right)^2}\right]\right.$$

$$\left. + \frac{1}{H_{3/2}^2}\left[\frac{1}{1-\left(\frac{D}{g_z\beta H_{3/2}}\right)^2}\right]\right\} - 5.25\left(\frac{B}{g_z\beta}\right)^2\left[\frac{1}{H_{-1/2}} - \frac{1}{H_{3/2}}\right]$$

for g_z,

$$\frac{1}{8}\left(\sum_m H_{1/2,m}\right) = \frac{h\nu}{g_z\beta} - 3\left(\frac{E}{g_z\beta}\right)^2\left[\frac{1}{1-\left(\frac{D}{g_z\beta H_{1/2}}\right)^2}\right]\frac{1}{H_{1/2}} - 5.25\left(\frac{B}{g_z\beta}\right)^2\frac{1}{H_{1/2}}$$

Similarly for the y axis and the value for E,

$$\sum_m \frac{H_{3/2,m} - H_{1/2,m}}{8} = \frac{D+3E}{g_y\beta}\left\{2 - \frac{3}{8}\left(\frac{D-E}{g_y\beta}\right)^2\left[\frac{1}{H_{3/2}^2}\left(\frac{1}{1-\left(\frac{D+3E}{2g_y\beta H_{3/2}}\right)^2}\right) + \frac{1}{H_{-\frac{1}{2}}^2}\times\right.\right.$$

$$\left.\left.\left(\frac{1}{1-\left(\frac{D+3E}{2g_y\beta H_{-1/2}}\right)^2}\right)\right] + \frac{27}{128}\left(\frac{D-E}{g_y\beta}\right)^4\left[\frac{1}{H_{3/2}^4}\left(1+\frac{10}{3}\left[\frac{D+3E}{2g_y\beta H_{3/2}}\right]^2\right) + \frac{1}{H_{1/2}^4}\left(1+\frac{10}{3}\left[\frac{D+3E}{2g_y\beta H_{1/2}}\right]^2\right)\right]\right\}$$

$$- 5.25\left(\frac{A}{g_y\beta}\right)^2\left[\frac{1}{H_{3/2}} - \frac{1}{H_{1/2}}\right]$$

$$\sum_m \frac{H_{1/2,m}}{8} = \frac{g_y\beta}{4|g_y\beta|H_{1/2}}\left[\frac{1}{1-\left(\frac{D+3E}{2g_y\beta H_{1/2}}\right)^2}\right] + \frac{9}{64}\frac{1}{H_{1/2}^3}\left(\frac{D-E}{g_y\beta}\right)^4 - 5.25\left(\frac{A}{g_y\beta}\right)^2\frac{1}{H_{1/2}}$$

Using the experimental data for the sums on the left hand side of the equations and evaluating the equations in a self-consistent manner yields the data listed in Tables 2 and 3, Chapter IV.

REFERENCES

1. W. Low, Solid State Physics, edited by F. Seitz and D. Turnbull, Academic Press, New York (1960), Supp. 2.

2. G. E. Pake, Paramagnetic Resonance, W. A. Benjamin, New York (1962), Frontiers in Physics Series.

3. J.D.E. Ingram, Spectroscopy at Radio and Microwave Frequencies, Academic Press, New York (1955).

4. J.D.E. Ingram, Free Radicals as Studied by Electron Spin Resonance, Academic Press, New York (1958).

5. C. P. Shlichter, Principles of Magnetic Resonance, Harper and Row, New York (1963).

6. B. Bleaney and K.W.H. Stevens, Repts. Prog. Phys., 16, 108 (1953).

7. K. D. Bowers and J. Owen, Rept. Prog. Phys., 18, 304 (1955).

8. H. S. Jarrett, Solid State Physics, Vol. 13, Academic Press, New York (1963).

9. E. Zavoisky, J. Phys. USSR, 9, 211, 245 (1945).

10. E. Zavoisky, J. Phys, USSR, 10, 197 (1946).

11. H. Bethe, Ann. Physik 3, 133 (1929)—English Translation, Splitting of Terms in Crystals, available from Consultants Bureau, New York.

12. J. H. Van Vleck, Electric and Magnetic Susceptibilities, Oxford University Press (1932).

13. C. J. Ballhausen, Introduction to Ligand Field Theory, McGraw-Hill Book Co., New York (1962).

14. NMR Table, 3rd edition, Aug. 1955, Varian Assoc., Palo Alto, Calif.

15. V. Heine, Group Theory in Quantum Mechanics, Pergamon Press, New York (1960).

16. B. Bleaney, D.J.E. Ingram, and H.E.D. Scovil, Proc. Phys. Soc., A64, 601 (1951).

REFERENCES (Continued)

17. W. Low, Phys. Rev., 101, 1827 (1956).

18. G. M. Zverev and A. M. Prokhorov, Soviet Physics (JETP), 34, 1023 (1958).

19. J. Lambe, R. Ager, and C. Kikuchi, Bull. Am. Phys. Soc., 4, 761 (1959).

20. A. Siegert, Physica, 4, 138 (1937).

21. J.V.D. Handel and A. Siegert, Physica, 4, 871 (1937).

22. M.H.L. Pryce and W. A. Runciman, Disc. Faraday Soc., 26, 34 (1958).

23. J. Lambe and C. Kikuchi, Phys. Rev., 118, 71 (1960).

24. H. J. Gerritsen and H. R. Lewis, Phys. Rev., 119, 1010 (1960).

25. G. M. Zverev and A. M. Prokhorov, Soviet Physics (JETP), 12, 160 (1960).

26. G. Andersson, Acta Chem. Scand., 10, 623 (1956).

27. C. K. Jorgensen, Acta Chem. Scand., 11, 73 (1957).

28. N. S. Garif'ianov and B. M. Kozyrev, Daklady Akad. Nauk (USSR), 98, 929 (1954).

29. B. M. Kozyrev, Disc. Faraday Soc., 19, 135 (1955).

30. G. E. Pake and R. H. Sands, Phys. Rev., 98, 266A (1955).

31. R. H. Sands, Phys. Rev., 99, 1222 (1955).

32. D. E. O'Reilly, J. Chem. Physics, 29, 1188 (1958), see also ibid., 30, 591 (1959).

33. R. J. Faber and M. T. Rogers, J. Am. Chem. Soc., 81, 1849 (1959).

34. C. M. Roberts, W. S. Koski, and W. S. Caughey, J. Chem. Phys., 34, 591 (1961).

35. B. Bleaney, Proc. Phys. Soc., A63, 407 (1950).

REFERENCES (Continued)

36. J. W. Searl, R. C. Smith, and S. J. Wyard, Proc. Phys. Soc., A74, 491 (1959).

37. J. A. Ibers and J. D. Swalen, Phys. Rev., 127, 1914 (1962).

38. H. M. McConnell, J. Chem. Physics, 25, 709 (1956).

39. R. N. Rogers and G. E. Pake, J. Chem. Phys., 33, 1107 (1960).

40. J. E. Wertz, P. Auzins, J.H.E. Griffiths, and J. W. Orten, Disc. Faraday Soc., 26, 66 (1958).

41. C. A. Hutchinson and L. S. Singer, Phys. Rev., 89, 256 (1953).

42. W. B. Gager, Personal Memorandum to C. Kikuchi.

43. C. J. Ballhausen and H. B. Gray, J. Inorg. Chem., 1, 111 (1962).

44. R. Wyckoff, Crystal Structures, 3, text page 39, Interscience Publishers.

45. A.E.H. Tutton, Crystalline Structure and Chemical Constitution, Macmillan and Co., London (1910).

46. J. Weiss, Nucleonics, 10, 28 (1952), see also Nucleonics, 17, 73 (1959).

47. M.H.L. Pryce, Proc. Phys. Soc., 63A, 25 (1950).

48. A. Abragam and M.H.L. Pryce, Proc. Roy. Soc., 205A, 135 (1951).

49. R. Lacroix and G. Emch, Helvetica Physica Acta, 35, 592 (1963).

50. H. A. Jahn and E. Teller, Proc. Roy. Soc., 161A, 220 (1937).

51. H. A. Kramers, Proc. Acad. Sci. Amsterdam, 33, 953 (1930).

52. K.W.H. Stevens, Proc. Phys. Soc., 65A, 209 (1952).

53. G. F. Koster and H. Staatz, Phys. Rev., 113, 445 (1959).

54. H. Staatz and G. F. Koster, Phys. Rev., 115, 1568 (1959).

REFERENCES (Concluded)

55. M. B. Palma-Vitorelli, M. U. Palma, D. Palumbo and F. Sgarlata, Nuovo Cimento, 3, 718 (1956).

56. L. Pauling, The Nature of the Chemical Bond, 3rd edition, Cornell Univ. Press, Ithica, New York (1960).

57. B. Bleaney, R. P. Penrose, and B.I.P. Plumpton, Proc. Roy. Soc., 198A, 406 (1949).

58. M. D. Sturge, Internal Memo., Bell Labs. (to be published).

59. H. Kulenkampff, Ann. Physik, 69, 548 (1922).

60. R. D. Evans, The Atomic Nucleus, McGraw-Hill Book Co., New York (1955).